Thermal energy harvesting from temperature fluctuations

Hongying Zhu

N° d'ordre 2011-ISAL-0086 Année 2011

THÈSE

Récupération d'Énergie Thermique à partir de Variations de Température

-

Thermal Energy Harvesting from Temperature Fluctuations

présentée devant
L'Institut National des Sciences Appliquées de Lyon

Pour obtenir
Le grade de DOCTEUR

École doctorale : Électronique, Électrotechnique et Automatique de Lyon
Spécialité : Énergie et Systèmes

Par
Hongying ZHU

INSA de Lyon, FRANCE

Soutenue le 29 Septembre 2011 devant la Commission d'examen

Rapporteur	Pr. Amen AGBOSSOU
Examinateur	Pr. François BAUER
Rapporteur	Dr. Yves BERNARD
Directeur	Pr. Daniel GUYOMAR
Co-directeur	Dr. Sébastien PRUVOST

Laboratoire de recherche : Laboratoire de Génie Électrique et Ferroélectricité (LGEF) de l'INSA de Lyon

SIGLE	ECOLE DOCTORALE	NOM ET COORDONNEES DU RESPONSABLE
CHIMIE	**CHIMIE DE LYON** **http://www.edchimie-lyon.fr** Insa : R. GOURDON	M. Jean Marc LANCELIN Université de Lyon – Collège Doctoral Bât ESCPE 43 bd du 11 novembre 1918 69622 VILLEURBANNE Cedex Tél : 04.72.43 13 95 directeur@edchimie-lyon.fr
E.E.A.	**ELECTRONIQUE, ELECTROTECHNIQUE, AUTOMATIQUE** **http://edeea.ec-lyon.fr** Secrétariat : M.C. HAVGOUDOUKIAN eea@ec-lyon.fr	M. Gérard SCORLETTI Ecole Centrale de Lyon 36 avenue Guy de Collongue 69134 ECULLY Tél : 04.72.18 60 97 Fax : 04 78 43 37 17 Gerard.scorletti@ec-lyon.fr
E2M2	**EVOLUTION, ECOSYSTEME, MICROBIOLOGIE, MODELISATION** **http://e2m2.universite-lyon.fr** Insa : H. CHARLES	Mme Gudrun BORNETTE CNRS UMR 5023 LEHNA Université Claude Bernard Lyon 1 Bât Forel 43 bd du 11 novembre 1918 69622 VILLEURBANNE Cédex Tél : 04.72.43.12.94 e2m2@biomserv.univ-lyon1.fr
EDISS	**INTERDISCIPLINAIRE SCIENCES-SANTE** **http://ww2.ibcp.fr/ediss** Sec : Safia AIT CHALAL Insa : M. LAGARDE	M. Didier REVEL Hôpital Louis Pradel Bâtiment Central 28 Avenue Doyen Lépine 69677 BRON Tél : 04.72.68 49 09 Fax :04 72 35 49 16 Didier.revel@creatis.uni-lyon1.fr
INFOMATHS	**INFORMATIQUE ET MATHEMATIQUES** http://infomaths.univ-lyon1.fr	M. Johannes KELLENDONK Université Claude Bernard Lyon 1 LIRIS - INFOMATHS Bâtiment Nautibus 43 bd du 11 novembre 1918 69622 VILLEURBANNE Cedex Tél : 04.72. 43.19.05 Fax 04 72 43 13 10 infomaths@bat710.univ-lyon1.fr
Matériaux	MATERIAUX DE LYON	M. Jean-Yves BUFFIERE Secrétaire : Mériem LABOUNE INSA de Lyon École Doctorale Matériaux Mériem LABOUNE Bâtiment Antoine de Saint-Exupéry 25bis Avenue Jean Capelle 69621 VILLEURBANNE Tel : 04 72 43 71 70 Fax : 04 72 43 72 37 ed.materiaux@insa-lyon.fr
MEGA	**MECANIQUE, ENERGETIQUE, GENIE CIVIL, ACOUSTIQUE (ED n°162)**	M. Philippe BOISSE Secrétaire : Mériem LABOUNE Adresse : INSA de Lyon École Doctorale MEGA Mériem LABOUNE Bâtiment Antoine de Saint-Exupéry 25bis Avenue Jean Capelle 69621 VILLEURBANNE Tel : 04 72 43 71 70 Fax : 04 72 43 72 37 mega@insa-lyon.fr Site web : http://www.ed-mega.com
ScSo	**ScSo*** M. OBADIA Lionel Sec : Viviane POLSINELLI Insa : J.Y. TOUSSAINT	M. OBADIA Lionel Université Lyon 2 86 rue Pasteur 69365 LYON Cedex 07 Tél : 04.78.69.72.76 Fax : 04.37.28.04.48 Lionel.Obadia@univ-lyon2.fr

*ScSo : Histoire, Geographie, Aménagement, Urbanisme, Archéologie, Science politique, Sociologie, Anthropologie

If we knew what we were doing, it wouldn't be called research, would it?

Albert Einstein

Abstract

The development of portable equipments, wireless sensors networks and self-powered devices in a general manner generates a strong demand for micro-energy harvesting devices. One of the most challenging ways to self power devices is the development of systems that recycle ambient energy and continually replenish the energy consumed by the system. Apart from electromechanical energy harvesting, it is also interesting to convert thermal energy, which is "available" everywhere, into suitable electrical energy.

In this thesis, the thermal to electrical energy conversion from temperature fluctuations was developed and improved, and the feasibility of this technique was also confirmed by implementing the experimental experiment. Among different ferroelectric materials, PZN-4.5PT single crystal and P(VDF-TrFE-CFE) 61.3/29.7/9 mol% were chosen as active materials due to their outstanding properties under electric field. By means of some intelligent thermodynamic cycles, e.g., Ericsson or Stirling cycle, which has been presented in previous research, the efficiency of energy conversion could be improved greatly.

In the first part, pyroelectric energy harvesting on PZN-4.5PT single crystals with an Ericsson cycle was mainly investigated from two aspects: frequency effect and phase transitions. It was shown that the harvested energy demonstrated a nonlinear decrease with an increase of frequency, and the optimal use of the phase transitions during the Ericsson cycle could greatly improve the harvested energy by choosing the appropriate working temperature range. Based on it, two asymmetric Ericsson models (L-H and H-L cycles) were attempted successfully, and it was confirmed that the H-L cycle is the most effective thermal energy harvesting cycle for this material.

The second part concentrated on electrostatic energy harvesting by nonlinear capacitance variation on P(VDF-TrFE-CFE) 61.3/29.7/9 mol% terpolymer. Ericsson cycle was tested experimentally between 25 and 0°C and compared with the simulation from dielectric constant values obtained under DC electric field. The identical result between simulation and

experiment proved the reliability of our theoretical evaluation. It was found, from simulation, that the harvested energy increased up to 240 mJ/cm^3 when raising the electric field at 80 kV/mm. The further study on Ericsson and Stirling cycle was also made under different temperature and electric field conditions for evaluation. The harvested energy increases with the rising of temperature variation and electric field in both cycles, but in contrast to Ericsson cycle, Stirling cycle can harvest more energy for the same injected energy.

Résumé

Le développement des équipements portables, des réseaux de capteurs sans fil et systèmes auto-alimentés d'une manière générale génère une forte demande pour les dispositifs de récupération de micro-énergie. Une des voies les plus intéressantes pour auto-alimenter des dispositifs consiste à développer des systèmes recyclant l'énergie ambiante afin de renouveler sans cesse l'énergie consommée par le dispositif. En dehors de la récupération d'énergie électromécanique, il est également intéressant de convertir l'énergie thermique, qui est «disponible» partout, en énergie électrique.

Au cours de cette thèse, la conversion d'énergie thermique en énergie électrique fondée sur des variations temporelles de température a été développée et améliorée. Parmi les matériaux ferroélectriques, des monocristaux de PZN-4.5PT et le terpolymère P(VDF-TrFE-CFE) 61.3/29.7/9 mol % ont été choisis comme matériaux actifs en raison de leurs propriétés remarquables sous champ électrique. En utilisant des cycles thermodynamiques intelligents, par exemple, Ericsson ou à cycle de Stirling, l'efficacité de la conversion de l'énergie pourrait être considérablement améliorée.

Dans la première partie, la récupération d'énergie pyroélectrique en utilisant des monocristaux de PZN-4.5PT a été principalement étudiée sous deux aspects: l'effet de fréquence et des transitions de phase sur les cycles d'Ericsson. Il a été montré que l'énergie récupérée diminue de façon non linéaire avec une augmentation de la fréquence. De plus, l'utilisation optimale des transitions de phase pendant le cycle d'Ericsson permet d'améliorer grandement l'énergie récupérée en choisissant une gamme de température de travail appropriée. A partir de ces résultats, deux cycles d'Ericsson asymétriques (LH et HL) ont été réalisés avec succès. Avec les monocristaux de PZN-4.5PT, le cycle HL est le cycle le plus efficace pour la conversion d'énergie thermique en énergie électrique.

La deuxième partie traite de la récupération d'énergie électrostatique via la variation non linéaire de la capacité du terpolymère P(VDF-TrFE-CFE) 61.3/29.7/9 mol %. Un cycle

d'Ericsson a été réalisé entre 25 et 0°C et comparé à sa simulation à partir de la valeur de la constante diélectrique sous champ électrique DC. La concordance entre la simulation et l'expérience a prouvé la fiabilité de notre évaluation théorique. A partir de la simulation, l'énergie récupérée augmente jusqu'à 240 mJ/cm^3 en appliquant un champ électrique de 80 kV/mm. Des cycles de Stirling et d'Ericsson ont également été simulés sous différentes variations de température et champ électriques. L'énergie récupérée augmente avec l'accroissment de la variation de température et de la valeur du champ électrique appliqué et ceci quelque soit le cycle réalisé. Contrairement au cycle d'Ericsson, un cycle de Stirling peut récupérer plus d'énergie pour une même énergie injectée.

Acknowledgements

First and foremost, I would like to sincerely thank Prof. Daniel Guyomar for serving as my advisor. It has truly been an honor to work with him on the cutting edge of research in the field of Energy harvesting. His strong work ethic and creative thinking is contagious to me and will influence me throughout my professional career. I would also like to thank Dr. Sébastien Pruvost for serving as my co-advisor, for his sense of responsibility, incredible patience, and numerous fruitful discussions. His enlightening guidance and encouragement is the powerful support for my work.

I would like to thank Pr. Amen AGBOSSOU, Pr. Francois BAUER, Dr. Yves BERNARD for their contributions as committee members and for their comments and suggestions that improved the quality of this work.

Next, I would like to thank Dr. Pierre-Jean Cottinet for his generous help, our pleasant cooperation made a great promotion to this thesis. I would also like to thank Dr. Gaël Sebald for his constructive advices on my work.

I would like to express my gratitude to Dr. Laurence Seveyrat for providing help and advice in synthesizing the polymers. Besides, the experimental work could not have progressed so quick without the support of Verinique Perin. Thanks also go to Mr. Frederic Defromerie for machining the art-like device for my design and experiment.

I am extremely thank Evelyne Dorieux, secretary of Laboratory, for her supporting. She is not only my colleague in lab, but also a bosom friend, I will never forget her kindly help.

I will not be able to list the names of all whom I feel grateful to, but I would like to express my gratitude to all of the members of LGEF. Without a doubt, I am proud to be one of them, their optimistic and positive spirit, their serious in work and humorus in life accompany with me during all the life in LGEF.

In addition, I would like to acknowledge the China Scholarship Council (CSC) for their financial support and the Co-operation program between CSC and UT-INSA.

Finally, I want to thank my father, ZHU Dezhou, mother, LI Shuilian, brother, ZHU Chaoqun. Their support is the source of power to pursue my life goal. I extremely want to express my deepest gratitude and love to my husband, SHI Xueyuan, without his considerable understanding, tremendous support at work and life, I could never reach this joyful moment. This thesis is dedicated to him.

Table of contents

Nomenclature & Abbreviations

Nomenclature

Symbol	Signification
A	Surface of electrode
c	Calorific capacity
C	Curie-Weiss constant
C_{max}	Maximum capacitance
C_{min}	Minimum capacitance
C_r	Capacitance
D	Electric Displacement
e	Strain
E	Electric field
E_c	Coercive field
f	Frequency
FOM	Figure of merit for pyroelectric energy Harvesting
p	Pyroelectric coefficient
P_{max}	Harvested power
P_s	Spontaneous Polarization
P_r	Remnant polarization
Q	Charge
Q_{hot}	Thermal energy taken from the hot medium
U	Internal energy
V	Voltage
W	Energy
$W_{harvest}$	Harvested energy
W_{inject}	Injected energy
W_{max}	Harvested energy per unit of volume
Γ	Entropy
δW_{cycle}	Harvested energy in one cycle
ε_0	Vacuum permittivity
η	Conversion ratio
η_{carnot}	Conversion ratio in Carnot cycle
θ	Temperature
θ_c	Curie temperature
σ	Stress
χ	Electric susceptibility
$\varepsilon_{33}^{\theta}$	Dielectric permittivity

Abbreviations

Symbol	Signification
ECE	Electrocaloric Effect
MEMS	Micro-Electro-Mechanical System
MsM	Magnetostrictive Materials
PZT	Piezoelectric
PVDF	Polyvinylidene Fluoride
PZN-4.5PT	$Pb(Zn_{1/3}Nb_{2/3})_{0.955}Ti_{0.045}O_3$
P(VDF-TrFE)	Poly(vinylidene fluoride-trifluoroethylene)
P(VDF-TrFE-CFE)	Poly(vinylidene fluoride-trifluoroethylene-chlorofluoroethylene)
P(VDF-TrFE-CTFE)	poly(vinylidene-fluoride–trifluoroethylene–chlorotrifluoroethylene)

Introduction

Over the years, there has been a growing interest in stand-alone systems in numerous application fields, such as embedded sensors in buildings, medical implants, and other remote wireless sensing nodes. In many applications, the problem posed by these devices is how to supply the required power. In addition, constant advances in electronics push past boundaries of integration and functional density toward completely autonomous microchips embedding their own energy source. In these cases, research continues to develop higher energy-density batteries, but the amount of energy available is finite and remains relatively weak, limiting the system's lifespan, which is paramount in stand-alone systems or portable electronics and may induce a costly maintenance, in the case of contaminated areas for instance. Moreover, batteries dying without warning poses serious problems in safety monitoring applications. Extended life is also particularly advantageous in systems with limited accessibility, such as biomedical implants, structure-embedded microsensors, or safety monitoring devices in harsh environments and contaminated areas. Accordingly, supplying systems with power over the lifespan of a structure is a significant challenge. To solve all these problems, sustainable power generation may be achieved in converting ambient energy into electrical energy.

Energy harvesting aims to collect ambient energy to help power systems, possibly storing energy when it is not required. Different systems are already available: solar cells and electromechanical conversion for harvesting from vibrations or from mechanical stress (i.e. produced by a person walking or an object movement). The interest of researchers is continuously increasing in the framework of clean energy sources. One energy source -- thermal energy -- is rarely harvested although being 'available' everywhere. In the daily life, large amounts of waste heat are released from power, refrigeration, and heat pump cycles. In this dissertation, we concentrate on a promising approach – thermal energy harvesting from temperature variation.

The objective and motivation of this study is to develop a new energy harvester that may be particularly suited to satisfying the small scale power generation demands of applications. There are two methods we mainly investigated for thermal energy harvesting: (1) pyroelectric energy harvesting in PZN-4.5PT single crystal, and (2) electrostatic energy harvesting in P(VDF-TrFE-CFE) 61.3/29.7/9 mol% terpolymer. We hope the results obtained in this work could promote the development of thermal energy harvesting.

Chapter 1
Literatures Review and General Concepts of Different Techniques of Energy Harvesting

1.1 Motivation

With the recent development of wireless and integrated electronics, the demand for portable electronics and wireless sensors has demonstrated a rapid growth, as has the demand for structural sensors in buildings, medical implants, global positioning system (GPS) tracking devices on animals in the wild or safety-monitoring devices in harsh environments and contaminated areas. Due to such devices being portable, it becomes necessary for them to carry their own power supply. Indeed, in most of the above-mentioned applications, the system is completely embedded in the host structure and physical connections with the outside world are impossible.

The conventional solution is to utilize electrochemical batteries. However, this entails drawbacks, e.g., the finite lifespan of such batteries. Moreover, retrieving the system simply to replace or recharge the battery is a very costly task, and is sometimes even impossible. Another great drawback, certain applications do not tolerate the chemicals they contain, even normally the batteries are encapsulated, there is still potential risk to cause serious problems once the exhausted batteries can not be replaced or recharged in time.

An optimum solution to build ‘perpetually powered’ systems is to include a microgenerator that converts available ambient energy into electrical energy. Some possible ambient energy sources are, for instance, thermal energy, light energy, mechanical energy and magnetic energy. Solar power and ocean tides are also frequently harnessed as most of the

available renewable energy sources in nature due to their huge radiant light and heat or mechanical energy, respectively. Thus, a portable small scale power generation system (alternative methods of power) that can either replace batteries entirely or recharge them to extend their lifetime is of considerable interest. Then, this small, portable, and lightweight power generation systems are currently in very high demand in the commercial markets, due to a dramatic increase in the use of personal electronics and communications equipments.

Energy harvesting (also known as "power scavenging" or "energy extraction") is the process by which energy is captured and stored. Frequently this term is applied when speaking about small autonomous devices, like those used in sensor networks. There are various sources of energy available for harvesting, and indeed, much work has been presented on generators capable of generating electrical energy from light[1-2], thermal gradients[3-6], solar power[7-10], ambient RF[9,11]. Scavenging energy from ambient vibrations, heat or light could enable smart sensors to be functional indefinitely. Several articles reviewing energy source for energy harvesting can be found in the literature[12-17]. Over the past decade, the amount of literature published on the topic of energy harvesting has increased drastically due to renewed interest in alternative energy sources.

Roundy[18] studied the energy conversion of ambient vibrations to electricity, which based on both piezoelectric and electrostatic (capacitive) coupling. By comparing the power densities between piezoelectric converters and electrostatic converters, he concluded that piezoelectric converters are capable of higher power output densities. However, electrostatic converters are more easily implemented in silicon micromachining processes. Randall[10] provided that ambient energy systems based on photovoltaic solar cells may be used for higher power devices (mW rating). L. Mateu and F. Moll[16] presented several different energy transducers for obtaining electrical energy from different types of energy available, including kinetic energy (piezoelectric generator, electrostatic energy generator, magnetic induction generator), electromagnetic radiation (solar energy, RF radiation) and thermal energy.

This chapter introduces a broad survey of potential energy sources or techniques for energy harvevsting. Also, it provides literatures review and a comparison of energy scavenging technologies.

1.2 Energy Harvesting Principles

Energy harvesting, also referred to as "energy scavenging" or "energy extraction", can be defined as "converting ambient energies such as vibration, temperature, light, RF energy, *etc*. to usable electrical energy using energy conversion materials or structures, and subsequently storage the electrical energy for powering electric devices". In other words, the general concept of energy harvesting is to convert energy from the environment that is in an unusable form or wasted form into a more useful form. Frequently the form of energy that is most useful in modern applications is electrical energy, where it can be stored in a battery or used to power electrical circuitry.

The wasted or unusable energy sources exist in various forms such as industrial machines, human activity, vehicles, structures and environment sources, as listed in **Table 1.1**[19]. Environment energy sources can be divided into vibration, solar power, RF, air flow sources, pressure variations, radioactive specks, temperature gradient... Several approaches have been explored during the last few decades in order to harvest energy from the environment to power low power wireless sensor networks. These sensor networks are employed to improve the comfort and health of intelligent buildings. The energy needed by a wireless sensor is in the order of hundreds of micro watts.

Human body	Vehicles	Structures	Industrial	Environment
Breathing, blood pressure, exhalation, body heat	Aircraft, UAV, helicopter, automobiles, trains	Bridges, roads, tunnels, farm house structures	Motors, compressors, chillers, pumps, fans	Wind, solar, temperature gradient, daily temperature
Walking, arm motion, finger motion, jogging, swimming, eating, talking	Tires, tracks, peddles, brakes, shock absorbers, turbines	Control-switch, HVAC systems, ducts, cleaners, etc.	Conveyors, cutting and dicing, vibrating mach.	Ocean currents, acoustic waves, EM waves, RF signal

Table 1.1 Sources of energy available in the surrounding.[19]

The main power sources studied for wireless sensor networks are solar power and mechanical vibration. Solar power technology employed for this application can be outdoor or indoor solar power which include light and thermal energy. The outside solar energy has the capability of providing power density of 15,000 $\mu W/cm^3$ which is about two orders of magnitudes higher than other sources. However, one of the major challenges is that the variation in light or heat intensity (cloudy vs. sunny day) can drop the efficiency greatly. The other most attractive source is kinetic energy comprising of mechanical vibrations, air flow and human power. The kinetic energy can be converted into electrical energy using piezoelectric, electromagnetic or electrostatic mechanism. A comparison of vibration

conversion to solar power and battery power is shown in **Fig. 1.1**. The shaded boxes in the figure indicate the range of solar (lightly shaded) and vibration (darkly shaded) power available based power generation[20]. Solar and vibration power output are not a function of lifetime.

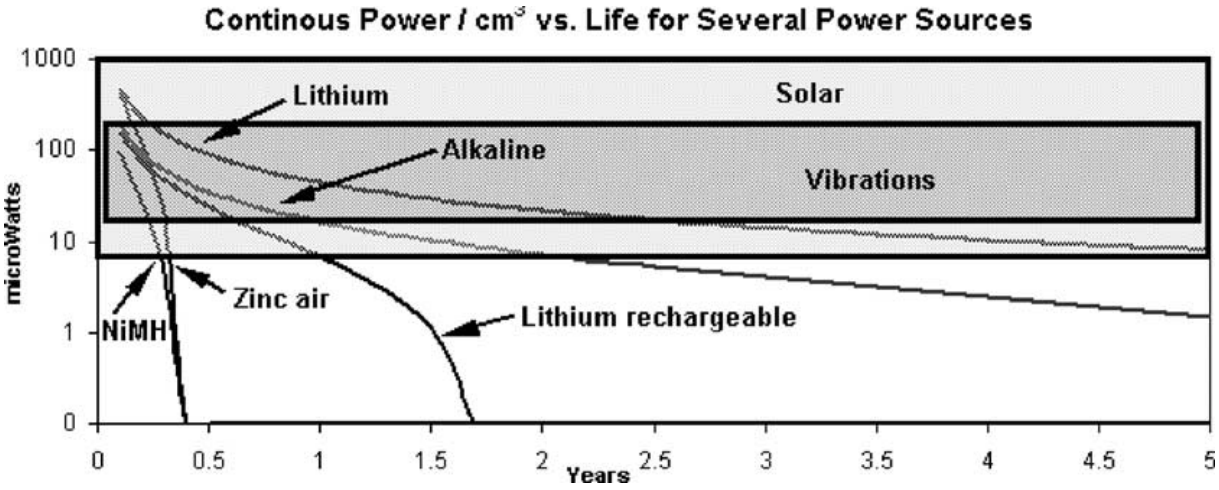

Fig. 1.1 Comparion of power from vibrations, solar and various battery chemistries.[20]

The continuous miniaturization and reduction of power consumption in modern electronic devices enables and demands the employment of alternative energy sources. In contrast to vibration, the energy-conversion from thermal energy has received more and more attention recently. Thermal energy is another form of energy which is available almost everywhere, thermoelectric and pyroelectric are the most universal techniques for thermal energy harvesting. Temperature gradient or temperature variation in energy converter is the necessary precondition for thermal energy harvesting. The temperature varies more slowly due to the large heat capacity of the materials. This causes the working frequency to be lower, and consequently, a maximum of available energy must be harvested in a single attempt. Roundy et al provided the result of a broad survey of potential energy sources for energy conversion, both fixed energy sources such as batteries and power scavenging sources, and showed in **Table 1.2**[20].

	Power density ($\mu W/cm^3$) one year lifetime	Power density ($\mu W/cm^3$) 10 year lifetime
Solar (outdoors)	15,000—Direct sun, 150—Cloudy day	15,000—Direct sun, 150—Cloudy day
Solar (indoors)	6—Office desk	6—Office desk
Vibrations (piezoelectric conversion)	250	250
Vibrations (electrostatic conversion)	50	50
Acoustic noise	0.003 at 75 dB, 0.96 at 100 dB	0.003 at 75 dB, 0.96 at 100 dB
Temperature gradient	15 at 10 °C gradient	15 at 10 °C gradient
Shoe inserts	330	330
Batteries (non-rechargeable lithium)	45	3.5
Batteries (rechargeable lithium)	7	0
Hydrocarbon fuel (micro heat engine)	333	33
Fuel cells (methanol)	280	28

Table 1.2 Comparison of power density and energy sources.[20]

Differing from battery-powered sensors, the energy harvesting device should be designed with high efficiency, which converts, collects, and stores the energy to power the sensor node as needed, as shown in **Fig. 1.2**[21], an energy harvesting wireless sensor has a complicated architecture including an energy harvesting module with harvesting device unit and energy harvesting circuit unit. To establish a congruent interface with the energy harvesting module, two additional submodules, power switching and power management modules, are integrated within the wireless sensor node.

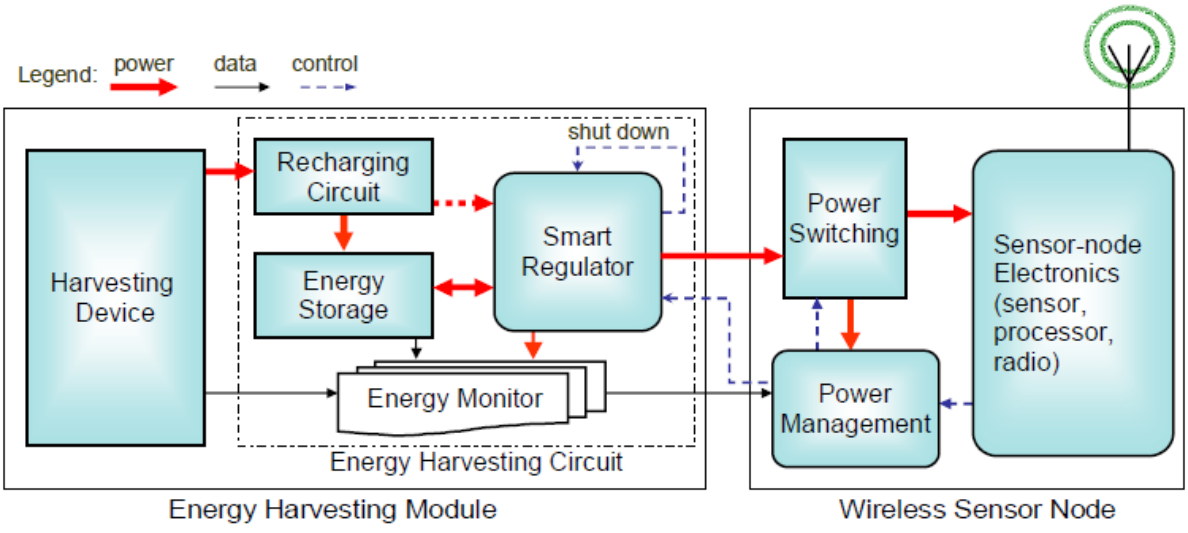

Fig. 1.2 General structure of an energy harvesting module and compatible wireless sensor nodes.[21]

The harvesting device generates usable electrical energy from ambient energy. It can be implemented by two mechanisms: one is based on materials for energy conversion such as piezoelectric material, electrostrictive material, pyroelectric material, thermoelectric material , solar cell, etc.; the other relies on structures for energy conversion such as electromagnetic

harvesters and electrostatic harvesters. Unlike battery supply, which is simply characterized by the amount of residual and reliably available energy, the characterization of environmental energy is time-dependent and more complicated, also, the environmental energy has the potential to be used permanently.

1.3 Summary of Potential Energy Sources and the corresponding technique

This part examines the potential ambient energy sources and current methods of harvesting electrical energy.

1.3.1 Solar Energy

Solar or other light energies can be converted into electrical power using solar cells, which are commercially mature and well characterized. On average, the earth's surface receives about 1.2×10^{17} W of solar power. It means that in less than one hour enough energy is supplied to satisfy the entire energy demand of the human population[22]. Photovoltaics is a method of generating electrical power by converting solar radiation into direct electrical current using semiconductors that exhibit the photovoltaic effect. It is well known as generating electric power by using solar cells.

Solar power has large potential for power generation due to the large input power from the sun, but many challenges limit its practical use. Different materials display different efficiencies and have different costs. The output energy depends on the material which must have characteristics matched to the spectrum of available light, for example, crystalline materials such as silicon and gallium arsenide have moderated absorption efficiency and high conversion efficiency about 15% ~ 30%; while thin film materials such as cadmium telluride have high absorption efficiency and lower conversion efficiency ($\leq$10%). The choice of materials also relies on its spectral response and the light source of interest[23].

Outdoor isolation levels offer approximately two to three orders of magnitude more electricity per unit area than indoor electric light sources[12,17,20]. Measurements taken in normal office lighting show that only 6 $\mu W/cm^3$ can be converted by a solar cell[12], which is not nearly enough for the targeted application under consideration and restricts its main use to areas where there is not enough sunlight. Therefore, using other techniques of harvesting energy such as vibration and thermal is suitable.

1.3.2 Radio Frequency Energy

Radio frequency energy is emitted by sources that generate high electromagnetic fields such as TV signals, satellites orbiting earth, wireless radio networks, wifi and cell phone towers. We are being bombarded with energy waves every second of the day. If it could be possible to gather the energy and store it, we could potentially use it to power other circuits.

Most commonly used as an application for radio frequency identification tags in which the sensing device wirelessly sends a radio frequency to a harvesting device which supplies just enough power to send back identification information specific to the item of interest (**Fig. 1.3**).

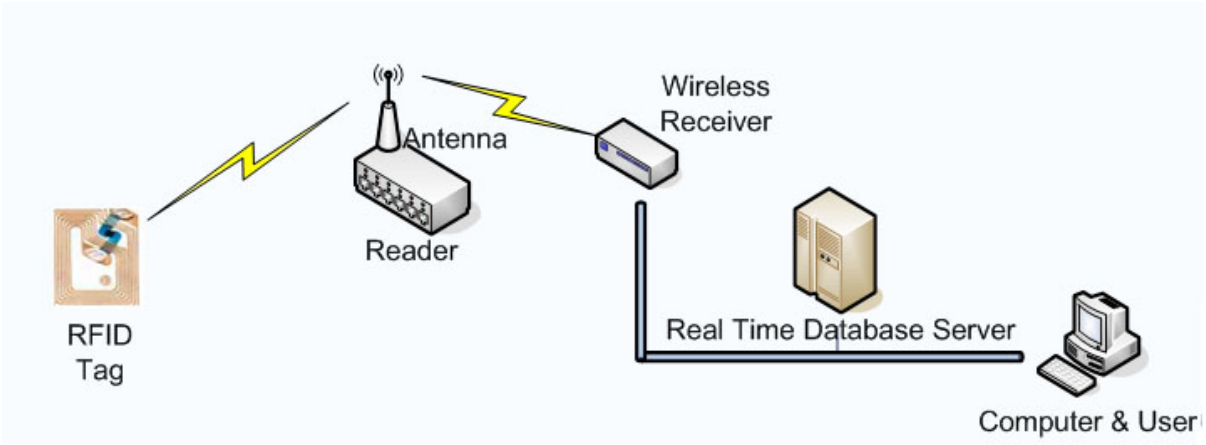

Fig. 1.3 RFID System Diagram.
(http://www2.egr.uh.edu/~mpark5/rfid.html)

RF energy harvesting needs a receiving antenna linked to a power generating circuit capable of converting AC voltage to usable DC voltage[24], as shown in **Fig. 1.4**. Although the total energy is fixed, RF antenna designs and the distance between the source and the device can vary the energy density. The increased concentration of RF energy by focusing is typically measured in terms of antenna efficiency. The efficiency of an antenna is related to the shape and impedance of the antenna and the impedance of the circuit. If the two impedances aren't matched then there is reflection of the power back into the antenna meaning that the circuit was unable to receive all the available power.

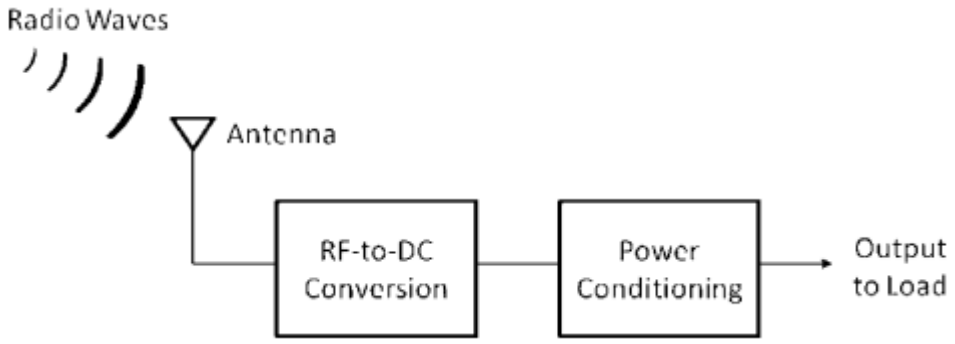

Fig. 1.4 Overview of a RF energy harvesting system.
(http://www.sensorsmag.com)

1.3.3 Human Power

Human power is defined as the use of human motion or body heat for energy generation to power an electronic device. That said, power might be scavenged indirectly from the user's everyday actions or might be intentionally generated by the user. The energy can be harvested from body heat, breathing, blood pressure, typing, arm motion, pedaling, and walking, **Table 1.3** provides a perspective on the amount of power used by the human body during various activities[25]. In general, most attraction is focusing on two fields about human power for energy harvesting: human motion and body heat.

Activity	*Kilocal/hr*	*Watts*
sleeping	70	81
lying quietly	80	93
sitting	100	116
standing at ease	110	128
conversation	110	128
eating meal	110	128
strolling	140	163
driving car	140	163
playing violin or piano	140	163
housekeeping	150	175
carpentry	230	268
hiking, 4 mph	350	407
swimming	500	582
mountain climbing	600	698
long distance run	900	1,048
sprinting	1,400	1,630

Table 1.3 Human energy expenditures for selected activities.[25]

1.3.4 Vibration Energy

Vibration energy harvesting is one approach where energy from parasitic vibrations can be converted into electrical energy by using piezoelectric or electromagnetic transducers. Parasitic vibrations come from a range of sources around the energy harvesting device, such as wind, seismic forces and traffic[26]. There are three main categories of vibration sources, as shown in **Table 1.4** Industrial, Structural, and Vehicular[27]. Existing approaches to vibration energy harvesting typically utilize a rectifier circuit, which is tuned to the resonant frequency of the harvesting structure and the dominant frequency of vibration.

Vibration energy harvesting techniques can rely on electromagnetic (inductive), electrostatic (capacitive), piezoelectric, and magnetostrictive approaches. Four common techniques will be discussed individually, and then a comparison table will be drawn to compare the features of different techniques.

Category	Vibration Sources	Recommended AdaptivEnergy Joule-Thief™ Module			
		JTF-060e5 (Fixed Frequency)	JTF-120e5 (Fixed Frequency)	JTRA-e5mini (Low Freq Random)	Custom Joule-Thief™
Industrial	Motors		X		
	Compressors		X		
	Turbines		X		
	Pumps	X	X		
	Smart Grid	X	X		
	Transformers	X	X		
	Chillers	X	X		
	Fans	X			
	Conveyors			X	X
	Cutting, Dicing			X	X
Structural	Bridges				X
	Roads				X
	HVAC Systems	X			X
Vehicular	Train			X	X
	Truck			X	X
	Automobile			X	X
	Helicopter			X	X
	Other Aircraft		X		X

Table 1.4 Categories of vibration and recommended Adaptivenergy Joule-Thief™ energy harvesting module.[27]

1.3.4.1 Electromagnetic Energy Harvesting

Since it is quite easy to keep a strong magnetic field with a permanent magnet, electromagnetic vibration-power generators are preferred in many applications. The basic electromagnetic energy generator consists of a mass mounted on a spring which vibrates relative to housing when subjected to an external vibrational force. The mechanical energy of the moving mass is transformed to electrical energy by having the mass move a magnet relative to a coil. The motion of such a system can be described as **Fig. 1.5** (a)[28]. Faraday's Law is a basic principle of electromagnetic system to operating principals of electric generator, as illustrated in **Fig. 1.5** (b)[29].

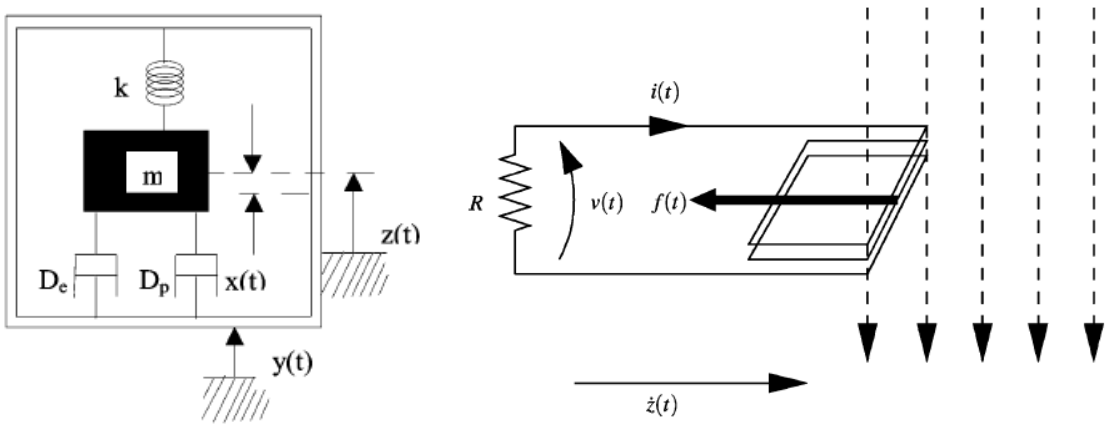

(a) (b)

Fig. 1.5 (a) Schematic diagram of electromagnetic generator. m - mass, k- spring D – damping, (b) the principle of operation of electromagnetic transducer.[29]

Electromagnetic-based generators have been demonstrated to generate power levels ranging from 0.3 to 800 μW from vibration frequencies of several hundred hertz. Williams and Yates proposed an electromagnetic energy harvesting device in 1996[30], the power they produced was proportional to the cube of the vibration frequency. For a typical device, the power generation was 1 μW at 70 Hz and 0.1 mW at 330 Hz. In order to maximize power generation, the mass deflection should be as large as possible. Glynne-Jones *et al.* presented that the output voltage is a function of vibration amplitude as well as its magnetic field strength. They designed the electromagnetic generator which can produce a peak power of 3.9mW with an average power of 157 μW when mounted on the engine block of a car[31]. However, due to low electromagnetic damping, the size and structure of the device, the optimization theory is difficult to be verified in practice.

In 2006, Chitta Ranjan Saha *et al.*[28] presented a model for an electromagnetic-based, vibrational power generator and investigated the optimum condition for electromagnetic damping and local resistance. Furthermore, they also verified the optimum condition by using measurements on two macrogenerators which have been built and tested. Their result showed that the power is maximum for the value of load resistance at which electromagnetic damping and parasitic damping are equal. The electromagnetic damping is always much less than the parasitic damping and the power is maximized for a load resistance equal to the coil resistance.

In 2009, Ibrahim Sari *et al.*[32] proposed a new electromagnetic micro energy harvester, employing array of parylene cantilevers on which planar gold coils are fabricated. The micro

harvester generates voltage by virtue of the relative motion between the coils and a stationary magnet. The fabricated device occupies a volume of 9.5 × 8 × 6 mm^3. A single cantilever of this device can generate a maximum voltage and power of 0.67 mV and 56 pW, respectively, at a vibration frequency of 3.4 kHz. These values can be improved considerably by increasing the coil turns and natural frequency of the cantilevers.

In summary, the electromagnetic energy conversion mechanism is simple without the need of smart materials, but it has relatively larger volume than the other vibration energy conversion system (e.g., piezoelectric energy conversion), because of the required permanent magnets and pickup coil. Due to its inductive property, comparatively high output current levels are achievable at the expense of low voltage. Voltage multiplier may be a suitable solution to increase the voltage level.

1.3.4.2 Electrostatic Energy Harvesting

An electrostatic transducer uses the force between charges stored on electrodes to couple the energy from the mechanical domain into the electrical domain. By placing charge on the capacitor plates and then moving the plates apart, mechanical energy can be converted into electrical energy which can then be stored and utilized by a load as depicted in **Fig. 1.6**[33].

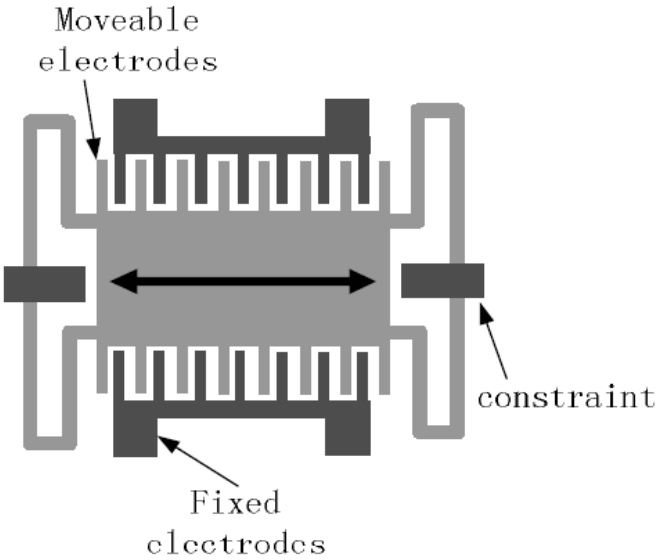

Fig. 1.6 Schematic of a typical electrostatic harvester vibrating horizontally.[33]

Meninger *et al.*[34] presented an electrostatic generator that employs a variable micromachined capacitor. Fundamentally, electrostatic harvesters harness the work ambient vibrations exert on the electrostatic force of a variable capacitor (i.e., varactor). In more

physical terms, vibrations cause the gap distance and/or overlap area of a parallel-plate capacitor (C_{VAR}) to vary with a net effect, under constant charge or voltage conditions, of producing electrical energy[35]. Two possible energy conversion cycles in the charge-voltage plane for the MEMS transducer are charge constrained conversion and voltage constrained conversion, respectively. **Fig. 1.7** illustrates the process of charging and discharging the capacitance following the constant charge (path A-B-D-A) or constant voltage (path A-C-D-A) approaches[34]. The energy enclosed by the total path is the energy harvested in the cycle. One basic constraint for both cycles is that there is some maximum allowable voltage, V_{max}, which is set by some process or system requirement.

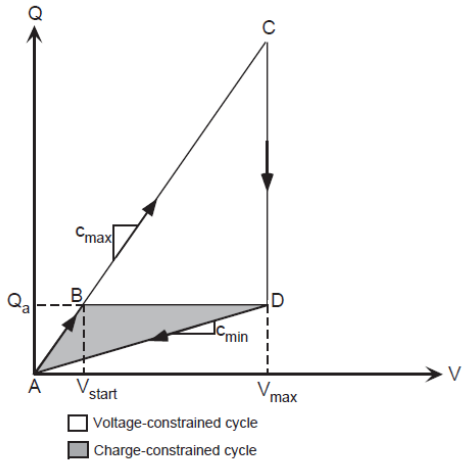

Fig. 1.7 Scheme of electrostatic energy conversion cycle.[34]

Fig. 1.8 (a) and (b) illustrate the principle of operation of the two possible electrostatic energy conversion[29], respectively. The name of the path depicts which property is held constant during the conversion process while the other changes in response to a varying capacitance. If the charge on the capacitor is maintained constant while the capacitance decreases (e.g., reducing the overlap area of the plates or increasing the distance between them), the voltage will increase, operation as **Fig. 1.8** (a). If the voltage on the capacitor is maintained constant while the capacitance decreases, the charge will decrease, operation as **Fig. 1.8** (b).

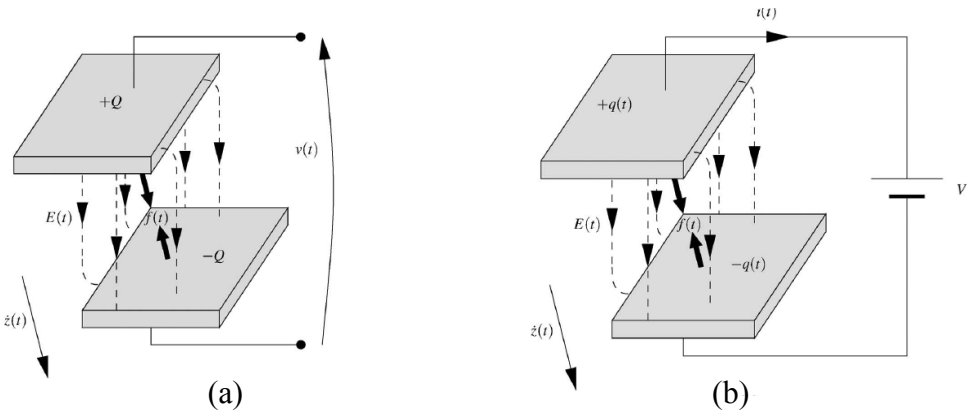

Fig. 1.8 Principle of operation of electrostatic transducer.
(a) charge constrained (b) voltage constrained.[29]

The electrostatic energy harvesting does not require smart materials and could be interested on MEMS. Due to capacitive-based device, it generates relative high voltage of 2~10 V and results in a limited current-supplying capacity[33]. Meninger *et al*.[34] compared two different conversion cycles using a variable capacitor under the condition of constant maximal applied voltage. In 2004, Roundy *et al.* optimized the electrostatic harvester and improved the output power density up to 110 μw/cm^3 at 120 Hz vibration[33].

1.3.4.3 Piezoelectric Energy Harvesting

The piezoelectric effect is a phenomenon whereby a strain in a material produces an electrical charge in that material, and conversely an applied electric field produces a mechanical strain[36] as shown in **Fig. 1.9**. It was discovered by Jacques and Pierre Curie in 1880. Curie's brothers found that certain materials, when subjected to mechanical strain, suffered an electrical polarization that was proportional to the applied strain. This is the piezoelectric effect used for mechanical to electrical energy conversion (**Fig. 1.9**[29]).

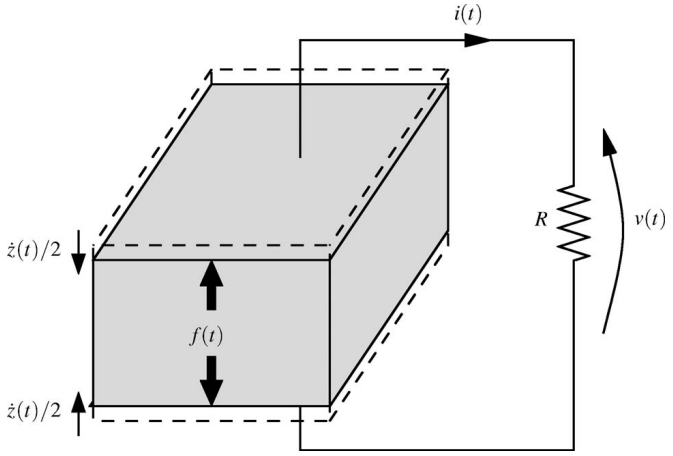

Fig. 1.9 Principle of operation of the piezoelectric transducer.[29]

Piezoelectric energy is the most popular among all these vibration-based methods because of reasonable electro-mechanical coupling coefficient, no bulky accessories (such as coil or permanent magnet), and feasibility of being deposited on substrates for MEMS application. Concept of utilizing piezoelectric material for energy harvesting has been studied by many researchers. Umeda et al.[37] investigated fundamentals of piezoelectric generator using a piezoelectric vibrator and a steel ball. This study quantified the energy produced when a steel ball impacted a thin piezoelectric plate. The authors used an equivalent circuit model to predict the energy while modifying numerous parameters in the system to find the best combination. It was determined that the efficiency increased if the mechanical quality factor increased, the electromechanical coupling coefficient increased and the dielectric loss decreased. The maximum efficiency of 52% could be obtained by simulation. Elvin *et al.*[38] used a polyvinylidene fluoride (PVDF) piezofilm sensor attached to a simply-supported Plexiglas beam to generate electric power. The goal of this energy harvesting experiment was to generate sufficient energy from the strain induced on the piezofilm by the bending beam to power a telemetry circuit. The energy generated from the PVDF patch was accumulated in a capacitor. A switch was added to the circuitry to allow the capacitor to charge or discharge, which produced the output voltage range of 0.8~1.1 V for a RF transmitter.

Other types of piezoelectric materials were also investigated for power harvesting purposes[39]. The two types being the commonly used monolithic piezoelectric (PZT) bimorph and Macro Fiber Composites (MFC), both transducers were used to charge nickel metal hydride batteries of varying sizes to compare their performance and ability to store electrical power. It was found that the MFC produced a much higher voltage while the current remains far smaller than that of the PZT. Because the use of interdigitated electrodes in the MFC limited the amount of current produced, and hence hindered its capabilities as a power harvesting device for charging batteries. The PZT, however, was able to charge 40 mAh and 80 mAh batteries within two hours. It was also shown that charging a battery by vibrating the PZT at resonance typically took less time than by using a random input signal to the PZT.

While significant headway has been made in the field of energy harvesting, the energy generated from piezoelectric material is still not sufficient to power the desired electronic systems. To dynamically optimize the power transfer efficiency, Ottman *et al.*[40] presented an adaptive approach to harvest electrical energy from a mechanically excited piezoelectric element. The harvesting circuit consists of an ac–dc rectifier with an output capacitor, an electrochemical battery, and a switch-mode dc–dc converter that controls the energy flow into

the battery. It was found that the power output could be increased by over 400% using the adaptive dc–dc converter. To further investigation, they continued their work using a similar circuitry[41], but modified it by removing the adaptive circuitry and used a fixed switching frequency. With this circuit, the power flow was increased by over a factor of 3 at a peak resonant excitation level of 70 V open circuit. Additionally, the efficiency of 70% at an optimal value of excitation was obtained.

Recently, Guyomar *et al.*[42-43] proposed a new approach for piezoelectric energy reclamation from mechanical vibrations, which is called "Synchronized Switch Harvesting on Inductor" (SSHI) by using a self-adaptive power harvesting circuit. **Fig. 1.10** shows (a) the model of vibrating structure including a piezoelectric element and (b) the SSHI energy harvesting device in steady state operation. This approach is derived from a popular method called 'Synchronized Switch Damping on Inductor' (SSDI)[44], a semi-passive technique that was developed to address the problem of vibration damping in mechanical structures. It consists in the switching sequence triggered on the maximal and minimal of the piezo mechanical displacement. It is shown that the SSHI technique increases the harvested power by a factor 8 compared to the standard technique[42].

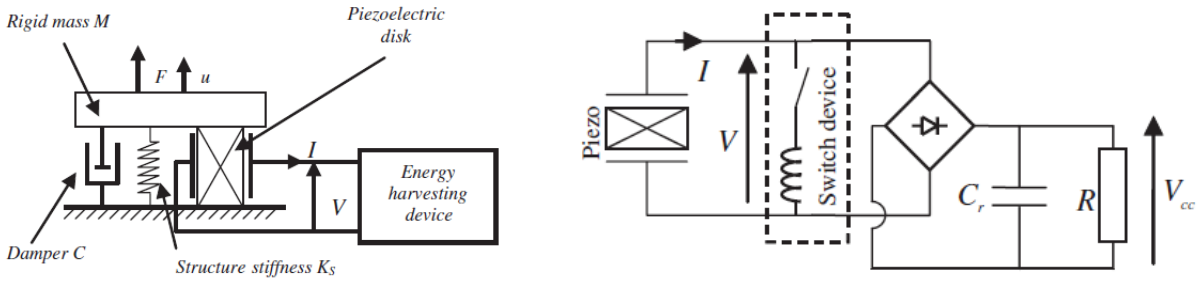

(a) (b)

Fig. 1.10 (a) model of vibrating structure including a piezoelectric element (b) SSHI energy harvesting device in steady state operation.

1.3.4.4 Magnetostrictive Energy Harvesting

Magnetostrictive materials (MsM) are a class of compounds which change their shape or dimension when they are subjected to a magnetic field. The reciprocal effect, vibration-induced strain of a MsM producing a change in the magnetization of the material, is called Villari effect. The mechanism of magnetostriction can be depicted by **Fig. 1.11**. The principle of vibration energy harvesting is mainly based on Villari effect.

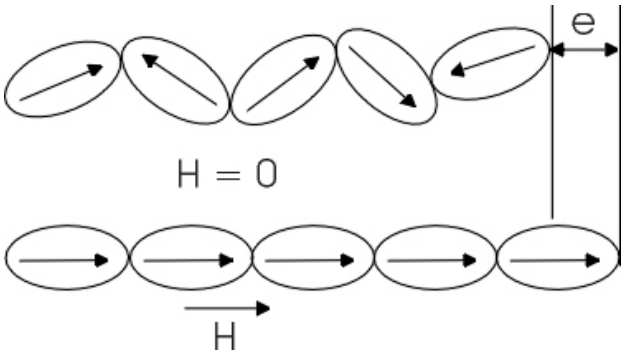

Fig. 1.11 Mechanism of magnetostriction (http://aml.seas.ucla.edu/research/areas/magnetostrictive/mag-composites/Magnetostriction%20and%20Magnetostrictive%20Materials.htm)

To convert ambient vibrations to electrical energy, current technology focuses mainly on piezoelectric materials, but its inherent limitations including aging, depolarization, brittleness, and high output impedance confine further applications in actual wireless sensor networks. To overcome such limitations, magnetostrictive materials (MsM) would be a promising candidate as depicted in **Fig. 1.12**[21]. It utilizes the Villari effect of magnetostrictive, where vibration induced strain from a MsM produces a change in the magnetization of the material. This change in magnetization is converted into electrical energy using a pick-up coil or solenoid surrounding the MsM according to Faraday's law.

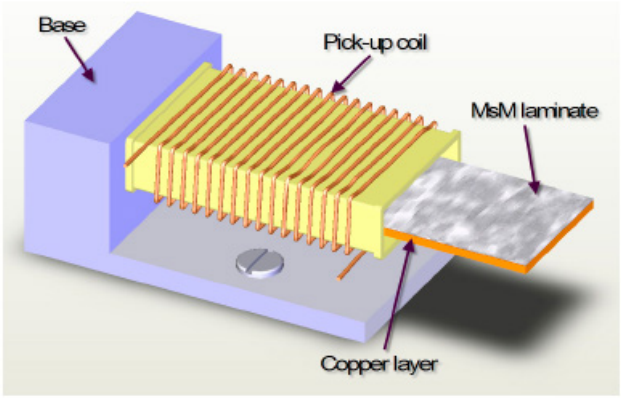

Fig. 1.12 Prototype of MsM energy harvesting device.[21]

Staley and Flatau attempted to apply a Terfenol-D alloy in vibration energy harvesting[45]. The Terfenol-D rod was operated in axial mode rather than flexural bending mode. The maximum output power was up to 45 μW at resonant frequency of 45 Hz, and the amplitude of AC output voltage was less than 0.35 V which was inapplicable to voltage rectification.

Wang and Yuan[46] firstly proposed the feasibility of using amorphous metallic glass (Metglas 2605SC) as MsM for harvesting energy from ambient vibrations. Compared to piezoelectric materials, Metglas-based harvesters displays more competitive due to its ultra-

high magnetomechanical coupling efficiency (>0.9), higher Curie temperature, and no depolarization problem. However, it has relatively large dimension, which is hard to be integrated with MEMS, because of the pick-up coil and permanent magnets.

1.3.4.5 Comparison of different vibration energy harvesting techniques

Electromagnetic, electrostatic, piezoelectric and magnetostrictive are four main energy harvesting mechanisms from ambient vibration. Each of the technologies described above has their own advantages and disadvantages and these are now summarized as in **Table 1.5**[21]. Currently, piezoelectric, or PZT, is the most popular material because of its compact configuration and compatibility with MEMS (Micro-Electro-Mechanical System), but its inherent limitations including aging, depolarization, brittleness, and high output impedance confine further applications in actual wireless sensor networks.

Type	Advantages	Disadvantages
Electromagnetic	• no need of smart material • no external voltage source	• bulky size: magnets and pick-up coil • difficult to integrate with MEMS • max voltage of 0.1V
Electrostatic	• no need of smart material • compatible with MEMS • voltages of 2~10V	• external voltage (or charge) source • mechanical constraints needed • capacitive
Piezoelectric	• no external voltage source • high voltages of 2~10V • compact configuration • compatible with MEMS • high coupling in single crystal (SiO_2)	• depolarization and aging problems • brittleness in PZT • poor coupling in piezo thin film (PVDF) • charge leakage • high output impedance
Magnetostrictive	• ultra-high coupling coefficient >0.9 • no depolarization problem • high flexibility • suited to high frequency vibration	• non-linear effect • pick-up coil • may need bias magnets • difficult to integrate with MEMS

Table 1.5 Summery of the comparison of the different vibrational types of harvesting mechanisms.[21]

1.3.5 Thermal Energy

Thermal energy is the other form of energy readily presenting in environment. Thermal energy harvesting devices could use thermal energy of different sources: persons and animals, machines or other natural sources. The search for an efficient way to convert thermal into useful electrical energy has been ongoing for decades. Ambient thermal energy commonly presents two forms: temperature gradient or temperature time-variation. Corresponding to

these two representations of thermal energy, majority attempts to generate electrical energy from heat mainly rely on two effects: thermoelectric effect and pyroelectric effect.

1.3.5.1 Thermoelectric Energy Harvesting

Semiconductor thermoelectric generators, which convert thermal energy to electrical energy, have been of great interest in recent years. Due to their merits, such as high reliability, silence, together with their capability of utilizing waste heat as an energy source make them an attractive way for energy harvesting from temperature gradients.

1.3.5.1.1 Global Conception of Thermoelectric Effect

Thermoelectric phenomena (often known simply as thermoelectric effects) encompasses three separately identified effects: the Seebeck effect, Peltier effect and Thomson effect. All of these three effects are thermodynamically reversible.

The Seebeck effect shows that an electrical current is present in a series circuit of two dissimilar metals, provided the junctions of the two metals are at different temperatures, as shown in **Fig. 1.13** (a).This was because the metals responded differently to the temperature difference, creating a current loop and a magnetic field.

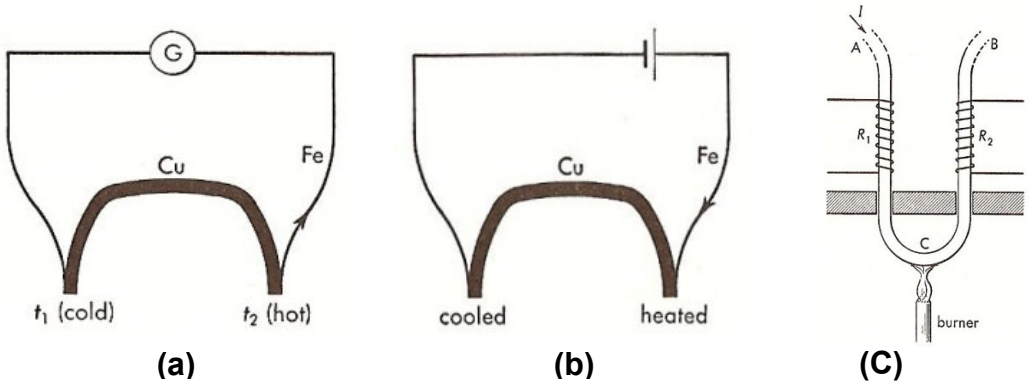

Fig. 1.13 Diagram of (a) Seebeck effect, (b) Peltier effect and (c) Thomson effect. (http://www.daviddarling.info/encyclopedia/S/Seebeck_effect.html)

The Peltier effect is the presence of heat at an electrified junction of two different metals, Peltier found that the junctions of dissimilar metals were heated or cooled, depending upon the direction in which an electrical current passed through them, as shown in **Fig. 1.13** (b). The Peltier effect can be used to create a refrigerator which is compact and has no circulating fluid or moving parts. The Thomson effect describes that an electromotive force (emf) would arise within a single conductor whenever a temperature gradient was present (**Fig. 1.13** (C)).

In summary, these three effects are not independent of, but is rather a combination of each other.

1.3.5.1.2 Global Conception of Thermoelectric Energy Harvesting

The thermoelectric effect is the ability to convert thermal heat flow to an electric current proportional to the heat flow based on Seebeck effect. Both cooling and energy harvesting are possible. A thermoelectric device creates a voltage when there is a different temperature on each side. Conversely when a voltage is applied to it, it creates a temperature difference.

Thermoelectric modules are the main way for energy harvesting from temperature. These are based on temperature gradients leading to heat flow through the thermoelectric generator and a small percentage of the heat flow is converted to electric energy.

Traditional thermoelectric systems are comprised of a number of doped semiconductor elements arranged electronically in series and thermally in parallel as shown in **Fig. 1.14**. If heat is flowing between the top and bottom of the thermoelectric device (forming a temperature gradient) a voltage will be produced and hence an electric current will flow.

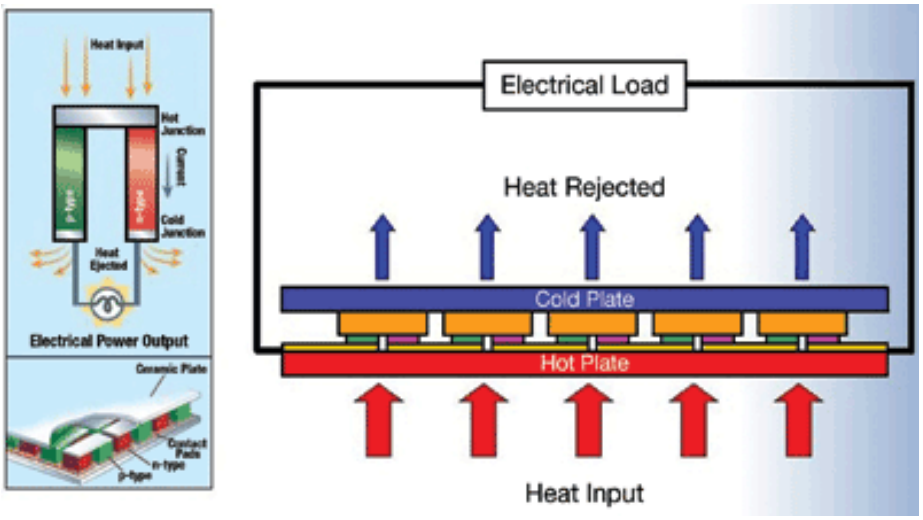

Fig. 1.14 Thermal-to-electric conversion with thermoelectrics. (http://www2.electronicproducts.com/)

A thermoelectric converter is a heat engine and like all heat engines it obeys the laws of thermodynamics. If we first consider the converter operating as an ideal generator in which there are no heat losses, the efficiency is defined as the ratio of the electrical power delivered to the load to the heat absorbed at the hot junction. For a given temperature difference, the conversion efficiency, which is limited by the material properties, may be obtained using[47].

$$\eta = \frac{\theta_2 - \theta_1}{\theta_2} \frac{\sqrt{ZT+1}-1}{\sqrt{ZT+1}+\theta_2/\theta_1} \qquad (1.1)$$

where θ_2 and θ_1 are temperatures at hot and cold ends of the converter, and ZT is figure of merit. **Fig. 1.15** depicts the figure-of-merit of a number of thermoelectric materials together with potential generating applications[48].

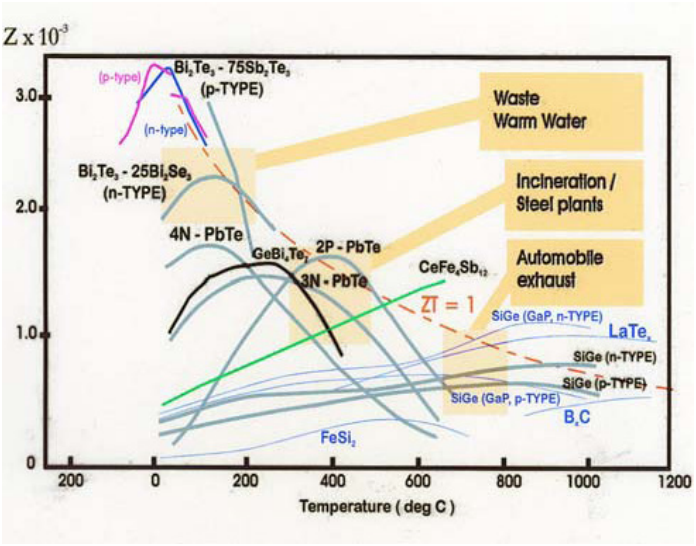

Fig. 1.15 Figure-of-Merit of a selection of materials.[48]

Material properties are the key parameter for improving both the output power (the increase of the thermal heat flow thus making it difficult to keep the temperature gradient) and the efficiency (improving the Seebeck coefficient and figure of merit).

However, when considering the limited heat exchange on the outer surfaces of the thermoelectric module, it was found that figure of merit does not really express the performance of a thermoelectric generator[49]. Apart from Seebeck effect and thermoelectric generator design, parameters such as the heat loss of the Joule and Peltier effects caused by the electric current largely affect the performance. This is due to the fact that a limited heat exchange on the outer surfaces results in a decrease of the actual temperature gradient and thus makes the Joule and Peltier effect much more important in the performance loss than what could be expected from the single figure of merit.

1.3.5.1.3 Evolution of Thermoelectric Energy Harvesting

Thermoelectric technology has been used for capturing ambient energy practically in wide areas recently. Wu et al[50] (1996) proposed the concept of a waste-heat thermoelectric generator, the specific power output of the generator was analyzed and compared with that of Carnot. They concluded that a completely reversible heat engine played a major role in the development of the performance of thermoelectric generators.

Rowe et al.[51] investigated the ability to construct a large thermoelectric generator capable of supplying 100 watts of power from hot waste water. The system tested used numerous thermoelectric devices placed between two chambers, one with flowing hot water and the other with cold water flowing in the opposite direction, thus maximizing the heat exchange. With a total of 36 modules, each with 31 thermocouples, 95 watts of power could be generated. Attempts are also being made to improve the competitiveness of thermoelectrics by increasing the electric power factor. In 2002, Rowe et al[52] synthesized intermediate valence compound $YbAl_3$. At temperatures below 100 K, the electrical resistivity exhibits a $\rho(\theta) = \rho_0 + A\theta^2$ dependence, the Seebeck coefficient exhibits a temperature dependence. Combination of a large Seebeck coefficient and low residual resistivity of single crystalline $YbAl_3$ leads to the appreciable electrical power factor of 340×10^{-6} W cm^{-1}K^{-2} at 80 K.

Stordeur et al.[53] developed a low power thermoelectric generator (micro-thermoelectric harvester) capable of generating tens of microwatts of power (15 μW/cm^2 from a 10°C temperature differential) out of a device that had previously generated nanowatts with the same size. The device was based on thin film thermoelectric materials, consisted of 2250 thermocouples, and operated in temperatures ranging from room to not higher than 120°C. Fleming et al.[54] investigated the use of thermoelectric generator (TEG) for powering microscale air vehicles. The idea is to integrate the TEGs as part of the airframe powerplant assembly to reclaim a portion of the engine's waste heat as electric power. A TEG was mounted on the exhaust system of an internal combustion engine that was shown to generate 380 mW of power.

The oil consumption of road transportation is one of the major issues in the world, automotive engines reject a considerable amount of energy to the ambience through the exhaust gas. The latest statistics indicates there is only about 25% of the fuel combustion energy is utilized for vehicle operation whereas about 40% is lost in the form of waste heat of exhaust gas. Significant reduction of engine fuel consumption could be attained by recovering of exhaust heat by using thermoelectric generators. Several research groups have studied the use of thermoelectric generators for obtaining waste energy from the exhaust of automobiles. Wojciechowski et al [55] designed and tested a prototype thermoelectric generator mounted on self-ignition (Diesel) engine. The designed model was able to recover even 25 kW of heat energy. Assuming the 5% efficiency of the thermoelectric modules it could allow to obtain the maximum electric power of app. 750 W. This power is comparable to the power of typical alternators used in cars with 1.3 dm^3 engine capacity. Birkholz et al.[56] fitted a TEG unit around the exhaust pipe. The unit was experimentally tested and found to generate an open

circuit voltage of 22 V and a total power of 58 W. Similarly, Matsubara[57] constructed an exhaust system using ten TEG modules and a liquid heat exchanger to maximize the thermal gradient. The system was tested on a 2000 cc class automobile and shown to produce 266 W of power.

Sodano et al[3] proposed a novel approach to thermal harvesting using a small greenhouse device to capture thermal energy from solar radiation. To increase the amount of thermal radiation captured by the power harvesting device, the hot side of the thermoelectric generator is placed in a small greenhouse, while the cold side is secured against a thermal sink.

Latest advancement in preparing new thermoelectric materials with good performance has made it available to fabricate feasible micro-generator. The most reported researches about thermoelectric micro-generators have been focusing on miniaturizing n-legs and p-legs in the micro-devices and the smallest size has already reached micrometer scale. But the properties of the thermoelectric material used in this form are almost the same as that in bulk. It has been verified by theory and experiments that the nanowires of thermoelectric material should have an enhanced figure of merit due to the quantum- size effects. Wang *et al*. have been successfully prepared one-dimensional n-type and p-type Bi_2Te_3 nanowire arrays by electrochemical deposition (ECD) technology. Based on those work, a new type of thermoelectric micro-generator comprised of n-type and p-type nanowire array was designed. This micro-generator can be used as not only an independent power generator, but also can be integrated with electric components together to convert waste heat into electric power.

In 2010, The National Institute of Advanced Industrial Science and Technology (AIST) publish news through their official website, a thermoelectric power generation module has been developed using new materials. The module has been demonstrated to have power generation performance equivalent to that of existing thermoelectric power-generation modules, with an output power of 1.7 W and a generation efficiency of about 4% for a temperature difference of 300°C (330°C on the hot side of the module and 30°C on the cold side).

1.3.5.1.4 Summary

According to the study of thermoelectric generator, it is found that with relatively small thermal gradients and only conductive heat transfer, a thermoelectric generator can be used for energy harvesting applications. In conclusion, the advantages of thermoelectrics as following:

1. No moving parts allow continuous operation for many years.
2. Thermoelectrics contain no materials that must be resupplied.
3. Heating and cooling can be reversed.

Thermoelectric energy conversion suffers from its low efficiency (currently less than 10%). The development of materials that are able to operate in higher temperature gradients, and that can conduct electricity well, without conducting heat, will result in increased efficiency. In brief, the generated voltage and power is proportional to the temperature differential and the Seebeck coefficient of the thermoelectric materials. Large thermal gradients are necessary to produce practical voltage and power level. Nevertheless, temperature differences greater than 10°C are rare in a micro-system, consequently producing low voltage and power level.

1.3.5.2 Pyroelectric Energy Harvesting

Pyroelectric energy conversion offers a novel and direct solution to convert waste heat into electricity by alternatively heating and cooling a pyroelectric material resulting in electricity generation. Contrary to the thermoelectric generator, pyroelectric materials do not need a temperature gradient, but time temperature fluctuations, thus the application targets are quite different.

1.3.5.2.1 Global Conception of Pyroelectric Energy Harvesting

Pyroelectricity is the ability of certain materials to generate an electrical charge when they are heated. The temperature variation slightly modifies the position of the atoms within the crystal structure, such that the polarization of the material changes. This polarization change creates a voltage across the material. This property was discovered before piezoelectric effect and is mainly used for pyroelectric infrared temperature sensor. Recently, it is found that it could be also used for the conversion of heat directly into electrical energy.

The pyroelectric effect can be used in a power generation system to force electrical charge from the pyroelectric material to an electrical storage device via heating. Subsequently, the electrical storage device can be used to satisfy the power demands of an electromechanical device.

Pyroelectric effect can be considered as the inverse electrocaloric effect. The electrocaloric effect is enhanced in the vicinity of a transition like antiferroelectric-ferroelectric or ferroelectric-paraelectric suggesting that the pyroelectric effect also increases

near a transition. Materials with high pyroelectric activity or those exhibiting a transition are always corresponding to larger polarization variations, thus it can be used to greatly increase the harvested energy.

The advantages of pyroelectric energy conversion are two-fold. First, it does not require the high source temperatures that a traditional thermoelectric power generator requires. Time varying temperature changes are necessary. Second, the combination of relatively low operating temperatures and almost no moving parts provides the potential for a power generating system with excellent reliability and a long lifetime.

1.3.5.2.2 Evolution of Pyroelectric Energy Harvesting

Pyroelectric power generation has been studied by a small number of researchers since the late 1950's. The feasibility of direct conversion of heat into electrical energy with ferroelectric materials was proposed in 1959[58] and widely reviewed[59-60]. Initial investigations of the principles of the conversion of heat energy directly into electrical energy were made by Clingman & Moore[61], Childress[62] and Hoh[63]. They studied the theoretical performance of ferroelectric materials operated in the neighbourhood of its Curie point (a molecular realignment phenomenon that is a strong function of temperature)[62]. Additionally, they determined the basic dielectric material properties necessary for meaningful power generation, e.g., a very large electric displacement, a very large breakdown voltage, and a strong temperature dependence of the electric displacement. The electric displacement is the amount of electrical charge that a dielectric material can store per unit surface area, and the breakdown voltage is the point at which the dielectric material suffers catastrophic failure (destruction of the charge storing capability). The product of these two properties describes the electrostatic energy density of the dielectric material, and this must be sufficiently large to extract significant quantities of electrical energy. A strong temperature dependence of the electric displacement is necessary to maximize the electrical charge that can be extracted from the dielectric material when it is heated and cooled.

In the mid 1960's, Fatuzzo et al[64] studied the efficiency for power converter by using of several different types of power generation cycles. They calculated and compared the thermal and electrostatic energy stored by their pyroelectric materials, as well as evaluate the performance of the power generation cycles by determining the thermodynamic states of their materials.

Gonzalo tackled the field of pyroelectric power generation in the mid 1970's[65], he concluded that with proper material selection, a pyroelectric power generator that used only one pyroelectric material could achieve a maximum efficiency of 4%, which corresponds to 17% of the Carnot efficiency. Additionally, Gonzalo proposed that several of these pyroelectric devices could be tailored to operate in sequential temperature ranges, such that they could be connected, creating a multistage converter. This device has a much larger temperature range of operation, increasing the maximum predicted efficiency to 14%, for a device operating between 300 and 1500 K.

A large advancement was obtained in the field of pyroelectric conversion by Olsen's group[66-68]. They proposed the first pyroelectric conversion cycle named 'Olsen cycle' or 'Ericsson cycle' (electric analogous of the Ericsson heat engine cycle). They measured this thermodynamic cycle in terms of charge-voltage (polarization versus applied electric field) behavior on a new materials -- copolymer P(VDF-TrFE). Between 23 and 67°C, each conversion cycle was able to generate 30 mJ/cm^3 of output electric energy density by applying maximum electric field 55 kV/mm[67]. Following this method, they also patented a pyroelectric power generator by the use of one or more capacitors having temperature dependent capacitance[69-70]. Olsen's group built, tested, and subsequently patented an experimental pyroelectric power generator that demonstrated the heat cascading effect in a pyroelectric device, shown in **Fig. 1.16**[71]. In this schematic, the ceramic stack consists of thin film materials separated by a working fluid, which is oscillated by the pump drive. The difference in temperature between the heater and the cooling unit induces temperature oscillations in the flow, which, in turn, generate temperature oscillations in the dielectric materials, providing the heating and cooling necessary for power generation.

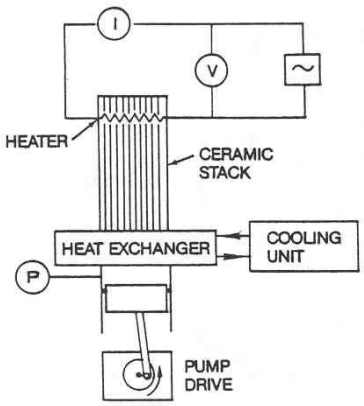

Fig. 1.16 Schematic View of the Thermal-Mechanical Portions of the Pyroelectric Conversion Experiment.[71]

Tiway[72] carried out experiments with thin film ferroelectric polymers polyvinyledene (PVF_2), attempting to quantify the maximum ratio of thermal to electrical energy conversion, as well as relate the performance of his ferroelectric material to other materials. The energy ratio, i.e. the ratio of the input heat energy to the obtainable electrical energy is assessed to be around 0.861. Most recently, Ikura's[73] experimental investigation implemented one of Olsen's theoretical operating cycles in a simple pyroelectric converter, demonstrating the ability to generate significant quantities of high voltage power of 15-52 mJ/cm^3 with a pyroelectric device. However, Ikura's device was highly inefficient, the ratio of electrical output to electrical input ranged between 1.2~1.5.

Entering the 21st century, significant breakthrough have been made in the framework of the pyroelectric energy conversion benefiting from the study on pyroelectric effect of materials, including linear pyroelectric effect and nonlinear pyroelectric effect (FE-FE and FE-PA phase transition) respectively.

First of all, utilizing linear pyroelectric effect, Guyomar et al[74] investigated the feasibility of heat energy harvesting on PVDF film combining with the synchronized switch harvesting on inductor (SSHI) technique. For amplitude variations of temperature from 0.5 to 8 K, the conversion efficiency is found about 0.02% of Carnot thermodynamic cycle with a standard interface, and the SSHI technique increases the converted energy by a factor which is about 2.5 times of the standard interface. The produced electrical power for temperature amplitude 7 K is more than 0.3 mW for an energy harvesting device composed for 8 g of active material. Sebald et al[75] also simulated the pyroelectric energy harvesting using linear pyroelectric properties of $0.75Pb(Mg_{1/3}Nb_{2/3})O_3$-$0.25PbTiO_3$ ceramic. They studied the output power as a function of the heat exchange coefficient for 20°C peak-to-peak temperature variation. Neglecting dielectric losses, increasing the heat exchange or frequency of temperature variation results in an increase of the harvested power. In addition, they estimated the output power under the same simulated conditions for different pyroelectric materials: linear and nonlinear as in **Table 1.6**.

Linear materials	Shape	p (μC m^{-2} K^{-1})	$\varepsilon_{33}^{\theta}$ (ε_0)	c_E ($\times 10^6$ J m^{-3} K^{-1})	P_{out} (μW cm^{-3})
111 PMN–0.25PT single crystals	SC	1300–1790	961–1100	2.5	100–169
PZT	C	533	1116	2.5	12.9
PMN–0.25PT ceramic	C	746	2100	2.5	13.4
PVDF	P	33	9	1.8	6.12
Nonlinear materials		Q_{ECE} (J cm^{-3})	Applied electric amplitude (kV mm^{-1})	θ_{cold} (°C)	P_{out} (μW cm^{-3})
$0.95PbSc_{0.5}Ta_{0.5}O_3$–$0.05PbSc_{0.5}Sb_{0.5}O_3$	C	4.2	2.5	−5	1570
$0.90Pb(Mg_{1/3}Nb_{2/3})O_3$–$0.10PbTiO_3$ ceramic	C	1.4	3.5	30	500
⟨110⟩ 0.955 $Pb(Zn_{1/3}Nb_{2/3})O_3$–$0.045PbTiO_3$ single crystal	SC	No measure	2	90	750
$0.90Pb(Mg_{1/3}Nb_{2/3})O_3$–$0.10PbTiO_3$ thin film	TF	15	90	75	4320
PZST75/20/5	C	9.8	3	160	2240
$PbZr_{0.95}Ti_{0.05}O_3$ thin film	TF	30	78	220	5960

Table 1.6 Properties of linear and nonlinear pyroelectric materials and the expected output power for an external temperature variation of 20°C peak-peak at 10^{-2} Hz.[75]

From the table above, it is obvious that the harvested energy enhanced greatly for nonlinear pyroelectric material, and the direct pyroelectric energy harvesting (connecting an adapted resistance, for example) is not effective. Therefore, in 2008, Sebald *et al.*[76] investigated pyroelectric energy harvesting using ferroelectric-paraelectric (FE-PA) phase transition in a relaxor ferroelectric ceramic $0.9Pb(Mg_{1/3}Nb_{2/3})O_3$-$0.1PbTiO_3$. Based on Ericsson cycles, the harvested energy reached 186 mJ/cm^3 with 50°C temperature variation and electric field cycle of 3.5 kV/mm. The harvested energy is 100 times higher than using simply the linear pyroelectric effect.

Pervious study on pyroelectric energy harvesting hinted that, in order to improve the energy harvesting ability, ferroelectric transitions may be of great interest due to the locally ultra-high pyroelectric activity. In the framework of energy harvesting over a small temperature variation, use of a ferroelectric-ferroelectric (FE-FE) transition may increase the energy conversion effectiveness. Guyomar et al[77] studied the pyroelectric energy harvesting based on FE-FE transition in ferroelectric single crystals <110> PZN-4.5PT. By applying an electric field, a FE-FE transition was induced, abruptly increasing the polarization. This transition minimizes the supplied energy in comparison with the use of the FE-PA transition and increases polarization variations and consequently the harvested energy. In addition, Sebald et al[78] also investigated the optimization principles of pyroelectric energy conversion. An energy harvesting figure of merit is defined to quantify and check the effectiveness of pyroelectric energy harvesting.

On the theoretical side, Vanderpool et al[79] simulated a prototypical pyroelectric converter using finite element methods. They estimated the pumping power and electrical power, and also analysed the dependent factor of energy efficiency and power density. Later, Nguyen et al[80] designed and tested a pyroelectric energy converter, consisted of a Teflon cylindrical chamber with a piston oscillating vertically and driving a working fluid back and forth between a heat source and a cold heat exchanger. A maximum energy density of 130 mJ/cm^3 was achieved at 0.061 Hz frequency of temperature oscillating between 69.3 and 87.6°C in the Ericsson cycle. Based on the previous work, in 2011, Navid et al[81] tested Ericsson cycle on three different types of P(VDF-TrFE) copolymer samples, namely commercial, purified, and porous films. By successively dipping the films in cold and hot silicone oil baths at 25 and 110°C under 20 and 50 kV/mm, the commercial and purified films produced a maximum energy density of 521 mJ/cm^3 and 426 mJ/cm^3, respectively. The porous films achieved a maximum energy density of 188 mJ/cm^3 between 25 and 100°C and electric field between 20 and 40 kV/mm. Furthermore, they discussed the result in light of recently proposed figures of merit for energy harvesting applications.

Some of the aforementioned papers and patents propose several designs for pyroelectric power generators. However, they provide practically no information about 1) The frequency effect on Ericsson pyroelectric energy conversion. 2) The temperature effect on the phase transition which have great influence on pyroelectric energy conversion. These are very interesting on pyroelectric energy harvesting, and we will resolve them in this dissertation.

1.3.5.2.3 Comparison between pyroelectric and thermoelectric energy harvesting

As stated before, dealing with small-power energy harvesting from heat, it can be achieved using both thermoelectric and pyroelectric effects. In the first case, temperature gradients are necessary, which is just the main difficulty of thermoelectric energy harvesting. In case of pyroelectric energy harvesting, a time varying temperature is necessary. In this part, we aim to compare energy harvesting using pyroelectricity and thermoelectricity.

Previous study on pyroelectric and thermoelectric energy harvesting showed that the overall output power using a linear pyroelectric material may be superior to that of a good thermoelectric material (by a factor of 10)[75]. Furthermore, using nonlinear pyroelectric materials (FE-FE transition) can result in a further gain of 10-100 on the performance. The advantages of pyroelectric energy conversion can be concluded in multi-fold. (1) In order to maximize the temperature gradient, thermoelectric generators need the bulky of sinks which

influence their performance to a great extent. Thus, pyroelectric materials are an alternative because of their ease of use. (2) The another major impediments for thermoelectric energy harvesting is toxicity of the available current thermoelectric materials. Typically, efficient thermoelectric materials contain heavy elements such as lead and tellurium that are toxic and not earth abundant. Many materials with unusual structures containing abundant and benign elements are known, but remain unexplored for thermoelectric applications. However, great progress has been made in creating artificial pyroelectric materials which is lead-free, for example polymers or ceramics with perovskite type structure, compared with thermoelectric materials, pyroelectric materials show more environmentally friendly. (3) Technically, for pyroelectric energy harvesting, the key parameter is the surface heat exchange combined with the heat capacity. On the contrary, thermoelectric energy harvesting requires ensuring the maximum temperature gradient, and this capability depends on the surface heat exchange and heat conductivity. That is to say, in the pyroelectric case, we face the optimization of periodic heat transfer whereas in the thermoelectric case, we face the optimization of the heat flow. Apparently, the latter is more difficult to control in practice[75].

1.4 Objective of this work

This study concerns on thermal energy harvesting using time varying temperature. Two different types of materials were attempted to realize this subject: single crystals and polymer films. Ericsson cycle as an efficiency thermodynamic cycle was carried out in both cases, and consequently made a great contribution to thermal energy harvesting.

For single crystal, we studied energy harvesting based on pyroelectric effect. <110> oriented PZN-4.5PT was chosen as the active pyroelectric element due to its high pyroelectric effect and FE-FE phase transition. The frequency effect was investigated and the inherent mechanism was also discussed from the perspective of domain engineering. We explored the different phase transitions under different electric fields and temperature conditions. In order to find the optimal parameters for pyroelectric energy harvesting (e.g., pyroelectric coefficient at different temperature, maximum electric field, working temperature range etc.), we detected the properties of PZN-4.5PT completely, then designed the asymmetric Ericsson cycle which greatly promoted the harvested energy and became the most effective energy harvesting cycle for this material.

Terpolymer P(VDF-TrFE-CFE) 61.3/29.7/9 mol% is the other research emphasis in this dissertation. Due to the low pyroelectric effect on polymer, we studied the low temperature electrostatic energy harvesting technique adopted nonlinear capacitance variation for thermal energy harvesting. First, we characterized the thermal property and dielectric properties, the electrical tunability of dielectric constant was also investigated at different temperature (25 and 0°C) in order to estimate the harvested energy by simulation. Finally, we carried out the experimental measurement and confirmed the feasibility of this solution for energy harvesting. All this research of thermal energy harvesting is based on Ericsson cycle, which is one of efficiency thermodynamic cycles. The other one – Stirling cycle – is also investigated for simulation.

Chapters 2 mainly states the principle of thermal energy harvesting used in this study, as well as the characterization of ferroelectric phenomena. Chapter 3 looks at the approaches for pyroelectric energy harvesting on single crystal <110> oriented PZN-4.5PT phase transition. Chapter 4 focuses on low temperature electrostatic energy harvesting on P(VDF-TrFE-CFE) 61.3/29.7/9 mol % based on nonlinear capacitance variations.

Chapter 2
Principle of Thermal Energy Harvesting and Characterization of Ferroelectric Phenomena

For the particular application in this dissertation, the initial energy is in the form of thermal energy. Pyroelectric effect and capacitance variation of ferroelectric material, which induced by temperature variation, were used to convert thermal energy into electrical energy.

2.1 Pyroelectric Effect

Before talking about pyroelectric effect, one should first distinguish three basic effects: piezoelectric, pyroelectric and ferroelectric effect. From the perspective of crystal classes as **Fig. 2.1**, of the thirty-two crystal classes, twenty-one groups, which are non-centrosymmetric (not having a centre of symmetry), possess one or more crystallographically unique directions (axes), and of these, twenty exhibit direct piezoelectricity (the 21st is the cubic class 432). The piezoelectric effect is the generation of an electrical charge upon application of mechanical stress. Ten of these represent the polar crystal classes, if the dipole moment can be reversed by the application of an electric field, the material is said to be ferroelectric. The ferroelectric effect is the generation of an electric voltage upon application of electric field. If it shows a spontaneous polarization without mechanical stress due to a non-vanishing electric dipole moment associated with their unit cell, and which exhibit pyroelectricity. The pyroelectric effect relates the generation of an electrical charge upon heating. The structure of crystal comprising cations and anions can be shown according to their polar behaviour in **Fig. 2.2**.

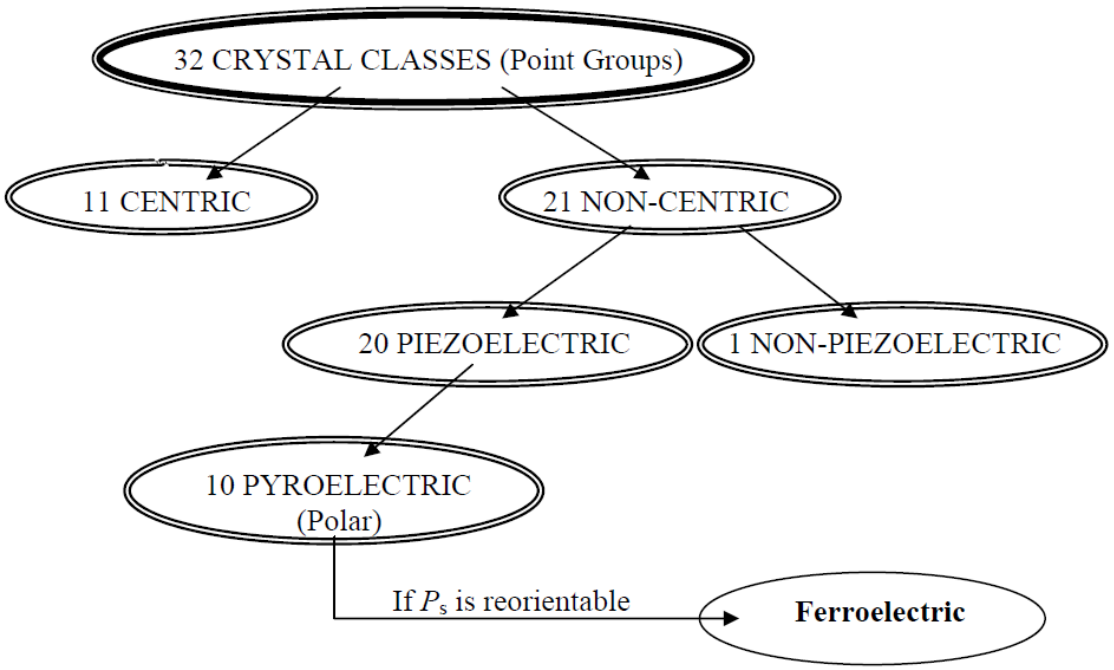

Fig. 2.1 A classification scheme for the 32 crystallographic point groups.

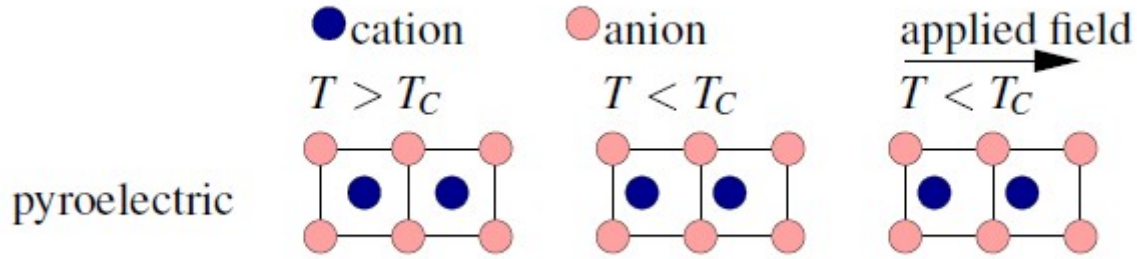

Fig. 2.2 Crystals comprising cations and anions for pyroelectric effect.
(http://www.mrl.ucsb.edu/)

Pyroelectric effect is defined as the temperature dependence of the spontaneous polarization in certain anisotropic solids, and frequently characterized by pyroelectric coefficient for quantification. The pyroelectric coefficient at constant stress σ and electric field E are defined as confining to scalar notations[82].

$$\left(\frac{\partial D}{\partial \theta}\right)_{E,\sigma} = \left(\frac{\partial D}{\partial \theta}\right)_{E,e} + \left(\frac{\partial D}{\partial e}\right)_{E,\theta}\left(\frac{\partial e}{\partial \theta}\right)_{E,\sigma} \tag{2.1}$$

where D, e, and θ represent, respectively, the electric displacement, strain, and temperature of the material. The first term of Eq. 2.1 is called the primary pyroelectric coefficient. The primary pyroelectric effect corresponds to the charges produced owing to the change in polarization with temperature when the dimensions of the pyroelectric material are fixed. For a material under constant stress, its dimensisons change with temperature due to

thermal expansion resulting in an additional contribution of piezoelectrically induced charge. This leads to the secondary pyroelectric effect which is defined as the final term of Eq. 2.1.

Measuring the primary effect directly is extremely difficult. But the secondary effect can be readily calculated from the values of the thermal expansion coefficient, the elastic stiffness, and the piezoelectric strain constant. **Table 2.1** lists the primary, secondary, and total pyroelectric coefficients of several materials for comparison[83]. Moreover, it shows a division between ferroelectric and nonferroelectric materials. In general, ferroelectric materials have larger pyroelectric coefficients than nonferroelectrics and are of greater interest for applications.

Material	Pimary Coefficient	Secondary Coefficient	Total Coefficient
Ferroelectrics			
Poled Ceramic			
$BaTiO_3$	-260	+60	-200
$PbZr_{0.95}Ti_{0.05}O_3$	-305.7	+37.7	-268
Crystal			
$LiNbO_3$	-95.8	+12.8	-83
$LiTaO_3$	-175	-1	-176
$Pb_5Ge_3O_{11}$	-110.5	+15.5	-95
$Ba_2NaNb_5O_{15}$	-141.7	+41.7	-100
$Sr_{0.5}Ba_{0.5}Nb_2O_6$	-502	-48	-550
$(CH_2CF_2)_n$	-14	-13	-27
Triglycine sulfat	+60	-330	-270
Nonferroelectrics			
Crystal			
CdSe	-2.94	-0.56	-3.5
CdS	-3.0	-1.0	-4.0
ZnO	-6.9	-2.5	-9.4
Tourmaline	-0.48	-3.52	-4.0
$Li_2SO_4.2H_2O$	+60.2	+26.1	+86.3

Table 2.1 Primary, secondary , and total pyroelectric coefficients of various materials.

Pyroelectric materials possess a so-called spontaneous polarization P_s, the spontaneous polarization presents strong temperature dependence due to the material's crystallographic structure[83]. Upon heating, P_s diminishes and becomes zero at the critical temperature of the ferroelectric—paraelectric phase transition. From the microscopic view to explain it, the displacement of the atoms from their equilibrium positions upon heating and cooling results in the pyroelectric effect. Imagine that conductive electrodes are then attached to the surfaces and connected through an current amplifier having a low internal resistance as shown in **Fig. 2.3**[83]. In most single crystals and ceramics, an increase in temperature causes the net dipole

moment and, consequently, the spontaneous polarization to decrease. The quantity of bound charge then decreases, and the redistribution of free charges to compensate for the change in bound charge results in a current flow—the pyroelectric current—in the circuit.

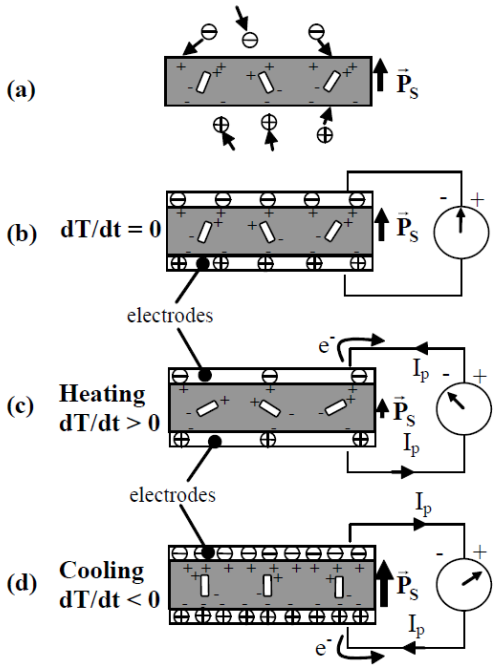

Fig. 2.3 Model of pyroelectric effect.[83]

Due to the material's spontaneous polarization, free charges accumulate at the surface of the material [**Fig. 2.3**(a)]. At steady-state ($d\theta/dt = 0$), the spontaneous polarization is constant, and no current is flowing as illustrated in **Fig. 2.3** (b). However, a rise in temperature ($d\theta/dt > 0$) reduces the spontaneous polarization through reduction in the dipole moment [**Fig. 2.3**(c)]. This results in a decrease in the quantity of bound charges at the electrodes, and the subsequent redistribution of charges results in current flowing through the external circuit. If the sample is cooled, the spontaneous polarization increases, and the current sign reverses as illustrated in **Fig. 2.3**(d).

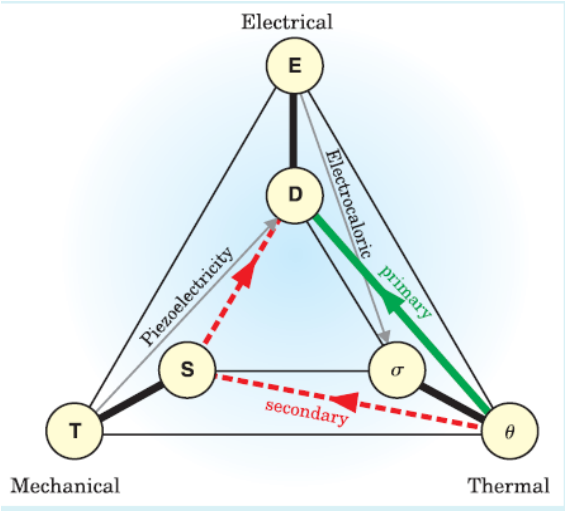

Fig. 2.4 Thermodynamically reversible interactions that may occur among the thermal, mechanical, and electrical properties of a crystal.[83]

Fig. 2.4 illustrates the thermodynamically reversible interactions that may occur among the thermal, mechanical, and electrical properties of a crystal[83]; magnetic properties are ignored for simplicity. The lines joining pairs of circles signify that a small change in one of the variables produces a corresponding change in the other. The three short bold lines that connect pairs of thermal, elastic, and electric variables define the physical properties of heat capacity, elasticity, and electrical permittivity, respectively[83]. The diagram also illustrates coupled effects, denoted by lines joining pairs of circles at different corners of the diagram.

Pyroelectricity is a coupled effect that relates a change in temperature to a change in electrical displacement D (with units of C/m^2),

$$dD = pd\theta \tag{2.2}$$

where p is the pyroelectric coefficient (with units of $C/m^2.K$). Both displacement and the pyroelectric coefficient are vectors or first-rank tensors. The pyroelectric coefficient is defined by

$$p = (\partial P_s / \partial \theta)_{\sigma,E,} \tag{2.3}$$

where the constraints are constant electric field E, and constant elastic stress σ.

The diagram's colored lines indicate that the two contributions make up pyroelectric effect. In the first, the crystal is rigidly clamped under constant strain S, to prevent expansion or contraction. A change in temperature causes a change in electric displacement as shown by the green line, which signifies the primary pyroelectric effect. The second contribution— the secondary pyroelectric effect—is a result of crystal deformation: Thermal expansion causes a strain that alters the electric displacement via a piezoelectric process, as shown by the dashed red lines.

2.2 Electrocaloric Effect

When talking about pyroelectric effect, it is inevitable to involve its reverse effect -- electrocaloric effect (ECE). It is a coupling between electrical and thermal properties of dielectrics wherein change in temperature occurs under adiabatic conditions in response to an applied electric field. When an electric field is applied to a dielectric material, it will induce a change in the material's polarization. The consequent changes in the entropy and temperature of the material are referred to as the electrocaloric effect. In the case of ferroelectric materials ECE is strongly correlated with the pyroelectric effect. Indeed the electrocaloric and pyroelectric effect may be seen as direct and inverse electrothermal conversion as for the electromechanical conversion. The large polarization change is the requirement of a large entropy change, this requirements make it advantageous to use ferroelectric material for the ECE. The ECE occurs in both ferroelectric and paraelectric phases, and is found to be larger in the paraelectric phase just above the ferroelectric--paraelectric phase transition[84]. In the vicinity of a transition, e.g., ordering-disordering transition, electrocaloric effect is greatly enhanced[85].

2.3 Modeling of Pyroelectric Energy Harvesting

When talking about energy harvesting from heat, we need first to establish the equations of pyroelectric materials[78]. It is assumed here idealized pyroelectric materials exhibiting no losses and purely linear properties.

$$dD = \varepsilon_{33}^{\theta} dE + p d\theta \tag{2.4}$$

$$d\Gamma = pdE + c_E \frac{d\theta}{\theta} \tag{2.5}$$

where D, E, θ, and Γ are electric displacement, electric field, temperature, and entropy, repectively. The coefficients are defined as:

$$\varepsilon_{33}^{\theta} = (\frac{dD}{dE})_{\theta}, p = \frac{dD}{d\theta} = \frac{d\Gamma}{dE}, c_E = (\frac{dU}{d\theta})_E \tag{2.6}$$

where U is the internal energy. $\varepsilon^{\theta}_{33}$, p, c_E, are the dielectric permittivity, pyroelectric coefficient and calorific capacity, respectively.

Analogying to electromechanical case in the work of Lefeuvre[86], the harvested power[87] in the pyroelectric case can be defined as

$$P_{\max} = \frac{p^2\theta^2}{2\pi\varepsilon_{33}^{\theta}} f \tag{2.7}$$

where f is the frequency. As a consequence, the harvesting energy for a cycle per unit of volume is given by

$$W_{\max} = \frac{p^2\theta^2}{2\pi\varepsilon_{33}^{\theta}} \tag{2.8}$$

For Eq. (2.6) the figure of merit for energy harvesting is

$$FOM = \frac{p^2}{\varepsilon_{33}^{\theta}} \tag{2.9}$$

From Eq. (2.9), pyroelectric properties of materials are one of the most significant factors of harvested energy. **Table 2.2** shows the pyroelectric properties of some common pyroelectric materials[78]. Here, the derivation and parameters are hypothesized under 'Ideal' linear pyroelectric effect, the pyroelectric coefficient and dielectric permittivity is constant as in **Table 2.2**, however, in practical energy harvesting experiment, the pyroelectric material is under external electric field, the pyroelectric coefficient and dielectric permittivity are variables, the detailed dependent relationship would be discussed in the following chapters.

Coefficient Unit	p $\mu C \cdot m^{-2} \cdot K^{-1}$	$\varepsilon_{33}^{\theta}$ ε_0	$c_E(\times 10^6)$ $J \cdot m^{-3} \cdot K^{-1}$	$-p/\varepsilon_{33}^{\theta}(\times 10^3)$ $V \cdot m^{-1} \cdot K^{-1}$
	PZN-PT and PMN-PT single crystals			
111 PMN-0,25PT	1790	961	2.5	210
110 PMN-0.25PT	1187	2500	2.5	54
001 PMN-0.25PT	603	3000	2.5	23
001 PMN-0,33PT	568	5820	2.5	11
011 PMN-0,33PT	883	2940	2.5	34
111 PMN-0,33PT	979	650	2.5	170
001 PMN-0,28PT	550	5750	2.5	11
011 PMN-0,28PT	926	2680	2.5	39
111 PMN-0,28PT	1071	660	2.5	183
001 PZN-0,08PT	520	3820	2.5	15
011 PZN-0,08PT	744	1280	2.5	66
111 PZN-0,08PT	800	950	2.5	95
	Bulk ceramics			
PZT	533	1116	2.5	54
PMN-0.25PT ceramic	746	2100	2.5	40
$(BaSrCa)O_3$	4000	16000	2.5	28
PLZT 0.5/53/47	360	854	2.5	48
PLZT 8/53/47	97	238	2.5	46
PLZT 14/53/47	19	296	2.5	7
	Thin films			
(PZT)/PZT composite	180	1200	2.5	17
$PbCaTiO_3$	220	253	2.5	98
PZT 700 nm	211	372	2.5	64
PMZT 700 nm	352	255	2.5	156
	Polymers and composites			
PVDF	33	9	1.8	314
PZT/P(VDF-TrFE) 50%	33.1	69.2	2	54
PZT/PVCD-HFP 50/50 vol%	450	85	2	598
PZT0.3/PU0.7 vol%	90	23	2	442

Table 2.2 Pyroelectric properties for different class of materials.[78]

2.4 Temperature Effect on Capacitance (Dielectric Constant) in Ferroelectric Materials

The previous report proposed an electrostatic energy-harvesting method using a variable capacitor[34]. Although the variable capacitor is realized by the electrostatic force through the ambient mechanical vibration, it still informs us that once we search the material with a temperature varying capacitance, why do not use it to harvest energy from temperature variation by electrostatic technique?

The dielectric constant is strongly dependent on structure of the material, thus how dielectric constant behaves with the temperature variation? It should also be considered from the perspective of molecular motion. The molecules in a structure always possess some energy and this induces stochastic thermal motion. Under equilibrium state, there is as much random motion in any one direction as in the opposite direction, consequently the average positions of molecules remain constant. As we all known that, if an electric field is applied to a polar material, the dipole will rotate to align with the electric field. However, due to thermal motion, not all the dipoles are perfectly aligned with the field. As a result of the temperature dependence of thermal motion, the dielectric constant also varies with temperature variation.

With the rise of the temperature, the thermal motion becomes intenser, the dielectric constant (capacitance) of the ferroelectric material goes down. However, this does not mean that the dielectric constant will increase continually as temperature is lowered, there are several discontinuities in the dielectric constant as temperature changes. Such as at phases transition temperature or below the freezing point.

In order to harvest energy from temperature variations, capacitance variation of materials provides a novel method. In this case, capacitance variation is the key parameter for electrostatic energy harvesting. To our best knowledge, this purpose can be accomplished with any charged capacitor in which the permittivity of the dielectric varies with temperature. This follows readily from the relation for the charge.

$$Q=C_r(\theta)V \tag{2.10}$$

A decrease in permittivity with varying temperature will decrease the capacitance C_r which in turn requires a rise in voltage V as long as the charge Q is held. The voltage rise is proportional to an energy rise because the electrical energy W is given by

$$W=1/2\ (QV) \tag{2.11}$$

This is just a sketch of energy harvesting by capacitance variation, the detailed study would be discussed in chapter 4.

2.5 Thermodynamic Cycles of Thermal Energy Harvesting

In the case of pyroelectric energy conversion, a Carnot cycle is not realistic because it is difficult to control successive adiabatic and isothermal conditions, and one needs excessive electric field paths and two isothermal paths. As a consequence, other cycles have to be

considered in our study, such as the Stirling cycle or Ericsson cycle, which were confirmed to be more efficiency.

2.5.1 Ericsson Cycle (Olsen Cycle)

The so-called Ericsson cycle is the electric analog of the Ericsson heat engine in the charge-voltage diagram (q-V). Energy conversion using Ericsson cycle (also called Olsen cycle) is achieved by alternatively placing an active material sandwiched between two electrodes in contact with a cold and hot source, respectively at low temperature and high temperature. For the Ericsson cycle, two isothermal and two constant electric field processes are necessary. The constant electric field path is associated with electric induction variations due to the temperature variation. To clarify the Ericsson cycle principle, electric and thermodynamic energy are determined for each segment of the cycle depicted in **Fig. 2.5** (**Table 2.3**)[76]. These curves were obtained with non-realistic coefficients for the sake of clarity.

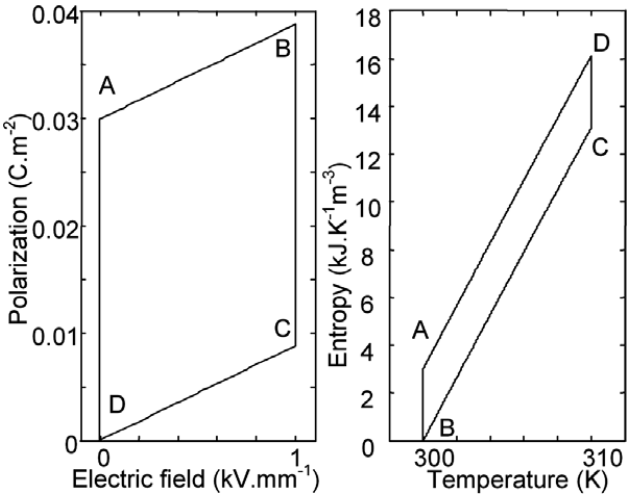

Fig. 2.5 Scheme of Ericsson cycle principle.[76]
Left: polarization–electric field plot. Right: corresponding entropy–temperature plot
Note: Here, $\varepsilon^{\theta}_{33} = 1000\varepsilon_0$, $p = 3000\ \mu$C m^{-2} K^{-1}, $c = 0.4 \times 10$ J m^{-3} K^{-1}.

Path	AB	BC	CD	DA
Electric induction	$\delta D_{AB} = \int_0^{E_M} \varepsilon_{33}^{\theta_1}\,\mathrm{d}E$	$\delta D_{BC} = \int_{\theta_1}^{\theta_2} p^{E_M}\mathrm{d}\theta$	$\delta D_{CD} = \int_{E_M}^{0} \varepsilon_{33}^{\theta_2}\,\mathrm{d}E$	$\delta D_{DA} = \int_{\theta_2}^{\theta_1} p^{0}\,\mathrm{d}\theta$
Entropy	$\delta \Gamma_{AB} = \int_0^{E_M} p^{\theta_1}\,\mathrm{d}E$	$\delta \Gamma_{BC} = \int_{\theta_1}^{\theta_2} c^{E_M}\frac{\mathrm{d}\theta}{\theta}$	$\delta \Gamma_{CD} = \int_{E_M}^{0} p^{\theta_2}\,\mathrm{d}E$	$\delta \Gamma_{DA} = \int_{\theta_2}^{\theta_1} c^{0}\frac{\mathrm{d}\theta}{\theta}$
Electric energy	$\delta W_{AB} = \int_0^{E_M} \varepsilon_{33}^{\theta_1} E\,\mathrm{d}E$	$\delta W_{BC} = E_M \int_{\theta_1}^{\theta_2} p^{E_M}\mathrm{d}\theta$	$\delta W_{CD} = \int_{E_M}^{0} \varepsilon_{33}^{\theta_2} E\,\mathrm{d}E$	$\delta W_{DA} = E_M \int_{\theta_2}^{\theta_1} p^{0}\,\mathrm{d}\theta$
Heat	$\delta Q_{AB} = \theta_1 \int_0^{E_M} p^{\theta_1}\,\mathrm{d}E$	$\delta Q_{BC} = \int_{\theta_1}^{\theta_2} c^{E_M}\mathrm{d}\theta$	$\delta Q_{CD} = \theta_2 \int_{E_M}^{0} p^{\theta_2}\,\mathrm{d}E$	$\delta Q_{DA} = \int_{\theta_2}^{\theta_1} c^{0}\,\mathrm{d}\theta$

Table 2.3 Electric and thermal quantities, and energies related to Ericsson cycles.[76]

As it can be seen in **Fig. 2.5**, the Ericsson cycle starts at temperature θ_1, applying the electric field E_1, the polarization subsequently increases to P_1 value (AB path). The temperature is changed to θ_2 (BC path), the polarization of the ferroelectric material decreases to P_2. Decreasing the applied electric field from E_1 to 0, the polarization also decreases to P_3(CD path), the temperature is finally come back to its initial value (DA path). In the case of the material with linear behavior, the polarization returns to its initial value, whereas for nonlinear materials, hysteresis polarization can be observed. In contrast to ceramics, a single crystal recovers nearly all of its initial polarization if the Curie temperature is not crossed.

During an Ericsson cycle, the sum of heat and sum of electrical energy are the same since the initial state and final state are the same (the internal energy is a state function). As a consequence, assuming that the pyroelectric coefficient is constant in the working temperature range, and assuming that the calorific capacity does not depend on the electric field, we can write

$$\delta W_{cycle} = -(\theta_2 - \theta_1)\int_0^{E_M} p dE \tag{2.12}$$

The energy taken from the hot temperature medium is

$$Q_{hot} = c(\theta_2 - \theta_1) + \int_0^{E_M} p\theta_2 dE \tag{2.13}$$

As a consequence, the conversion ratio defined as the net electric work on energy taken from hot temperature medium can be expressed as

$$\eta = \frac{|W_{cycle}|}{Q_{hot}} = \frac{\int_0^{E_M} p\theta_2 dE}{c + \frac{\theta_2}{\theta_2 - \theta_1}\int_0^{E_M} p dE} \tag{2.14}$$

Compared to the Carnot cycle conversion ratio

$$\eta_{carnot} = \frac{\theta_2 - \theta_1}{\theta_2} \tag{2.15}$$

We obtain

$$-\frac{\eta}{\eta_{carnot}} = \frac{\int_0^{E_M} p\theta_2 dE}{c(\theta_2 - \theta_1) + \int_0^{E_M} p\theta_2 dE} = \frac{1}{\frac{c(\theta_2 - \theta_1)}{\int_0^{E_M} p\theta_2 dE} + 1} \tag{2.16}$$

The conversion ratio compared to the Carnot conversion ratio decreases with the temperature difference.

2.5.2 Stirling Cycle

The Stirling cycle consists of two isothermal and two constant electric induction processes[88]. The isothermal process corresponds to electric field variations. The constant electric induction process corresponds to temperature variations, and voltage variations are due to the pyroelectric effect or dielectric permittivity variation of the ferroelectric materials. On a polarization versus electric field (P-E) diagram **Fig. 2.6**, the energy exchanged during the cycle is equal to the area of this cycle. For energy harvesting, the cycle must follow a clockwise closed path[77].

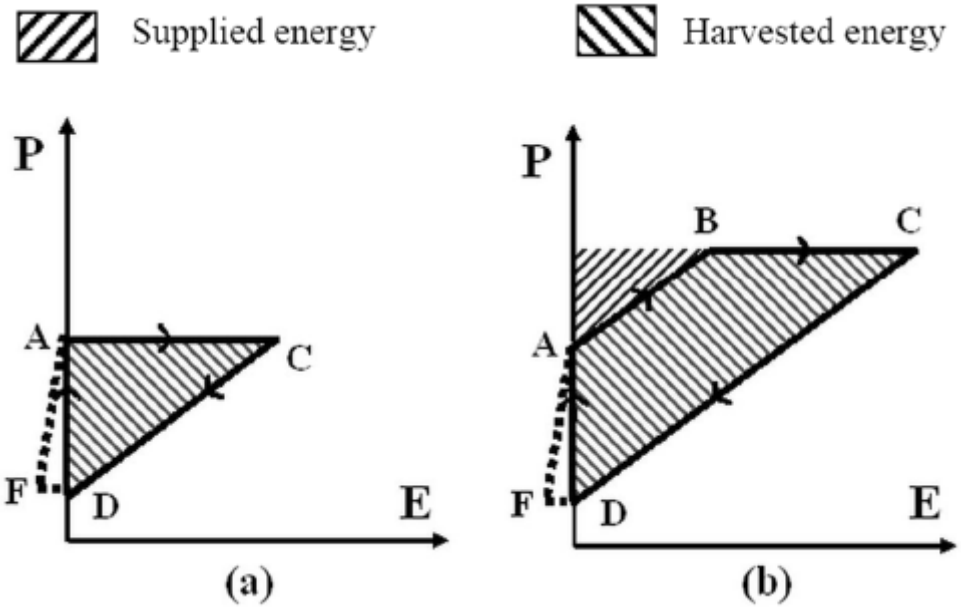

Fig. 2.6 Scheme of Stirling cycle.
(a) Stirling cycle with no starting electric field (b) Stirling cycle.[77]

The Stirling cycle may be described as follows, see **Fig. 2.6**, after increasing the electric field at θ_1 (AB path), the single crystal is open-circuited, cutting off the voltage applied to the sample at point B. The temperature is changed to the θ_2 value. The polarization of the specimen remains constant, and its voltage increases to the E_2 value (BC path). The sample is discharged isothermally by short-circuiting it (CD path). To close the Stirling cycle, the DA path is a constant electric field process[77]. Technically, the constant polarization process corresponds to the DF path. Experimentally, due to the small harvested energy in the DFA part of the cycle, as the temperature is come back to its initial value, the sample remains short-circuited. The paths are expressed in **Table 2.4**[77].

	Stirling cycle
AB and CD paths	$P = \int \varepsilon(E, \theta = \text{cste}) dE$
BC path	$E = -\int \frac{p(E,\theta)}{\varepsilon(E,\theta)} d\theta$
DA path	
DF path	$E = -\int \frac{p(E,\theta)}{\varepsilon(E,\theta)} d\theta$
FA path	$P = \int \varepsilon(E, \theta = \text{cste}) dE$

Table 2.4 Thermodynamic equations of the Stirling cycle.

2.6 Ferroelectric Materials Background

The following part provides overview and characterization on ferroelectrics utilized during this project.

2.6.1 Ferroelectric Phase and Curie Temperature

Most ferroelectric materials undergo a structural phase transition from a paraelectric phase above the Curie temperature (θ_c) into a ferroelectric phase of lower crystal symmetry below the Curie temperature. The phase transformation from paraelectric to ferroelectric results in a local domain structure with zero net polarization. Slight changes in the composition near the morphotropic phase boundary can change the crystal structure into tetragonal, monoclinic, orthorhombic or rhombohedral phase. It is generally believed that the ferroelectric structure of a crystal is created by a small distortion of the paraelectric structure such that the lattice symmetry in the ferroelectric phase is always lower than that in the paraelectric phase[89]. The temperature dependence of the dielectric constant above the Curie point ($\theta > \theta_0$) in most ferroelectric crystals is governed by the Curie-Weiss law:

$$\varepsilon = \varepsilon_0 + \frac{C}{(\theta - \theta_0)} \tag{2.17}$$

where ε is the permittivity of the material, ε_0 is the permittivity of the vacuum, C is the Curie-Weiss constant and θ_0 is the Curie-Weiss temperature. The Curie-Weiss temperature θ_0 is, in general, different from the Curie point θ_c. In a first-order ferroelectric-paraelectric phase transition, P_s has a substantial value at temperatures very close to θ_c, and undergoes a

paraelectric phase in discontinuous transition, whereas in a second-order phase transition, the decrease in P_s as θ approaches θ_c is more gradual.

2.6.2 Polarization Reversal and Hysteresis Loop

A ferroelectric crystal, as grown, has multiple domains. A single domain can be obtained by domain wall motion made possible by the application of an appropriate electric field. A very strong field could lead to the reversal of the polarization in the domain, known as polarization (or domain) reversal[89]. In a normal dielectric, the polarization, or electric displacement, vanishes when the electric field returns to zero. In a ferroelectric material, there is a spontaneous polarization (an electric displacement) which is inherent to the crystal structure of the material and does not disappear in the absence of the electric field.

An additional property of ferroelectric materials is the double-valued nature of their response to an electrical excitation, resulting in a hysteretic behaviour. In ferroelectrics, when an electric field via a voltage is applied, polarization increases. Upon removal of the voltage, the polarization decreases but does not return to zero. The result is a remnant polarization P_r. If the voltage is swept up and down, the result will be what is known as a hysteresis loop, as shown in **Fig. 2.7**[89].

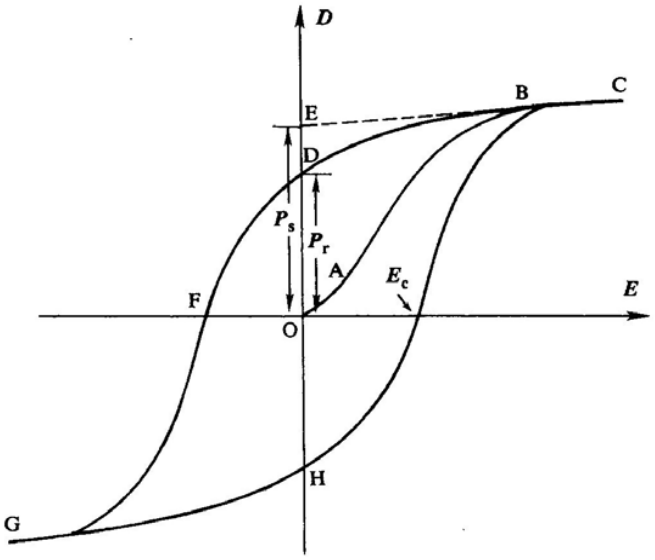

Fig. 2.7 A typical hysteresis loop in ferroelectrics.

The observation of hysteresis loops is still frequently used for the identification of ferroelectrics. In the P-E loop, the coercive field E_c, represents the magnitude of the field required to cancel out the remnant polarization, it depends not only on temperature, but also on the measuring frequency. The extrapolation of the linear segment BC of the hysteresis loop back to the polarization axis (CBE) represents the value of the spontaneous polarization (P_s),

in the case of an appropriately oriented, fully poled crystal. The area within the loop is a measure of the energy required to twice reverse the polarization.

Hysteresis occurs in ferroelectric materials because some of the dipole molecules or molecular groups are displaced in an inelastic manner when an electric field is applied. These dipoles keep their new alignments, even after the removal of the electric field. When an electric field is re-applied, they re-align themselves based on the magnitude and rate at which the external electric field changes, their previous orientation, and their degree of freedom. The occurrence of these inelastic dipoles makes ferroelectric polarization much larger than the polarization in normal dielectrics.

A dielectric material exhibits pyroelectric behavior if its polarization is a function of temperature under a null electric field. As the temperature of the material increases, the polarization of the material decreases, thus causing the electric displacement decreases. When the electric displacement decreases, some of the electric charge is forced off of the surface of the material, and can thus be captured by an external device. Additionally, very small amounts of charge may travel through the material without damaging it, i.e., without breakdown occurring; this is referred to leakage. Non-linear dielectric materials may have a much more complex dependence of the electric displacement on the temperature and electric field. In general, the amplitude of the electric displacement and the size of the hysteresis region decrease with increasing temperature.

2.6.3 Domain Engineering of PZN-PT Relaxor Ferroelectric Single Crystal

Rhombohedral phase relaxor ferroelectric single crystals, e.g., PZN-xPT, $0<x<0.1$, which are poled along <110> or <001> direction, could exhibit extraordinary dielectric and electromechanical properties. This is associated with “engineered domain states” formed within the crystals.

Ferroelectrics may exhibit one or more ferroelectric (polar) phases that show a domain structure. In most cases, the spontaneous polarization in a ferroelectric crystal is not uniformly distributed through out the whole crystal, but rather forms small regions, called domains. These domains in a crystal are separated by interfaces called domain walls. The spontaneous polarization is discontinuous across the domain wall. The origin of the ferroelectric domain can be explained from the energy viewpoint, the polydomain system may be in the state of minimum energy balanced from both electric and mechanical contributions. The polarization direction of each domain is determined by the crystal symmetry of the

ferroelectric crystal. The process of applying an electric field, which exceeds a certain field to orient the domains toward the field direction, is termed as poling. The physical properties of ferroelectric crystals are related to their phase states and domain structure, which change with composition, orientation, temperature, and applied fields.

"Domain engineering" refers to the processes and techniques used to form stable multi-domain states so that the crystals exhibit enhanced ferroelectric performance. These processes and techniques include cutting and poling the ferroelectric single crystals along certain crystallographic directions to form the expected multi-domain states, controlling the material compositions and temperature so that the crystals stay in certain structural phases, and controlling the applied stress and electric field in order to stabilize the preferred multi-domain states. The benefits of an engineered domain state are larger or tunable piezoelectric coefficients, reduced domain wall motion and hysteresis[90].

Relaxor PZN-xPT single crystals have the perovskite type structure. This structure shows a high temperature cubic phase, which is centrosymmetric and therefore is paraelectric. It becomes ferroelectric after undergoing a structure phase transition in the following order: tetragonal, orthorhombic and rhombohegral. Another characteristic feature of this relxor-based ferroelectric crystals is their complex domain structure. External loading causes polarization reorientation among multiple possible poling directions. This is the evolution process of crystal variant volume fractions. There are 90°/180° domain walls and polarization reorientations possible in the tetragonal phase, 70.5°/109.5°/180° domain walls and reorientations in the rhombohedral phase, and 60°/90°/120°/180° domain walls and reorientations in the orthorhombic phase. Banded and apparent crossing domain patterns are usually formed in the single crystals. Different domain structures observed in <111>, <001>, and <110> poled PZN-4.5PT single crystals are shown in **Fig. 2.8**[90] for comparison. Multi-domain structure as well as multi-phase coexistence around the morphotropic phase boundary (MPB) make major contributions to the enhanced electromechanical properties of relaxor single crystals.

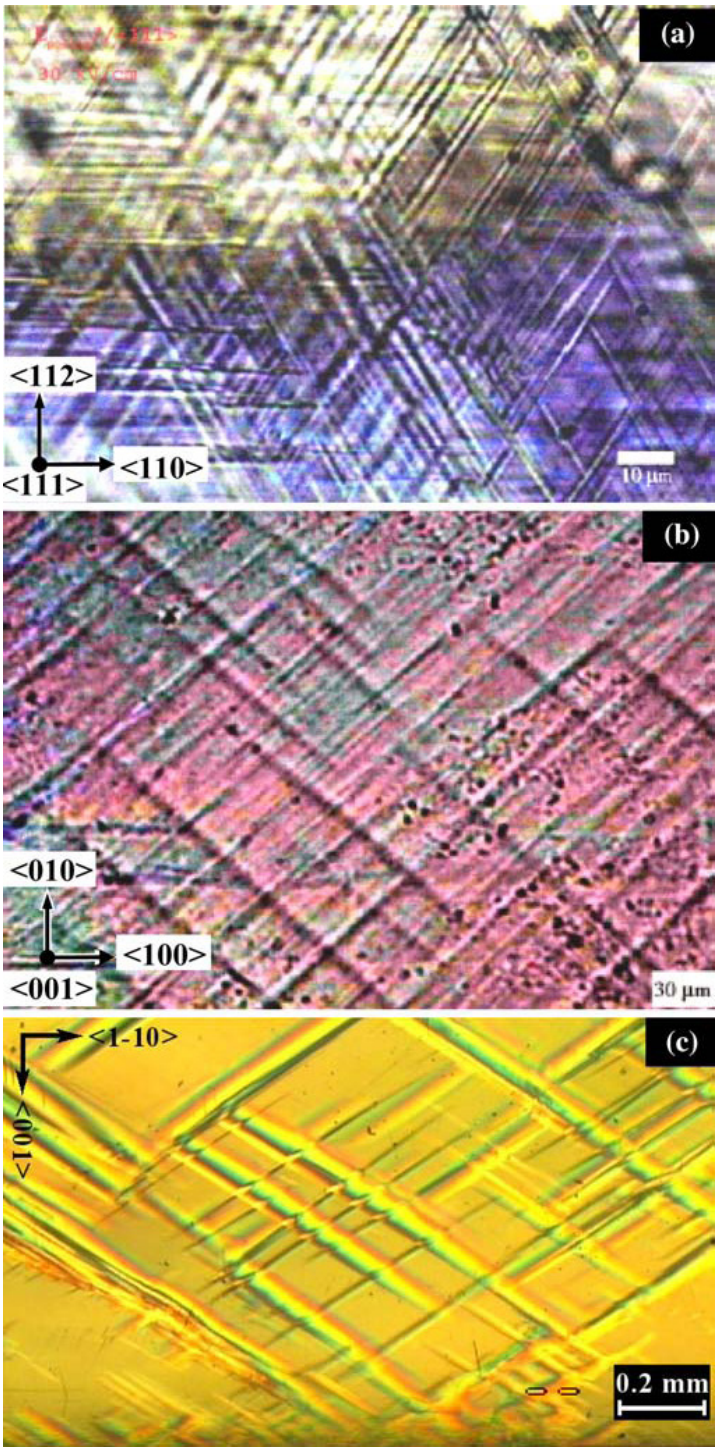

Fig. 2.8 Domain patterns observed in PZN-4.5PT single crystals under polarizing microcope. a <111> poled, b <001> poled , c <110> poled.[90]

Chapter 3
Thermal Energy Harvesting from $Pb(Zn_{1/3}Nb_{2/3})_{0.955}Ti_{0.045}O_3$ Single Crystals Phase Transitions

As previously reviewed in Chapter 2, the principle and modeling of pyroelectric energy converters have been investigated past[66,76,78], however, to the best of our knowledge, the optimization of experimental parameters is the bottle neck for further enhancement of pyroelectric converted energy, e.g., frequency effect and phase transition of ferroelectric materials. The factors which influence significantly the thermal energy harvesting by pyroelectric effect, have not been investigated.

This chapter devotes to study the influence of frequency and phase transition on thermal energy harvesting using pyroelectric effect, $Pb(Zn_{1/3}Nb_{2/3})_{0.955}Ti_{0.045}O_3$ (PZN-4.5PT) was chosen as the active material. In the first part, we introduce the basic characterization of relaxor single crystal, especially the phase transition at different temperature stage. Then, the high-temperature flux technique is presented for growing the high-quality PZN-4.5PT single crystal. XRD and weak field permittivity property are characterized in order to detect the crystal structure and phase transition temperature. The second part concentrates on the thermal electric energy harvesting on PZN-4.5PT single crystal under different frequency and temperature range between 100 and 130°C. Ericsson cycle is the basic thermodynamic cycle, and FE-FE phase transition is used during the cycle, e.g., R-O and O-T. The inherent mechanism of the frequency effect is also discussed in detail. Based on this research, we

developed the asymmetric Ericsson cycles which corresponds to the most effective energy harvesting cycle for this material.

3.1 Introduction

As stated in previous chapters, a majority of innovative solutions for harvesting energy arise from vibration[14,42-43,86], while very few address the possibility of energy harvesting from temperature fluctuations. The thermal energy can come from many different sources, such as ambient temperature, human body, solar energy and the other systems with time varying temperatures. Time varying temperature may also be obtained from heat reservoirs with alternative pumping fluid. Because large amounts of low grade heat are emitted from various industrials and wasted into the environment, the need and opportunity exist for converting waste heat into high-value electricity[91]. The energy harvested with a thermodynamic cycle using temperature variations is important but the 'frequency' (corresponding to the slope of the applied electric field during charging and discharging processes, same below) of the cycle being low (0.1 – 10 Hz in comparison to some hundreds of hertz for vibration), the conversion system must be efficient.

When considering energy converted from heat, it is necessary to differentiate between thermoelectric and pyroelectric energy conversion. For thermoelectric energy conversion based on temperature gradients, which leads to heat flow through the thermoelectric generator, a small fraction of the heat flow is converted into electrical energy. This technology has been practically used in wide range of areas[92]. However, in certain cases, thermal energy is difficult to transform into a stable temperature gradient. In a microgenerator, for instance, temperature differentials across a chip are typically low. In contrast, pyroelectric materials do not require temperature gradients since they can generate electric charges under temperature variations. This property has been widely used both on earth and in space, e.g., for IR detectors[93-94].

In the present case, cycles that are degraded as compared to the Carnot cycle have been used to harvest energy. These are either the Stirling cycle (with two constant electric induction paths and two isothermal paths) or the Ericsson cycle (with two constant electric field paths and two isothermal paths)[66-67,95]. The Stirling cycle is more interesting for low electric fields under the condition of the same injected energy, whereas for high electric fields, both cycles give almost the same harvested energy, but the Ericsson cycle is preferred due to the possibility of controlling the electric field withstood by the sample[77].

Previous studies on pyroelectric and electrocaloric effect[87], and energy harvesting through a pyroelectric effect[77,96] on single crystals have been performed, and it has been suggested that the pyroelectric effect increases near a phase transition. It has also been observed that the electrocaloric effect (a converse effect to its pyroelectric counterpart) became improved in the vicinity of a structural transition[97-99]. Materials with elevated pyroelectric effects or those displaying phase transitions can be used for energy harvesting, since a phase transition always enhances the polarization variations, thus improving the energy harvesting efficiency. Proper material plays important role on pyroelectric energy harvesting.

3.2 Materials Consideration

3.2.1 Brief Description of Relaxor Ferroelectric Single Crystals

In recent years, relaxor ferroelectric single crystals with complex perovskite structure have emerged as a group of promising materials for various applications. So-called "domain engineered" crystals exhibit extraordinarily large properties in one direction compared to the others. With the new explorations in these relaxor based single crystals, understanding the nature of polarization switching may be helpful to the study of energy harvesting on relaxor single crystal.

Relaxor ferroelectrics, which have extraordinarily high dielectric constants, can be distinguished from normal ferroelectrics by the presence of a broad, diffused, and dispersive phase transition on cooling over the so called Curie maximum, θ_c, at which the dielectric permittivity shows a maximum. Relaxor behavior appears due to the existence of a lattice disorder and polar nanodomains at a temperature much higher than θ_c.

Due to the frequency effect of the ferroelectric properties of relaxors, the Curie maximum shifts to higher temperatures with increasing frequency. Also, the maximum of the dielectric constant and dielectric loss do not coincide at the same temperature (**Fig. 3.1**)[100]. The dielectric constant maximum does not characterize the exact paraelectric to ferroelectric phase transition as in normal ferroelectrics. For ferroelectrics which have a diffuse phase transition, for example relaxors, the remnant polarization, P_r, gradually decreases to zero on increasing the temperature towards θ_c [101-102].

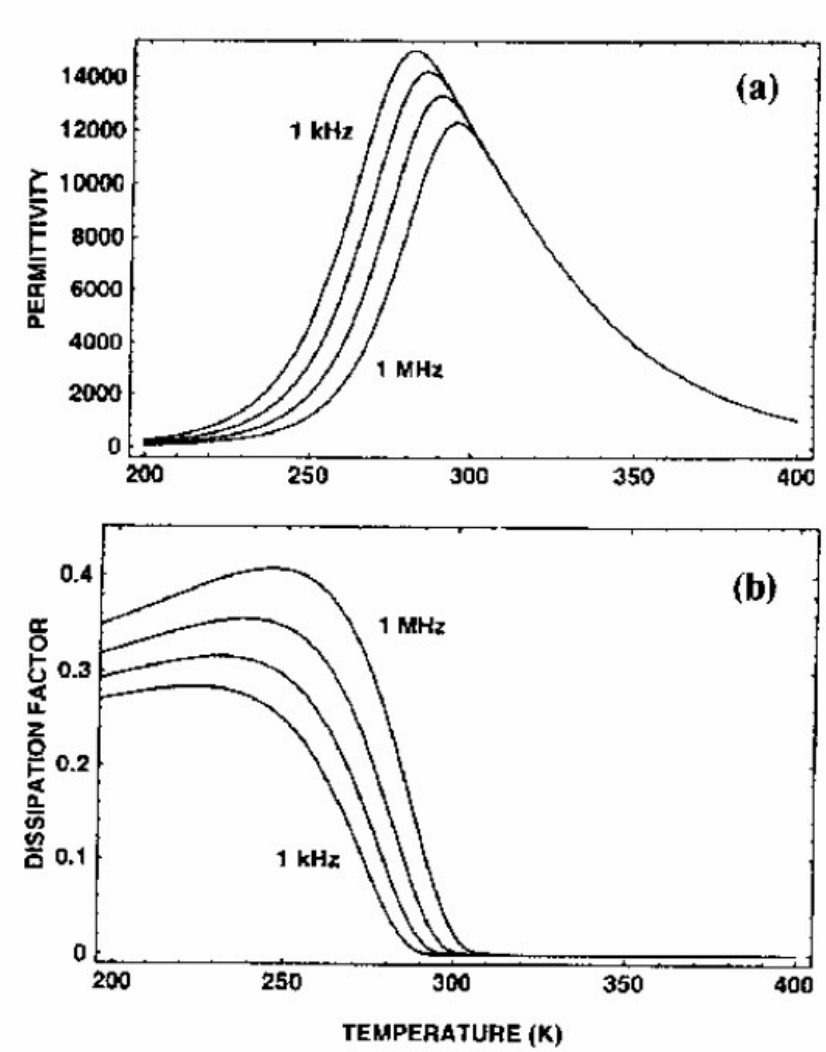

Fig. 3.1 Variation of the dielectric properties of a relaxor ferroelectric PMN single crystal with temperature at frequencies of 1, 10, 100 kHz and 1 MHz.
(a) dielectric permittivity, and (b) dissipation factor.[100]

With decreasing temperature, the number of polar regions increases, so that the regions are in contact and grow; however, since these regions are randomly oriented along different polarization directions, the crystal still appears isotropic. Larger and more stable macropolar regions will be formed at still lower temperatures. **Fig. 3.2** gives the schematic description of Micro- to Macro-domain transition in relaxor ferroelectrics[103]. In the absence of external field, the domain structure of relaxor ferroelectrics contains randomly oriented micropolar regions (**Fig. 3.2** (a)), applying electric field, micro domains orient along the field direction and macrodomains occur[104].

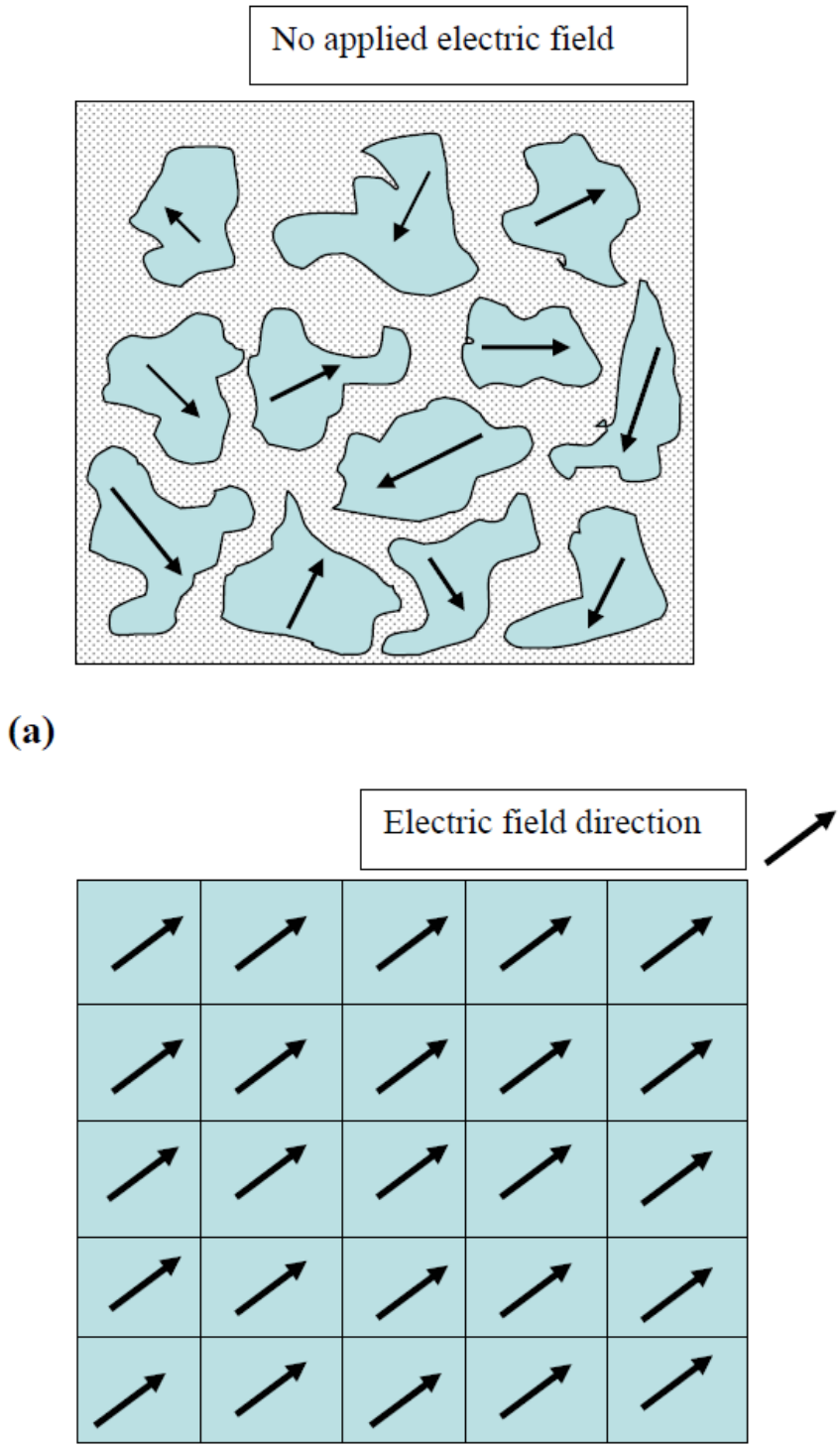

Fig. 3.2 Illustration of the electric field induced microdomain to macrodomain transition in a relaxor ferroelectric.
(a) no applied field and $T<T_f$;freezing temperature.
(b) applied electric field in a given direction.[104]

Relaxor ferroelectric lead zinc niobate, $Pb(Zn_{1/3}Nb_{2/3})O_3$ (PZN) crystals possess a maximum dielectric constant (~70,000 at 120 Hz) near 140°C where the paraelectric to

ferroelectric phase transition occurs. The room temperature crystal structure of PZN was reported by Kuwata *et al* [105] to be a rhombohedrally distorted perovskite. Lead titanate, $PbTiO_3$ (PT) is a simple perovskite normal ferroelectric with tetragonal symmetry below its Curie point of 490 °C. The addition of PT shifts the θ_c of PZN towards higher temperatures. The phase diagram is illustrated in **Fig. 3.3**[106].

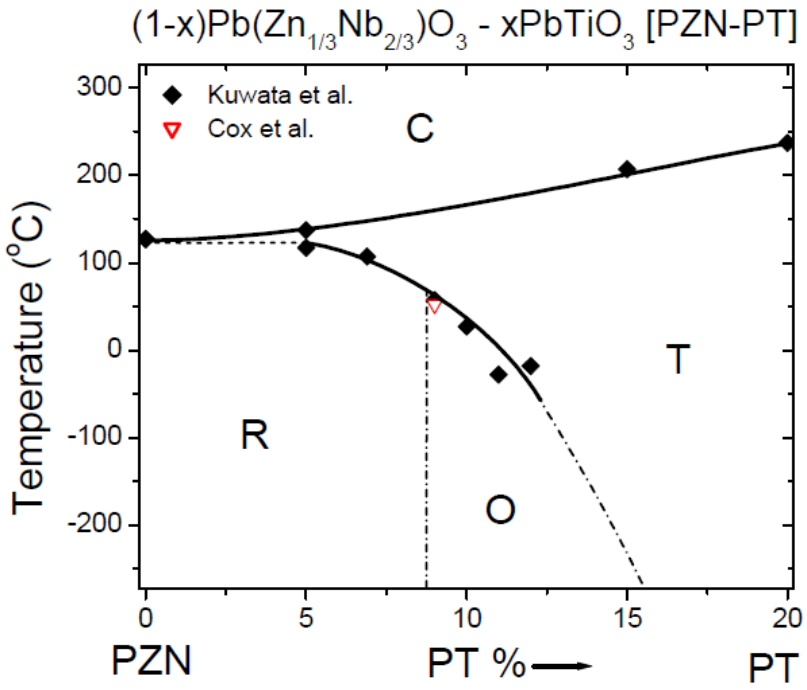

Fig. 3.3 Phase diagram for PZN-PT solid solution. (R: Rhombohedral, O: Orthorhombic, T: Tetragonal, C: Cubic).[106]

3.2.2 Ferroelectric Phase Transitions in PZN-4.5PT

In most cases, ferroelectrics may exhibit one or more ferroelectric (polar) phases (**Fig. 3.4**), and have a transition temperature called the Curie temperature, θ_c. Exceptions involve melting or decomposition before a θ_c are obtained, At a temperature $\theta>\theta_c$, the crystal does not exhibit ferroelectricity, while for $\theta<\theta_c$ it is ferroelectric[107-109]. On decreasing the temperature through the Curie point, a ferroelectric crystal undergoes a phase transition from a non-ferroelectric phase to a ferroelectric phase. If there are more than one ferroelectric phases as shown in **Fig. 3.4**, the temperature at which the crystal transforms from one ferroelectric phase to another is called the transition temperature. Early research studies on ferroelectric transitions has been summarized by Nettleton[110-111]. **Fig. 3.5** shows the variation of the relative permittivity (ε_r) (or dielectric constant) with temperature as a $BaTiO_3$ ferroelectric crystal is cooled from its non-ferroelectric (or paraelectric) cubic phase to the ferroelectric

tetragonal, orthorhombic, and rhombohedral phases. Near the Curie point or phase transition temperatures, thermodynamic properties including dielectric, elastic, optical, and thermal constants show an anomalous behavior. This is due to a distortion in the crystal as the phase changes. The temperature dependence of the dielectric constant above the Curie point ($\theta > \theta_c$) in most ferroelectric crystals is governed by the Curie - Weiss law (Eq. 2.17).

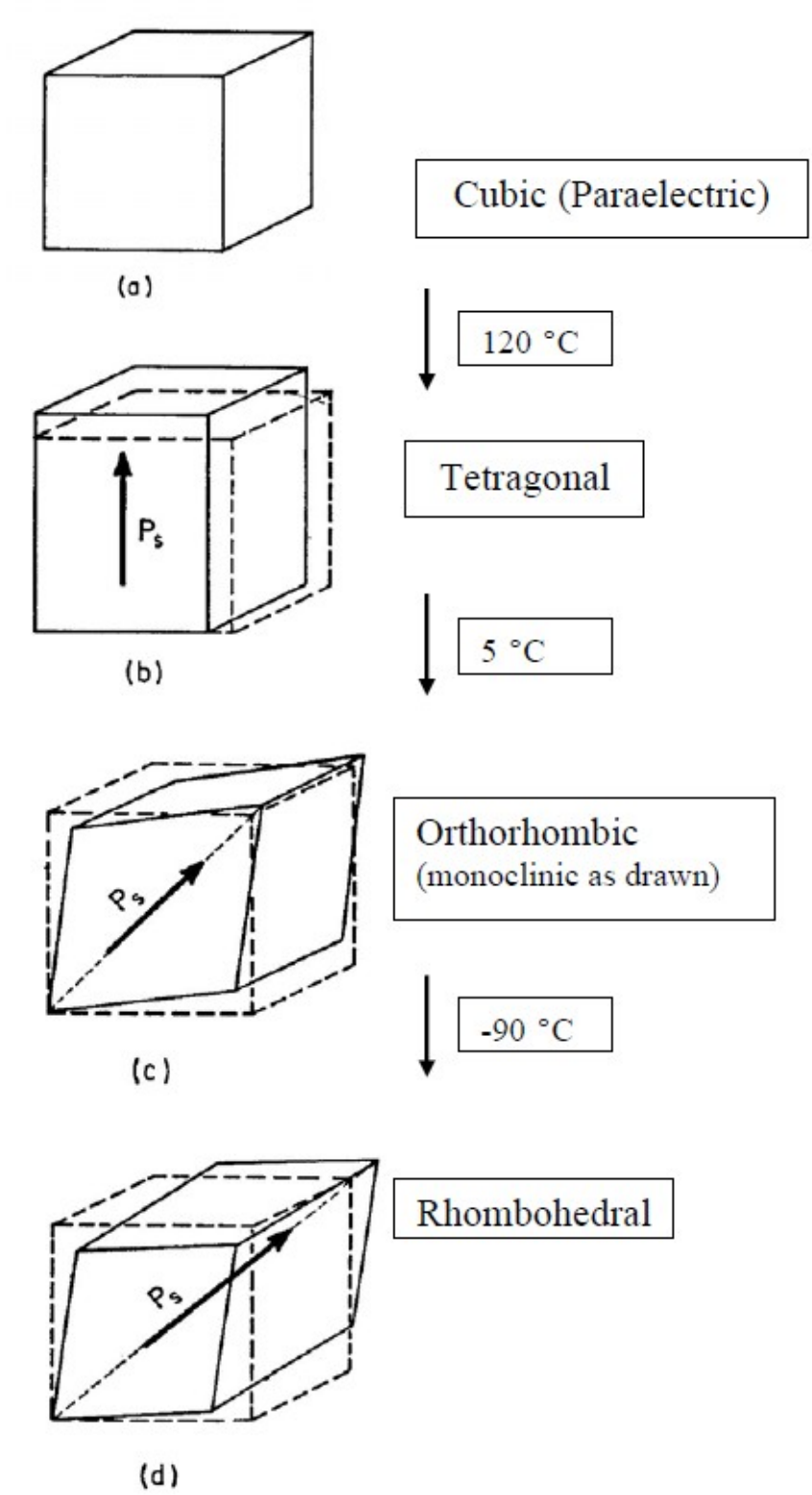

Fig. 3.4 Unit cells of the four phases of $BaTiO_3$. a) Cubic, stable above 120°C (T_C), b) Tetragonal, stable between 120°C and 5°C, c) Orthorhombic, stable between 5°C and -90°C, (monoclinic as drawn), d) Rhombohedral, stable below -90°C. (The dotted lines in (b), (c), and (d) delineate the original cubic cell. Arrows indicate the direction of the spontaneous polarization, *P*s, in each phase.). [109]

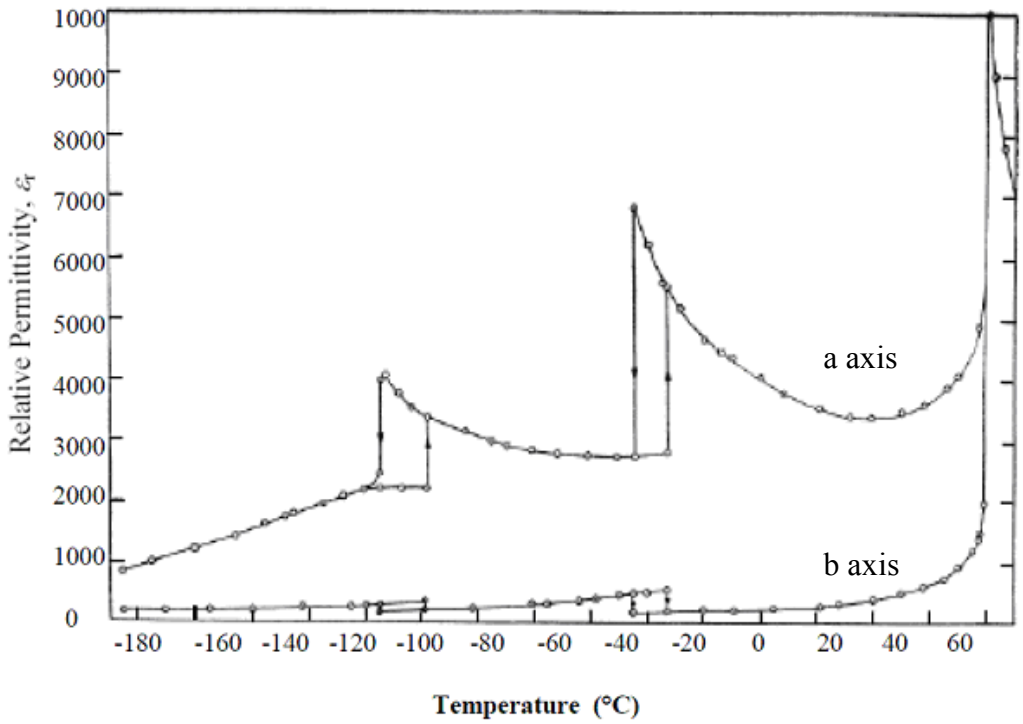

Fig. 3.5 Relative permittivities measured along the *a* and *c* directions of a poled tetragonal $BaTiO_3$ crystal versus temperature in a ferroelectric.[112] Note that the samples were not repoled at lower temperatures. It is a residual poling that yields the apparent anisotropy in the rhombohedral phase.[112]

Also, **Fig. 3.6** shows the temperature dependence of the permittivity ($\varepsilon^{\theta}_{33}/\varepsilon_0$), at 10 kHz and E = 0.1 kV/mm for PZN-4.5PT in <110>-oriented single crystal. The temperature dependence of $\varepsilon^{\theta}_{33}/\varepsilon_0$ shows three abrupt variations, characteristic of phase transitions, at quite comparable temperatures: $\theta \approx 425$, 385 and 345 K . These results show that an intermediate phase is electric field induced between the *T* and *R* ones. In the temperature range of this phase, the permittivity $\varepsilon^{\theta}_{33}/\varepsilon_0$ is lower than for the *T* and *R* phases[113].

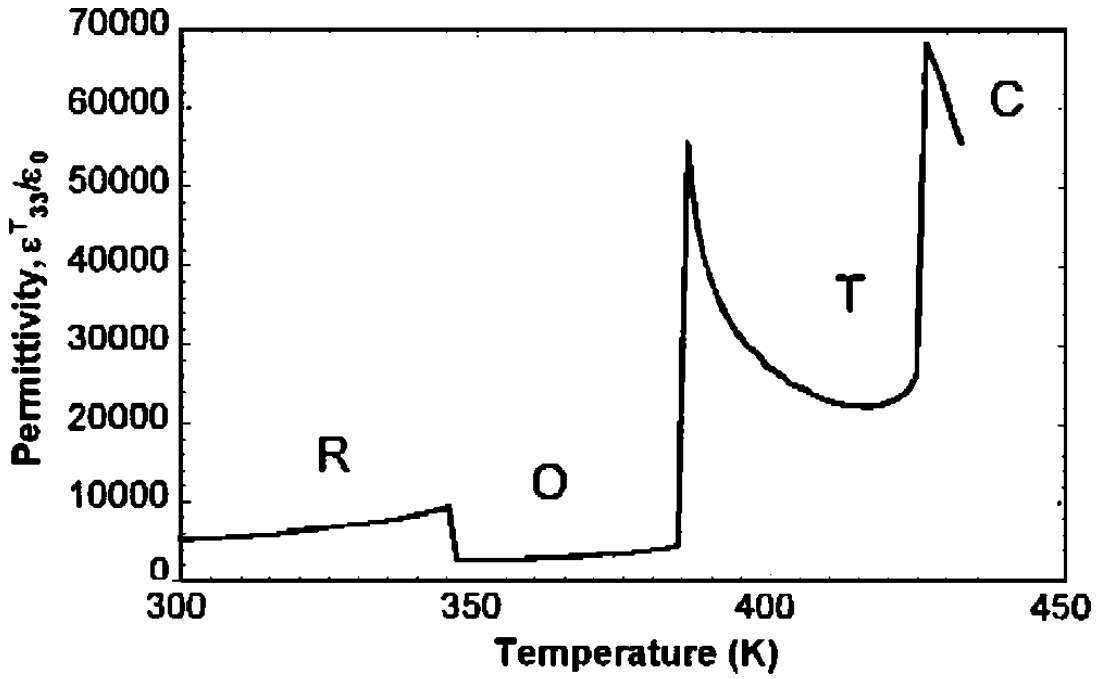

Fig. 3.6 Cooling Temperature dependence of permittivity $\varepsilon^{\theta}_{33}/\varepsilon_0$ measured at 10 kHz (*E*=100kV/m), for the PZN-4.5PT <110> -oriented single crystal[113].

Fig. 3.7 shows the temperature dependence of the displacement current *I* on <110>-oriented PZN-4.5PT single crystals. At 300 K, the domain configuration of a virgin (unpoled) PZN–4.5%PT crystal is 8*R*. The transition temperatures, determined from dielectric anomalies, are reported in the *E-T* diagram (**Fig. 3.8**).

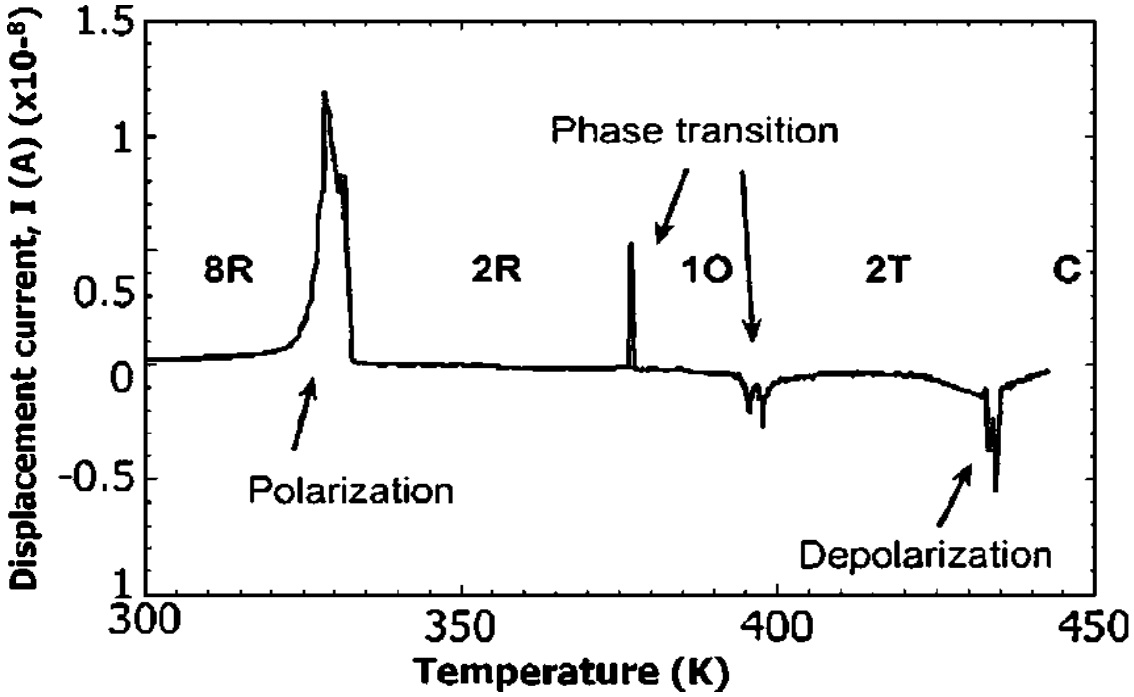

Fig. 3.7 Temperature dependence of the displacement current I(θ), measured in E=100kV/m, for PZN-4.5PT <110> -oriented single crystals.[113]

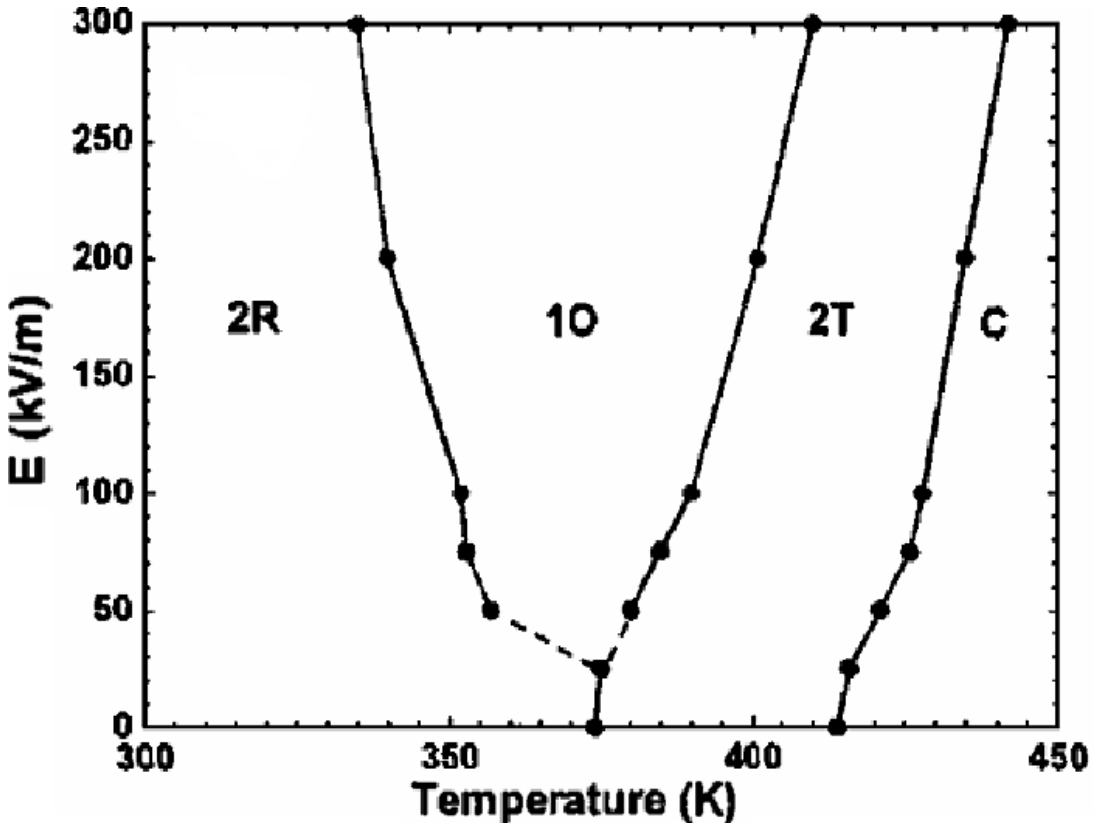

Fig. 3.8 Field-Temperature (E-θ) diagrams, resulting from the field cooling experiments, for the <110> -oriented single crystals.[113]

In a previous investigation, thermal energy harvesting was measured on <110> oriented $Pb(Zn_{1/3}Nb_{2/3})_{0.955}Ti_{0.045}O_3$ (PZN-4.5PT) single crystals[96]. This composition was chosen due to the occurrence of a FE-FE transition in a poled sample which could be induced by an electric field or temperature[113-114]. Based on the study of Renault et al.[113], during heating under a null electric field, PZN-4.5PT exhibited the following phase transitions: at room temperature, the stable phase was rhombohedral; in the temperature range of 120-130°C, the transition from rhombohedral (R) to tetragonal (T) occurred; and when the temperature was continuously raised up to nearly 160°C, a tetragonal to cubic phase transition emerged. Moreover, under an electric field, an intermediate ferroelectric orthorhombic phase (O) was induced at temperatures between those of the R and T phases[113]. The R-O transition induced an increase in the polarization and yet the O-T transition was associated with a drop in polarization. These polarization variations were of interest for improving the pyroelectric properties, and subsequently for increasing the harvested energy. Other studies have shown that since the properties of single crystals are recovered when returning to ambient temperature, the samples could be reversibly depolarized when the R-T transition was

crossed[115]. By the analysis above, PZN-4.5PT is chosen as the promising candidate for thermal energy harvesting in our study.

Since phase transition has close connection with working temperature, which temperature range should be chosen? Khodayari et al.[96] studied the Ericsson cycle at different temperature. Their study revealed that the transition does not always present an improvement in energy harvesting. Sometimes, it leads to lost energy. For example, Ericsson cycle between 25 and 50°C, the FE-FE transition occurs at an intermediate electric field as shown in **Fig. 3.9** (a), but the effect of phase transition is negative for energy harvesting, which lead to a supplied energy is higher than the harvested one due to the unsuitable position of phase transition. In contrary, Ericsson cycle between 50 and 100°C as shown in **Fig. 3.9** (b), it absolutely leads to harvest energy, whatever at low electric field or high electric field (0.5 kV/mm or 2 kV/mm). Compared the two Ericsson cycles at 2 kV/mm (**Fig. 3.9** (a) and (b)), the only difference is the working temperature and the temperature variation, which consequently result in the phase transition in different stage. Therefore, temperature is an important parameter which determines if the energy is harvested or lost.

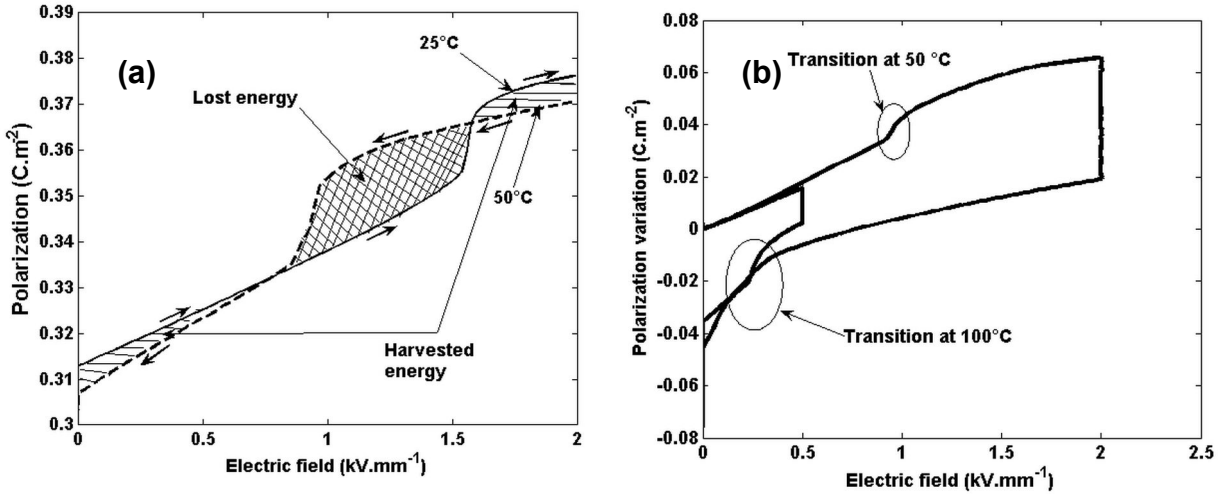

Fig. 3.9 (a) simulation of an Ericsson cycle between 25 and 50°C (b) Ericsson cycles between 50 and 100°C with an applied electric field of 0.5 kV/mm and 2 kV/mm, respectively.[96]

Based on the previous analysis, 100 and 130°C was chosen as the working temperature in our case. By this way, the Ericsson cycle exhibits a dramatic harvested energy by using the R-O transition during the first isotherm path, a large pyroelectric coefficient of the orthorhombic phase during the electric field constant path and O-T transition during the second isotherm path.

3.2.3 Preparation of PZN-4.5PT

PZN-4.5PT single crystals were prepared using the high-temperature flux technique[77,116-118]. Flux growth is a very efficient self-purification process. The use of high-purity charge is thus not a necessity. In the flux growth of PZN–PT single crystals, local cooling arrangement is often made to enable single-crystal nucleation at the base of the Pt crucible. When perfect single-crystal nucleation is initiated in the middle of the base of Pt crucible, the crystal will grow in a stress-free manner with minimum constraint and is totally protected by the PbO-rich solution. The latter is important because most relaxor-PT systems, in particular PZN–PT, are unstable at high temperatures even in PbO-rich vapor environments[116].

In this work, high-purity chemical powders PbO (99%), TiO_2 (≥99%), ZnO (≥99%) , Nb_2O_5 (99.9%) and Pb_3O_4 (99%) were used as starting materials. $ZnNb_2O_6$ and $PbTiO_3$ were prepared using a solid-state synthesis route at 1100℃ and 850℃, respectively. These precursors were mixed with Pb_3O_4 flux in the ratio PZNT:PbO = 40:60, molar percentage. Pb_3O_4 flux (which decomposed at 580°C to PbO) is usually used to inhibit the crystallization of pyrochlore phase. The mixture was loaded in a platinum crucible that was then placed in the three zones furnace where the gradient was the highest (around 30°/mm). The platinum crucible was covered with a platinum lid which has a hole of ~200 μm in order to equilibrate the pressure and placed in a pedestal in an alumina column inside the vertical furnace equipped with a gas cooling arrangement under the crucible. The bottom of the crucible was cooled by the oxygen gas to establish a preferential growth axis[119]. The loaded crucible was heated at 1300℃, soaked for 4 h at the same temperature, and the solution was slowly cooled at 1°/min down to 980℃. Later, the furnace was cooled at a fast rate of 200°C/h to about 500°C. Centimeter size crystals were leached out from the flux in hot nitric acid. X-ray diffraction on ground crystals confirmed the presence of a pure perovskite phase[117]. **Fig. 3.10** shows the electrical furnace with three zones, used to growth PZN-4.5PT single crystal. This furnace was completely designed at the laboratory, with an aim of reaching temperatures 100°C higher than melting point of the reagents in order to have the temperature of crystallization positioned in the central zone[117]. The resulting crystals are show in **Fig. 3.11**, the weight of these crystal was 195g, the yield obtained was more than 60% in weight. The color of the pure PZN-4.5PT is brown-yellow.

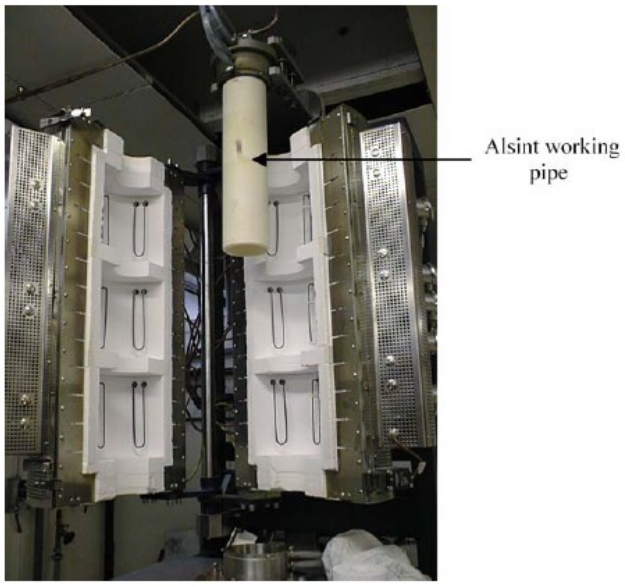

Fig. 3.10 Furnace used for growth of PZN-4.5PT single crystals by flux method.[117]

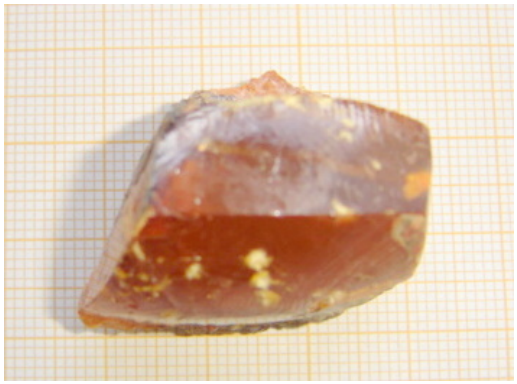

Fig. 3.11 Single crystal grown by flux method.

3.2.4 Characterization of PZN-4.5PT

To confirm the structure of grown single crytal better, X-ray diffraction was performed on ground crystals with the help of a Philips X'pert Pro diffractometer using a monochromatic selecting CuKα radiation (λ=1.5418Å). The XRD diffraction patterns in **Fig. 3.12** confirm a perfect perovskite structure solid solution of PZN-4.5PT single crystals with the orientation <110>. The single crystals were oriented by recording the pole figure corresponding to the <110> desired direction. Samples were then sliced into thin plates. The density of the material was equal to 8000 kg/m^3. For Ericsson cycle or other measurements in this study, 1.1 mm thick samples were electroded with silver paste.

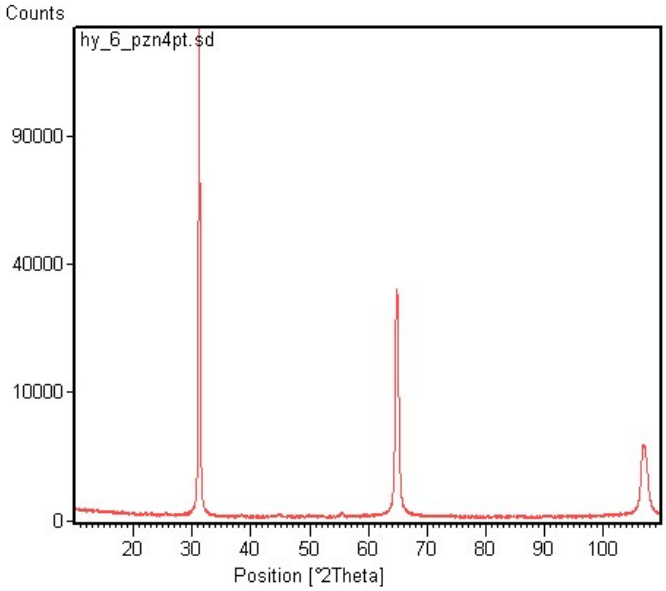

Fig. 3.12 XRD patterns for perovskite phase of <110> oriented PZN-4.5PT Single crystals.

The weak field dielectric properties in this thesis were measured by an impedance/Gain-phase Analyzer (HP4194A) with a controlled temperature chamber. The weak dielectric constant was measured as a function of temperature at various frequencies (100 Hz, 1 kHz, 10 kHz, 100 kHz) from 50°C to 250°C on two samples, unpoled and poled PZN-4.5PT <110>-oriented single crystal (**Fig. 3.13** (a), (b)). Compared **Fig. 3.13** (a) and (b), it is interesting to find that there is an additional phase transition just occurred on the poled sample at around 130°C, which corresponds to the rhombohedral to tetragonal ferroelectric phase transition. It provides the proof for choosing the working temperature range in the thermodynamic cycle.

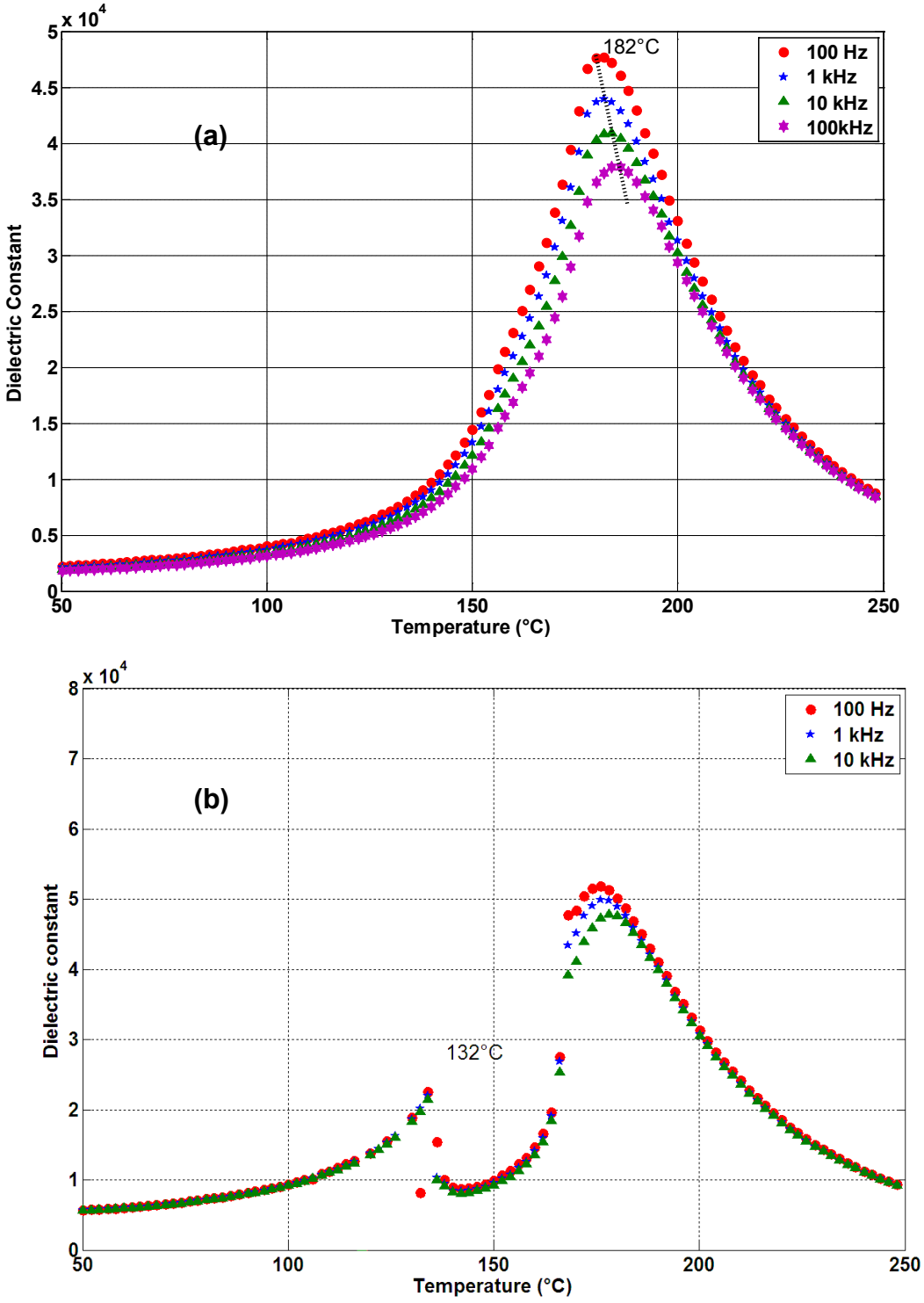

Fig. 3.13 Temperature dependences of dielectric constant for <110> oriented PZN-4.5PT single crystal.
(a) unpoled and (b) poled, dashed line for pointing out the dielectric maximum shifts with frequency.

In order to confirm the phase transition under electric field, bipolar and unipolar cycle were implemented on <110>-oriented PZN-4.5PT single crystal under the electric field of 2 kV/mm. **Fig. 3.14** shows the polarization hysteresis loop of virgin PZN-4.5PT single crystal with <110>-orientation at the ambient temperature and 0.1 Hz. In this figure, the single crystal exhibits low-temperature ferroelectric rhombohedral (R) phase. **Fig. 3.15** shows the polarization versus electric field at 100°C and 130°C, 0.1 Hz. Unipolar cycle was executed because it is similar to the isothermal processes of Ericsson cycle and more clearly to show the phase transition. Considering the phase transition in unipolar cycle occurs in rising electric field sequence. At 100°C under electric field, the phase transition from rhombohedral (R) to orthorhombic (O) occurs at 0.2 kV/mm. This phase transition causes a remarkable increase in the polarization. At 130°C under electric field, the phase transition from tetragonal (T) to orthorhombic (O) occurs at around 0.8 kV/mm, at it also causes an abrupt polarization variation. Both phase transitions are exactly what we will use in our study and together improve the harvested energy greatly.

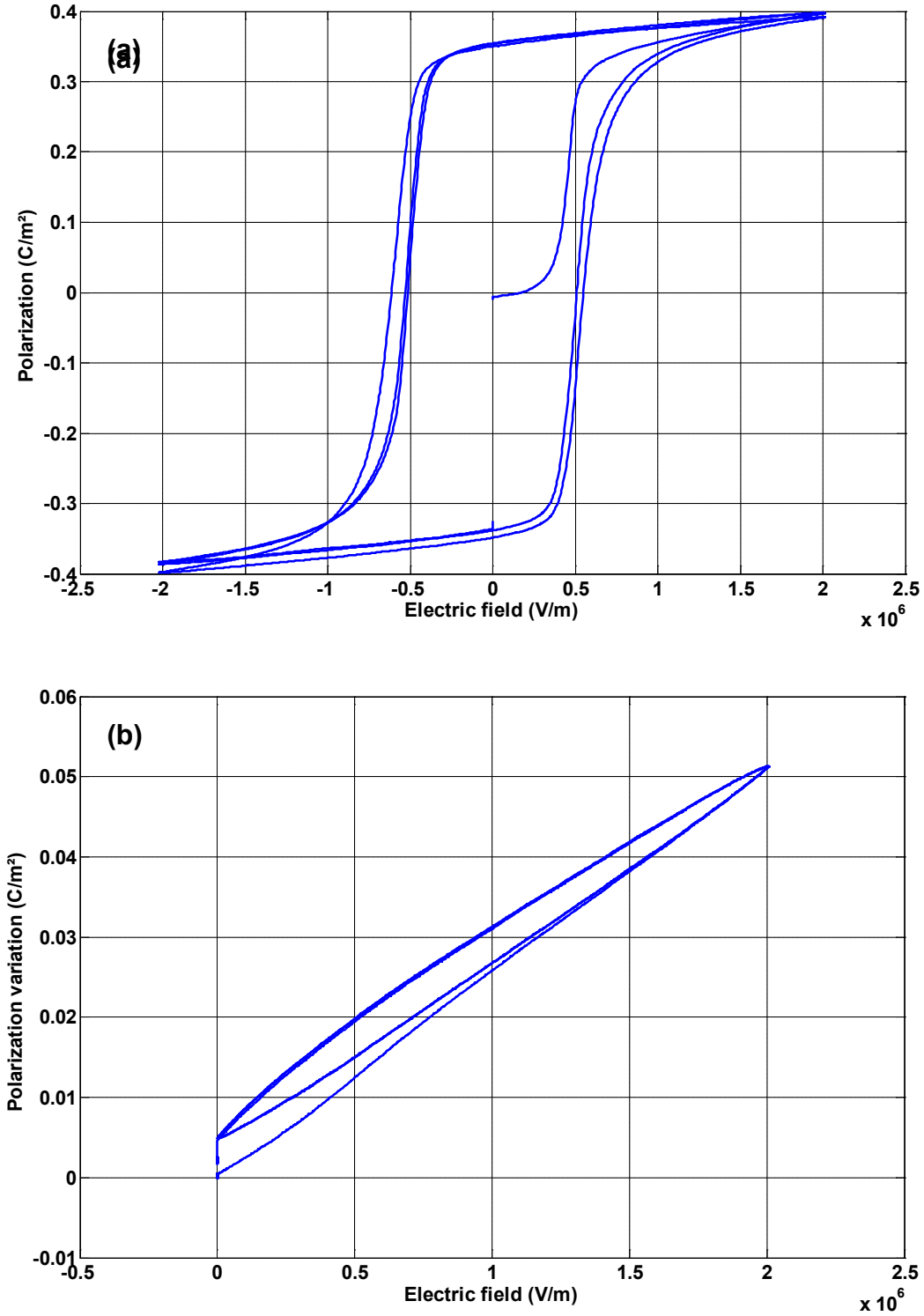

Fig. 3.14 Ferroelectric hysteresis loop of bipolar and unipolar cycle on <110> oriented PZN-4.5PT at ambient temperature, 2kV/mm and 0.1Hz.

Frequency effect was investigated at 100°C and 130°C respectively as shown in **Fig. 3.16** (a) and (b). Ferroelectric hysteresis loops were carried out at 10, 5, 1, 0.05 Hz in descending order. As we all know that, the process of polarization switching in ferroelectric needs a period of time, so the coercive electric field and remnant polarization are related to the frequency. It can be seen from **Fig. 3.16** that the hysteresis loop becomes narrow with decreasing frequency, which indicate that the coercive field decreases, and meanwhile, the remnant polarization increases. The reason for this could be that the polarization under a low frequency experiences a period of time to switch, while in the high frequency, there is not enough time to experience the polarization switching process, which leads to a high coercive field and the remnant polarization is not as well as that in low frequency. The frequency influence in energy harvesting will be also discussed in detail in the next part, and it will be used to improve the traditional energy harvesting cycle.

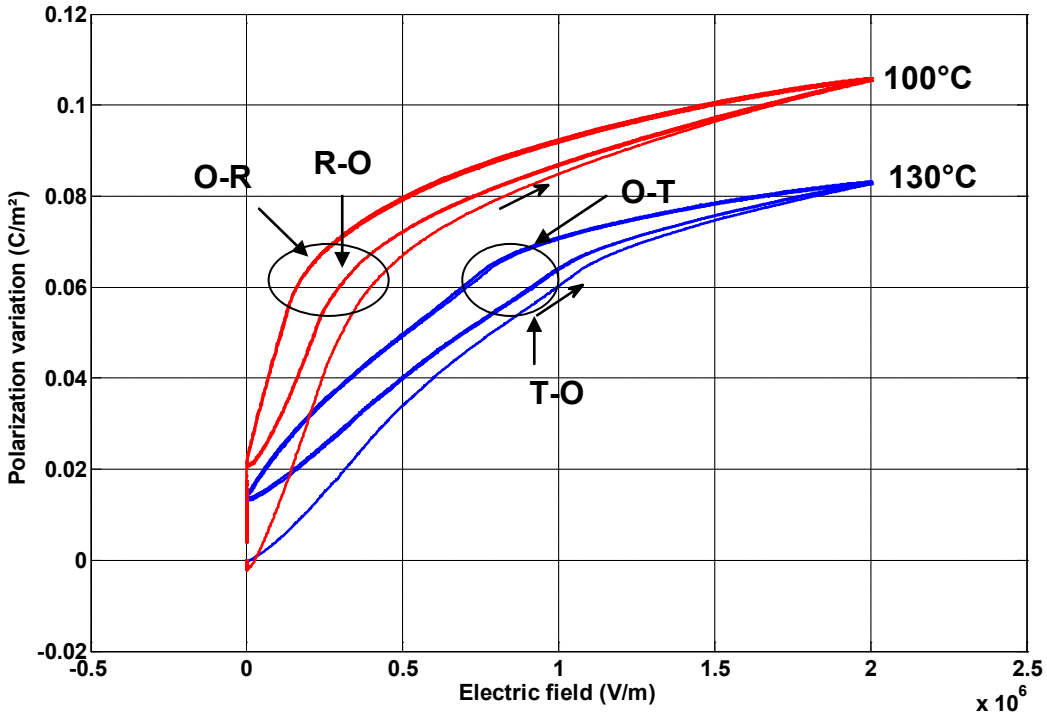

Fig. 3.15 Polarization vs. unipolar electric field at 100°C and 130°C on <110> oriented PZN-4.5PT .

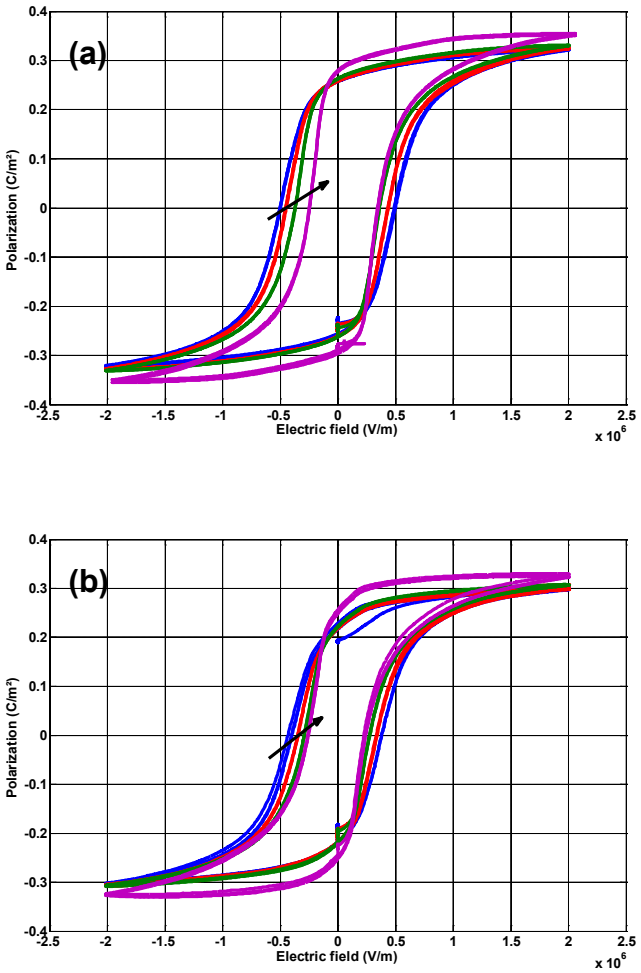

Fig. 3.16 Ferroelectric hysteresis loops with different frequencies on <110> oriented PZN-4.5PT at (a) 100°C and (b)130°C.
(The direction of arrow represents decrease of frequency)

In this part, we aim to introduce the general property of ferroelectric relaxor. We analysed the temperature and electric field dependence on polar regions. Due to its several different ferroelectric phases, the permittivity of PZN-4.5PT single crystals under different temperature changed and depends on the orientation of the crystals. Especially for <110> orientation, the intermediate orthorhombic phase is induced applying the electric field. This phase has a lower permittivity than that in the rhombohedral and tetragonal phases.

By the analysis, PZN-4.5PT is chosen as the best candidate for thermal energy harvesting in our work. The electric field induced R-O transition generated an increase in polarization and the temperature induced O-T transition provoked a drop in polarization. These transitions are of interest for improving the pyroelectric effect, subsequently for

increasing the harvested energy. We shew the preparation of PZN-4.5PT, and characterized their weak field dielectric properties in order to determine the working temperature for energy harvesting. Finally, bipolar and unipolar cycles were carried out under electric field at 100°C and 130°C for confirming the phase transition under electric field.

3.3 Thermal Energy Harvesting from $Pb(Zn_{1/3}Nb_{2/3})_{0.955}Ti_{0.045}O_3$ Single Crystals

In this part, we will introduce the experimental measurement of pyroelectric energy harvesting on PZN-4.5PT single crystal. Some valuable results (e.g., "frequency effect" on Ericsson cycle) and promising modeling (e.g., Asymmetric Ericsson cycles) are also discussed in detail.

3.3.1 Experimental Section

The traditional Ericsson cycle consists of two isothermal and two constant electric field processes, as shown in **Fig. 3.17** (a). In the present case and as portrayed in **Fig. 3.17** (b), the Ericsson cycle was modified by the phase transitions of a PZN-4.5PT single crystal. Similar to the traditional Ericsson cycle, it started at the lowest temperature θ_1 and the polarization variation equalled zero. The two isothermal processes could be assimilated to branches of a unipolar P-E cycle. The isothermal process in the Ericsson cycle at the lowest temperature θ_1 (AB path in **Fig. 3.17**) corresponded to the step when increasing the electric field from zero to the same maximum electric field E_1 in a unipolar cycle. Due to the transition from a rhombohedral to an orthorhombic phase, which induced the injected energy decreased greatly. The polarization increased up to P_1, the polarization variation was seen to be larger during this process and than its counterpart in a traditional Ericsson cycle. When increasing the temperature to θ_2 at the constant electric field (BC path), the polarization became reduced to P_2 due to the pyroelectric effect. Similarly, the other isothermal process at higher temperature θ_2 (CD path) corresponded to the step when decreasing the electric field from E_1 to zero in the unipolar cycle. The polarization variation became larger again due to the occurrence of a transition from an orthorhombic to a tetragonal phase. Finally, the temperature was lowered to its initial value (DA path) and the sample returned to its original state with a phase transition from tetragonal to rhombohedral. The whole cycle was closed according to a clockwise path.

When comparing the two cycles in **Fig. 3.17**, the modified Ericsson cycle demonstrated a great improvement of the energy harvesting.

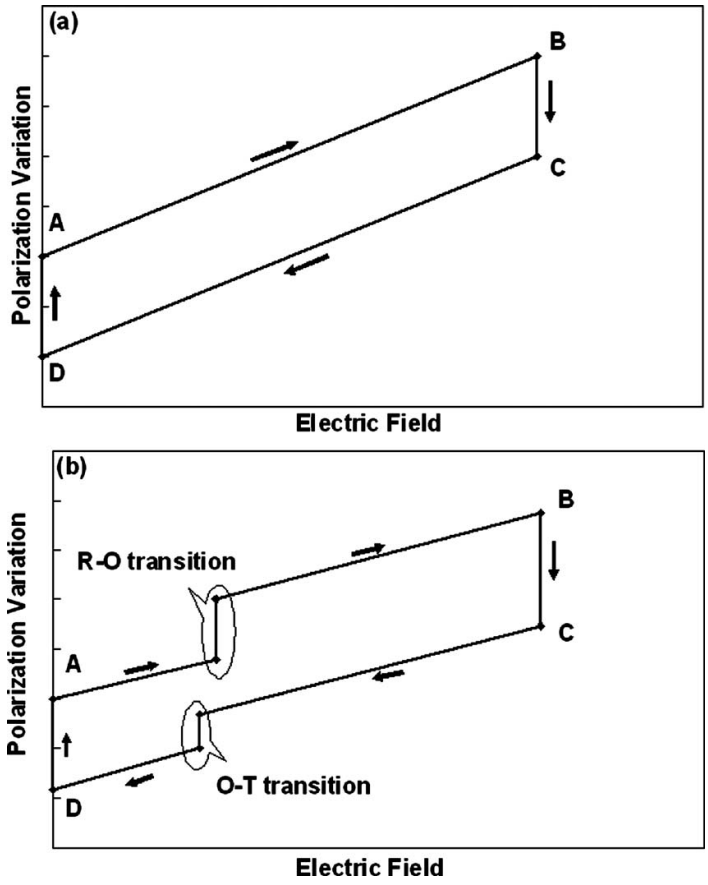

Fig. 3.17 Schemes of Ericsson cycle on pyroelectric material with (a) linear pyroelectric effect and (b) a FE-FE transition.

Measurements of the polarization versus the electric field cycles were carried out in a thermostatic silicone oil bath so as to ensure a control of the temperature and avoid arcing. A scheme of the experimental setup is shown in **Fig. 3.18**. The polarization was calculated by a time integration of the current ($P=\int idt$). The experimental setup required for the Ericsson cycle consisted of two temperature oil-baths at 100°C and 130°C. Due to the use of two oil baths, temperature variations could be realized by quickly moving the sample from one bath to the other. During the change, the sample was immersed in oil thus preventing an electric arc. A waveform generator (Agilent 33220A) and a high voltage amplifier (TREK Model 10/10B) were used to apply the voltage on the single crystal. The current was continuously monitored with a low-noise current preamplifier (STANDFORD Model 570), and an oscilloscope (Agilent MEGAZOOM DSO6034A) was employed to portray the output signal and record the data.

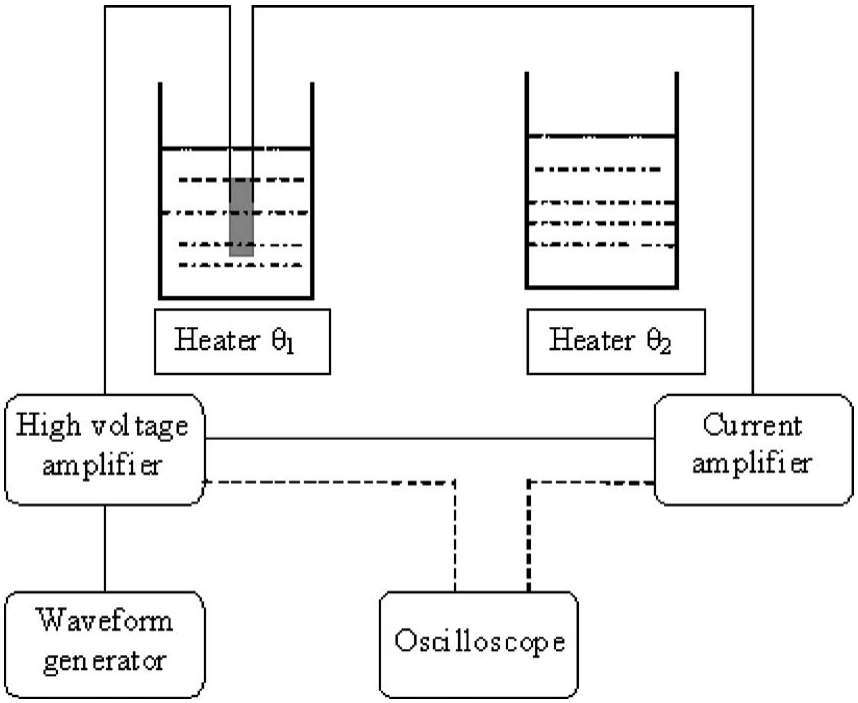

Fig. 3.18 Scheme of the experimental setup.

First, the electric field was increased to its maximum value with a chosen slope dE/dt. Following a decrease in the current down to zero (the end of the polarization process), the sample was moved to the bath with the higher temperature while maintaining the elevated voltage on the sample. Due to the change in temperature, a pyroelectric current was produced. After the diminution of the current down to zero (end of the pyroelectric process), the sample was moved back to the bath with the lower temperature. The increase and decrease in the electric field were considered as isothermal conditions due to the small electrocaloric effect (<1 K at 2 $kVmm^{-1}$) being too low to lead to a significant change in the sample's temperature. Moreover, since the sample was immersed in oil, the temperature remained perfectly constant due to the fast heat exchange between the sample and the oil. In order to confirm the repeatability of our experiment, all the measurements on Ericsson cycles have been implemented on 15 samples.

3.3.2 Ericsson Pyroelectric Cycle

For energy harvesting, the cycle needed to be executed in a clockwise manner. After reaching the lowest temperature, the single crystal recovered almost all of its initial polarization[120], and the harvested energy could be calculated as the area of the cycle in **Fig. 3.17**,

$$W_{harvest} = \oint E dP \tag{3.1}$$

where P is the polarization of the sample.

According to the first thermodynamic law: the change in internal energy of a closed thermodynamic cycle is equal to zero and consequently, the following relation can be deduced:

$$-(Q_{cold} + W_{output}) = Q_{hot} + W_{input} \tag{3.2}$$

Here, W_{input} is the electric energy injected into the material, and W_{output} is the electrical energy recovered from the material. As shown in **Fig. 3.17**:

$$W_{harvest} = W_{output} - W_{input} \tag{3.3}$$

Equally,

$$W_{harvest} = Q_{hot} + Q_{cold} \tag{3.4}$$

Thus, if the aim is to harvest energy, the heat extracted from the hot source should be larger than that emitted to its cooler counterpart. The thermal energy difference is exactly the energy converted into electrical energy.

The injected energy corresponding to the AB segment of the cycle depicted in **Fig. 3.17** is calculated as:

$$W_{inject} = \int_0^{E_1} E \frac{\partial P}{\partial E} dE \tag{3.5}$$

and the gain in term of electrical energy is defined as:

$$\eta = \frac{W_{harvest}}{W_{inject}} \tag{3.6}$$

In the present case, the injected energy corresponded exactly to the electrical energy stored during the increase in the electric field (AB path). Although the temperature increased during the BC path, this thermal energy originated from outside the system and was not included in the injected energy. Moreover, the energy referred to in this thesis as harvested was not the output electrical energy but more accurately the energy gained during the entire process as described by the equation (3.3). It is helpful to estimate the energy harvesting capability by way of the gain, since this parameter has a more practical significance for the implementation of the technique in a device. The application of a technique inevitably leads to certain unavoidable losses, reducing the actual harvested energy. A large gain is necessary to compensate these losses, rendering it possible to implement the technique in a device.

3.3.3 Results and Discussion

This section investigates the frequency effect on energy harvesting based on an Ericsson cycle. Several experimental Ericsson cycles were carried out with the same temperature variation between 100ºC and 130ºC, and the same maximum value of the electric field at 2 $kV.mm^{-1}$. For the sake of convenience, the value of frequency in the present study corresponded to its equivalency in the bipolar electric cycle and not to the actual frequency of the Ericsson cycle. In other words, at the same frequency, the slope of the changing electric field (dE/dt in AB, CD path) in the Ericsson cycle was equal to that in the bipolar cycle. For example, at f = 0.1 Hz, the electric field increased with a slope of dE/dt = 800 $V.mm^{-1}.s^{-1}$ in the bipolar cycle with a maximum electric field value of 2 $kV.mm^{-1}$. Thus, for the Ericsson cycle, the electric field was applied with the same slope during both the AB and CD paths.

In a first step, the Ericsson cycle was measured at f = 0.01 and 10 Hz (slopes at dE/dt = 80 $V.mm^{-1}.s^{-1}$ and 80 $kV.mm^{-1}.s^{-1}$ respectively). Electric field waveform and the corresponding current during Ericsson cycle were shown in **Fig. 3.19**, the energy corresponding to each segment could be obtained by the electric field integral with respect to current. **Fig. 3.20** presents the typical Ericsson cycle (P-E cycle) and several interesting pieces of information significantly influencing the harvested energy have been underlined. When the electric field was increased from zero to 2 kV mm^{-1} at 100 °C (AB path in **Fig. 3.7**), an abrupt positive peak in the current signal was observed due to the charge of the sample. At low frequency, the peak became deconvoluted into two peaks, which corresponded to the charge of the sample and the phase transition. The R-O phase transition increased the polarization due to the domain engineering for the <110> direction[121]. At high frequency, the current peak was sharper rendering the deconvolution difficult. Moreover, the electric field associated with the phase transition was no coincident for the various frequencies at a fixed temperature. As can be seen from **Fig. 3.20**, at f = 0.01 Hz, the electric field corresponding to the transition was approximately 100 V mm^{-1}, whereas at f=10 Hz, it increased to close to 400 V mm^{-1} and the transition appeared to be more diffuse.

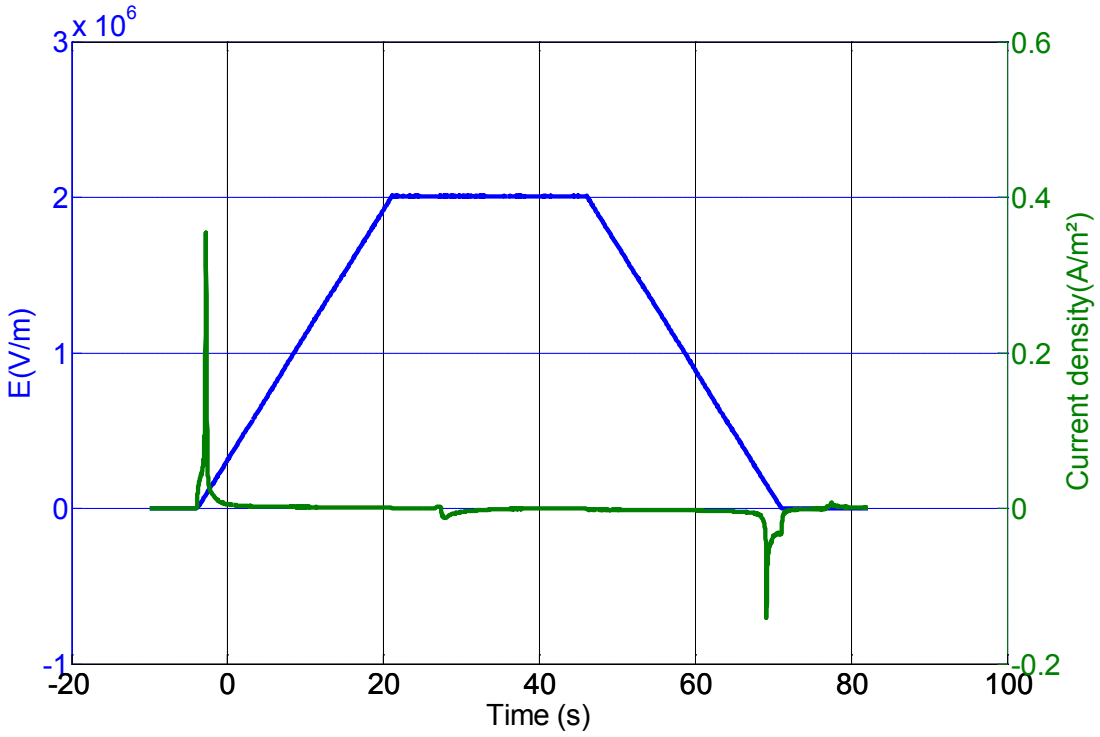

Fig. 3.19 Electric field waveform and the induced current in Ericsson cycle at f=0.01 Hz.

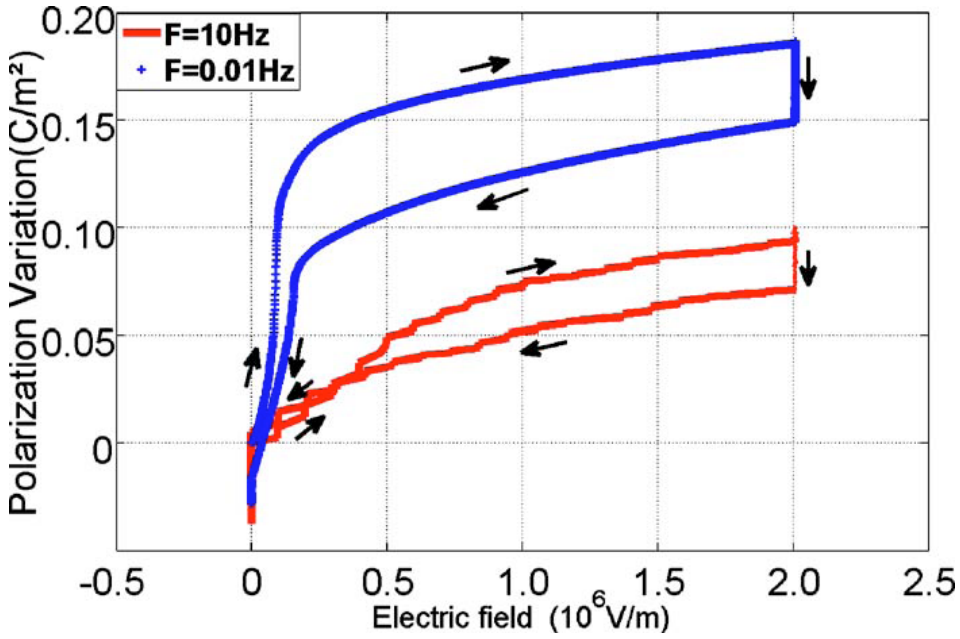

Fig. 3.20 (Color online) A comparison of experimental Ericsson cycles for f = 0.01 Hz (blue crosses) and f = 10 Hz (red curve).

From the theoretical analysis of the Ericsson cycle, the R-O phase transition was expected to occur as early as possible in order for the area of the Ericsson cycle to be increased. In other words, the switching electric field should be as low as possible. This way, at constant

polarization variation, one can harvest more energy due to the decrease in the injected energy. By integrating over the two cycles, the harvested energy equaled 86 mJ cm^{-3} at f =0.01 Hz, but only 30 mJ cm^{-3} for f =10 Hz. The phase transition observed during the AB path was not the only reason for the decrease in harvested energy when the frequency was raised. At 10 Hz, the two isothermal paths (AB and CD) crossed each other, as demonstrated in **Fig. 3.20**. The occurrence of this crossing modified the area of the cycle and the origin of this behavior will be explained below and in Sec. 3.3.4. The injected energy increased up to 72 mJ cm^{-3} and the harvested energy was reduced to 30 mJ cm^{-3}.

Fig. 3.20 also shows that with the same temperature variation and maximum electric field, the polarization variations of the two isothermal processes (AB, CD paths in **Fig. 3.20**) were smaller even though the frequency was higher. This effect is well known and is denoted a frequency effect. Another phenomenon that catches our attention on the AB path is the relaxation of the polarization caused by the external electric field for the highest frequency (i.e., f=10 Hz). At the end of the polarization, the current should decrease to zero. But in this case, the current did not immediately drop to zero when the electric field reached its maximum value. Consequently, the polarization did not stop at the maximum electric field, but rather increased somewhat. This augmentation of the polarization induced a large increase in the injected electrical energy.

Based on the illustration above, certain factors, such as a switching electric field, the crossing of the cycle, polarization variations and relaxations, influence the energy harvesting. The lower electric field frequency is preliminarily considered to benefit the energy harvesting. But a relevant question is whether the relationship between frequency and energy harvesting is linear or nonlinear. Moreover, how does one explain these phenomena and relationships from the perspective of the inherent physical mechanism of the sample? To answer these questions, the Ericsson cycle was further measured at several frequencies, f=10, 5, 1, 0.5, 0.1, 0.05, and 0.01 Hz, according to the slope in descending orders.

In **Fig. 3.21**, the harvested energy is plotted versus the frequencies for the application of the electric field. With an increasing frequency, the injected energy increased and the harvested energy demonstrated a diminution. For the critical frequency f=1 Hz, the slope of the energy curve was not linear. Moreover, at frequencies lower than 1 Hz, both the injected energy and harvested energy evolved smoothly. In contrast, at f=5 and 10 Hz, the injected energy versus frequency displayed an abrupt increase, whereas the harvested energy decreased significantly. This nonlinear tendency was also demonstrated by the gain which was defined by Eq. (3.6). At f = 0.01 Hz, the gain was maximum at 1.65 and it dropped down

to 1.26 for f = 1 Hz. At f = 5 and 10 Hz, it began to decrease abruptly; at f=10 Hz, the gain just equalled to 0.42. Comparing with that at 0.01 Hz, the difference value became 1.22. The gain at f = 0.01 Hz is nearly four times higher than that at f =10 Hz.

In order to obtain a better understanding of the frequency dependence of the harvested energy, the variation in polarization associated with the phase transition in each process of the Ericsson cycle was studied. **Fig. 3.22** gives this polarization variation as a function of all the studied frequencies corresponding to three processes of the Ericsson cycle (i.e., the AB, BC, and CD paths). According to the figure, the tendencies of the polarization variation during an increase and decrease in the electric field were nearly parallel. Originally, despite a slight decrease in the polarization variation, the general tendencies were mainly steady until the frequency was below 1 Hz, at which level a distinct descent was observed. It is interesting to note that the sample portrayed almost the same behavior with regard to harvested energy and polarization variation.

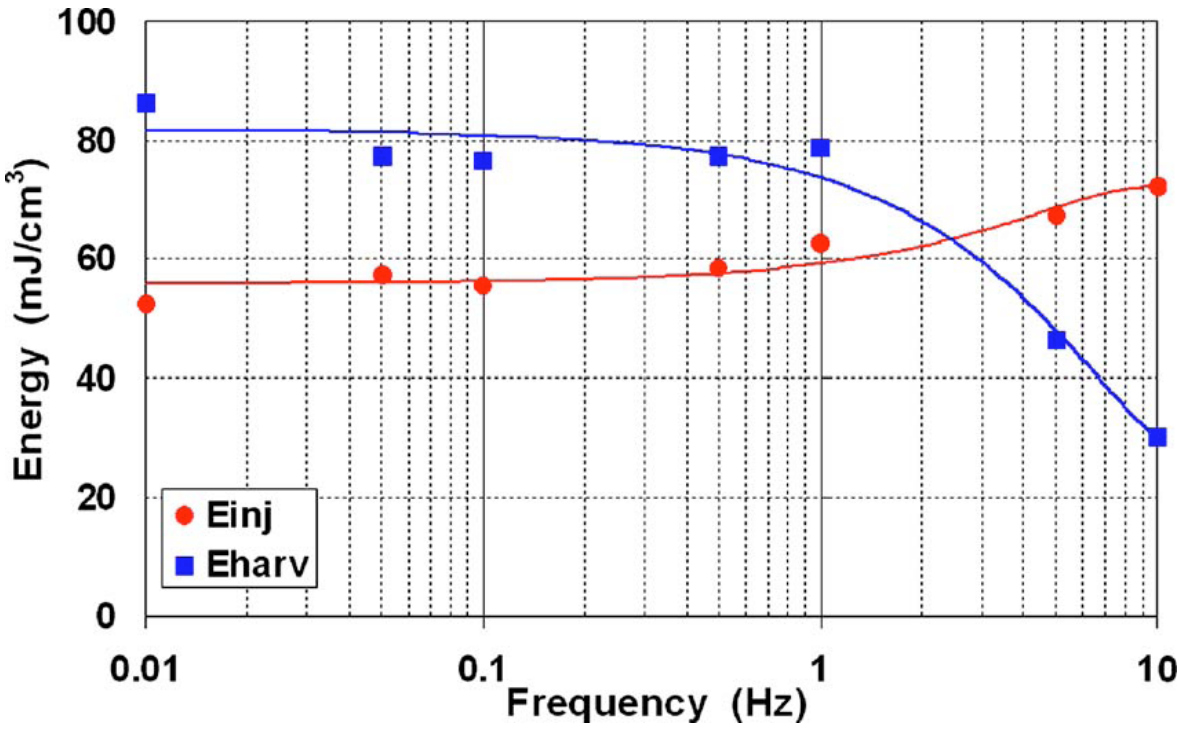

Fig. 3.21 (color online) The harvested energy (blue squares) and injected energy (red circles) as function of the logarithm of the frequency when applying the electric field. The solid line has been added to indicate the evolution tendency with the frequency.

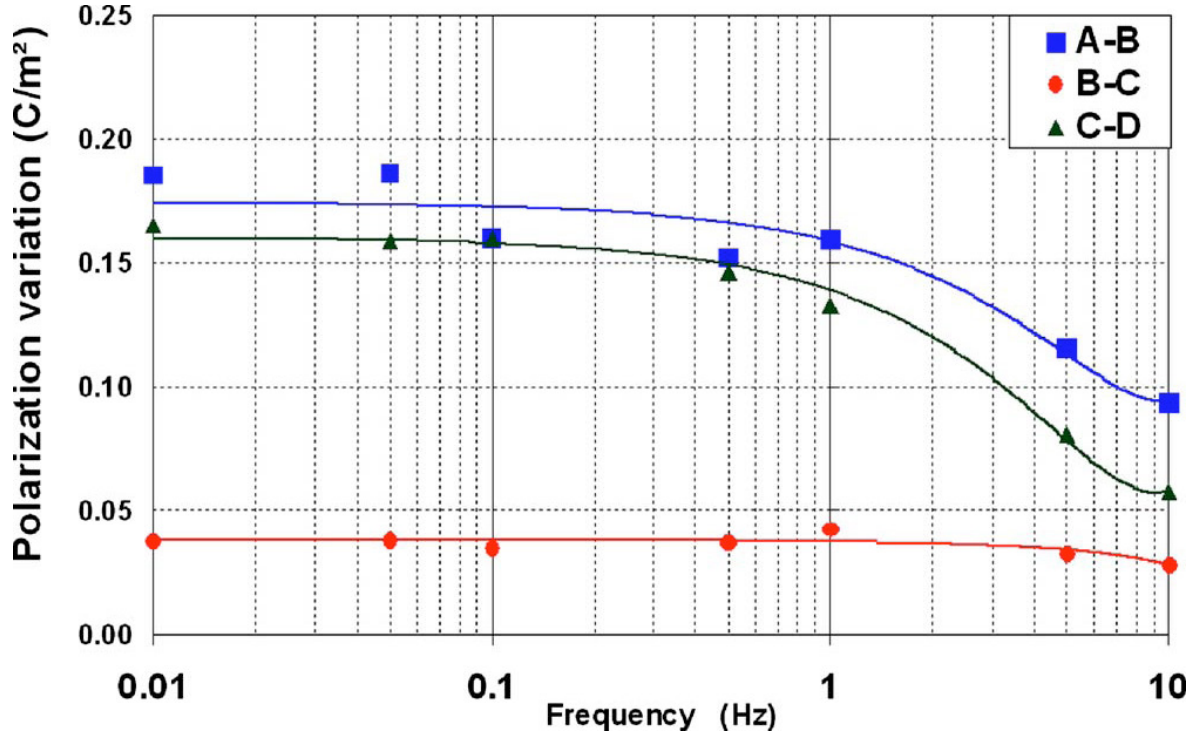

Fig. 3.22 (Color online) The polarization variation corresponding to each process. Blue squares: an increase in the electric field (AB path); red circles: a constant electric field (BC path); green triangles: a decrease in the electric field (CD path). The solid line has been added to indicate the evolution tendency with the frequency.

With these results, the inherent physical mechanism induced by the frequency on an energy harvesting cycle in PZN-4.5PT single crystals is starting to become clearer. At first, when applying the increasing electric field on the sample at 100 °C, the polarization variation occurred due to the R-O phase transition. It was also greatly influenced by the frequency of the electric field. As a relaxor single crystal, PZN-4.5PT required a sufficient amount of time to undergo the phase transition. If the frequency was too high, certain unexpected phenomena could take place: a polarization relaxation at the end of the first isothermal process (cf. **Fig. 3.20** with an Ericsson cycle at f = 10 Hz) and insufficient polarization. It was found that the polarization variation during the AB path at f = 1 Hz was 0.16 C m^{-2}, whereas at f =10 Hz, it decreased down to 0.09 C m^{-2}. The relaxation was not sufficient enough to obtain the same polarization variation prior to the constant electric field process. Moreover, the pyroelectric activity of the material below the electric field drove this process (BC path) and represented the key factor determining the harvested energy due to the fact that the maximum electric field was applied during this step. In this case, a low polarization variation could induce a large harvested energy.

In order to highlight this point, the pyroelectric coefficient during the constant electric field (BC path) was calculated using $p=(\partial D/\partial\theta)_E$ and data from **Fig. 3.22**. **Fig. 3.23** plots the pyroelectric coefficient for several frequencies. For an identical temperature variation (30°C), the pyroelectric coefficient was nearly stable around the mean value of 1250 μC m^{-2} K^{-1} from 0.01 to 1 Hz. However, a similar tendency appeared at frequencies above f =1 Hz in which range the pyroelectric coefficient decreased rapidly from 1250 to 934 μC m^{-2} K^{-1}. Between 1 and 10 Hz, the loss of the harvested energy was equal to 48.5 mJ cm^{-3}, i.e., a reduction of more than half the initial value. The difference in the polarization variation was mainly caused by the frequency effect. When increasing the frequency for the application of the electric field, the polarization time became shorter and the slope of the electric field steepened. Consequently, at the lowest frequency (0.01 Hz), there was sufficient time for the crystallographic structure change and the whole sample underwent phase transitions: R-O during the polarization process at lower temperature and O-T during the discharging processes at higher temperature.

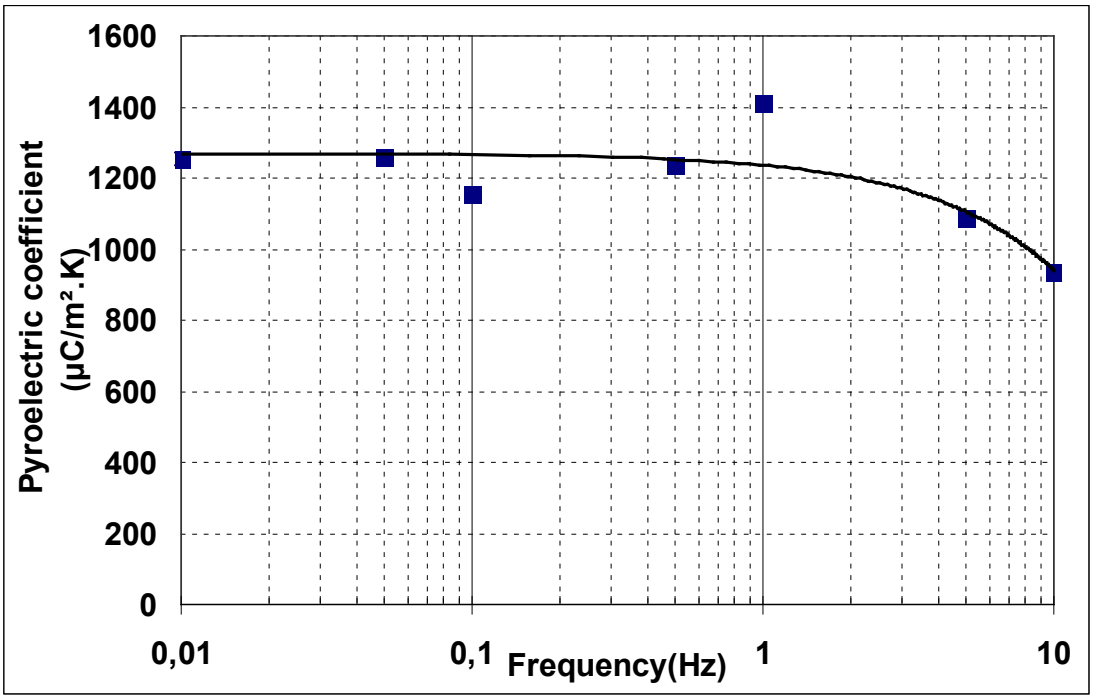

Fig. 3.23 The pyroelectric coefficient at a constant electric field (2 kV/mm^{-1}) for various frequencies. The solid line has been added to indicate the evolution tendency with the frequency.

Based on this set of phase transitions, both the polarization variations during the AB, CD paths and the pyroelectric coefficient during the BC path (orthorhombic phase) were at a maximum, as was the harvested energy. When increasing the frequency, a reduction in the polarization time resulted in an inadequate phase transition, a gradual decrease in the

polarization variation and, at f = 1 Hz, the achievement of a threshold value for the polarization time. When further increasing the frequency, only part of the crystalline unit cells took part in the phase transition from R to O during the first isothermal process. More importantly, during the constant electric field path, the incomplete phase transition led to a coexistence of the orthorhombic and rhombohedral phases in the sample. During the constant electric field process, the remaining rhombohedral phase was able to transit into the orthorhombic phase generating a positive current peak with the opposite sign to that of the pyroelectric peak. This was due to the fact that for the <110> direction, the rhombohedral to orthorhombic transition was associated with an increase in the polarization. As a consequence, the global pyroelectric coefficient weakened. The diminution of the polarization variations during the BC path gave rise to the emergence of a crossing between two isothermal processes for high frequencies. Consequently, the harvested energy of the Ericsson cycle decreased.

3.3.4 Asymmetric Ericsson Cycle

Based on the analysis of the experimental results above, it was found that the electric field frequency affected the phase transition and polarization in the whole Ericsson cycle and also significantly influenced the harvested energy. Thus, one can imagine that the Ericsson cycle can be modified by applying an electric field with different frequencies in the AB and CD paths. Indeed, **Fig. 3.24** shows an interesting Ericsson cycle. Two kinds of asymmetric cycles were measured. The first one, denoted the L-H Ericsson cycle, corresponded to a low frequency f=0.01 Hz for the electric field applied during the AB path and a high frequency f=1 Hz for the electric field applied during the CD path. The second cycle was equivalent to the first but with an opposite frequency sequence of the electric field. It was denoted the H-L Ericsson cycle. As can be seen in **Fig. 3.24**, owing to the frequency effect on the polarization variation, a crossing was once again observed in the L-H Ericsson cycle, which negatively influenced the harvested energy. In contrast, the H-L Ericsson cycle greatly promoted the harvested energy. When integrating the whole Ericsson cycle, the harvested energy even increased up to 106 mJ cm^{-3}, i.e., twice that of the supplied electric energy. The H-L Ericsson cycle exhibited a surprising capability for energy harvesting. From this cycle, advantage was taken to the fact that all the material was in the orthorhombic phase. This way, the pyroelectric activity was as high as possible. When decreasing the electric field, the lower the frequency, the higher were the polarization variations. This led to the harvested energy increasing.

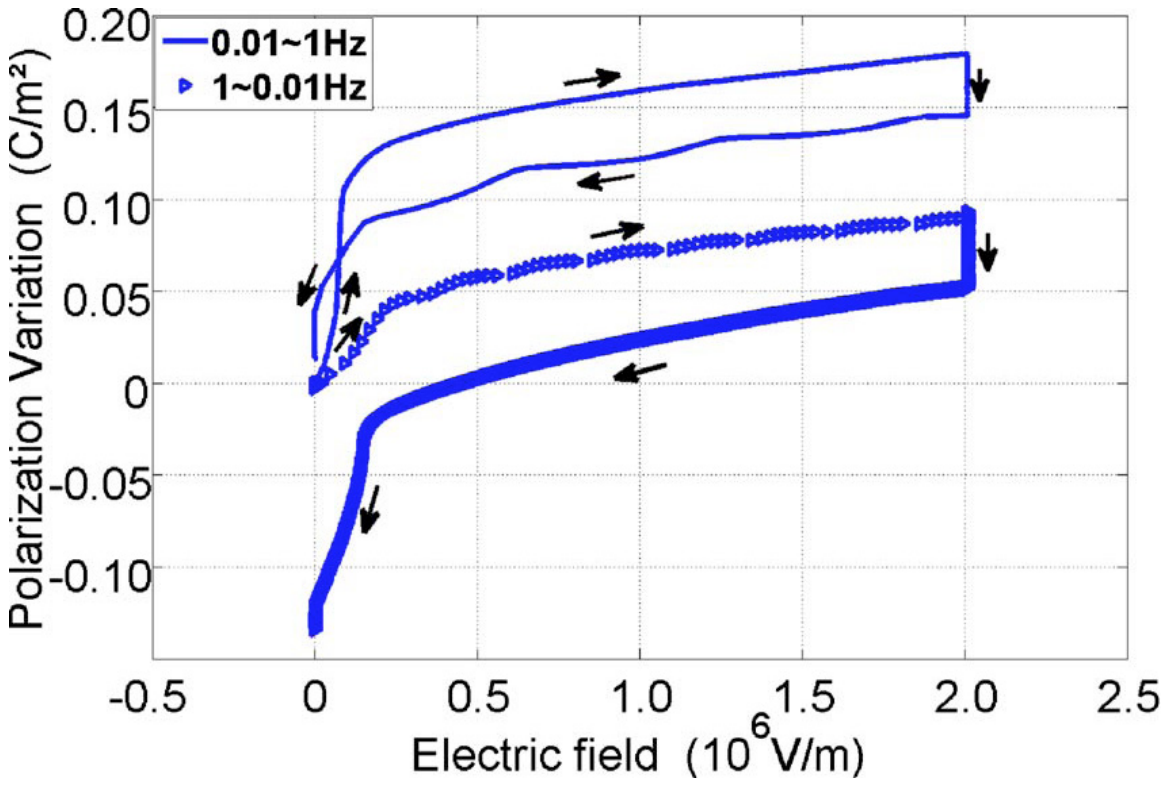

Fig. 3.24 (Color online) The polarization vs. the electric field for a modified experimental Ericsson cycle. Solid line: L-H Ericsson cycle; triangles: H-L Ericsson cycle.

3.4 Conclusions

This chapter focused on the pyroelectric energy harvesting on relaxor ferroelectric single crystal. Firstly, we presented the general definition of ferroelectric, including their micro- and macro domain regions. Phase transition is of more interest for energy harvesting, accordingly introduced in detail. The temperature effect on phase transition and the bipolar or unipolar P-E loops were investigated for detecting the appropriate parameters of working temperature and frequencies in Ericsson cycle. The experimental work has mainly been focused on two aspects of pyroelectric energy harvesting by means of Ericsson cycles on PZN-4.5PT single crystals.

A. The effect of the electric field frequency on energy harvesting

Considering the experimental measurements and theoretical analysis presented above, it was confirmed that energy harvesting depended to a large extent on the frequency of the electric field. The maximum harvested energy, corresponding to a value of 86 mJ cm^{-3}, was obtained at the lowest frequency f = 0.01 Hz. Compared with the Ericsson cycle at the highest

frequency (10 Hz) for which the harvested energy only reached 30 mJ cm^{-3}, the difference was as much as 56 mJ cm^{-3} between the two cycles for an equivalent temperature variation.

In order to precisely evaluate the frequency effect, the Ericsson cycle was measured for frequencies descending from 10 to 0.01 Hz, and the inherent physical mechanism of the frequency effect on energy harvesting cycle was analyzed. The phase transition at each process (R-O during the AB path and O-T during the CD path) due to domain engineering was a key factor for promoting the energy harvesting. Other factors, such as applied electric field, and relaxation of the polarization at high frequency, also influenced the energy harvesting to different degree. Furthermore, with an increasing frequency, an inadequate phase transition and relaxation occurred, which led to the coexistence of the orthorhombic and rhombohedral phases. These two phases influenced the energy harvesting adversely, and consequently, the harvested energy displayed a decreasing tendency with regard to the frequency of the electric field.

B. Asymmetric Ericsson cycles with varying frequencies

By applying the electric field with different frequencies during the two isothermal processes, two kinds of asymmetric Ericsson cycles were implemented: an L-H cycle and an H-L one. With the H-L Ericsson cycle, the crossing of the two isothermal processes could be avoided and the harvested electric energy reached a maximum of 106 mJ cm^{-3}. The H-L Ericsson cycle thus optimized the energy harvesting and constituted the best choice for energy harvesting when using a pyroelectric effect.

C. Summary of pyroelectric energy harvesting

In this work, author made a great deal of effort for thermal energy harvesting by pyroelectric effect. It is mainly focused on PZN-4.5PT single crystal, benefiting form the FE-FE phase transition and frequency effect. We developed H-L asymmetry Ericsson modeling and consequently improved harvested energy greatly. Meanwhile, there are also other groups make great deals of contribution for this subject. So here, we make a brief summary of the development on pyroelectric energy harvesting over the recent years in **Table 3.1**.

As we can see in the table, under the same conditions (e.g., temperature range, electric field) our work shows an obvious advantage in harvested energy. For example, comparing to the work on PMN-10PT ceramics, our work on PZN-4.5PT single crystal can harvest more energy, further increases the conversion ratio greatly (around 2.18 in H-L Ericsson cycle) due to the decrease of injected energy. Whereas, it was developed rapidly on pyroelectric energy harvesting from PVDF-base copolymers recently for its outstanding pyroelectric coefficient, their gratifying results provide us a hint that by P(VDF-TrFE) copolymers, perhaps, we can

find another solution to make further improvement on energy harvesting through the study on their key parameters (e.g., frequency or temperature effect, transition, thermodyelectric cycle etc.), it would be a next promising avenue to pyroelectric energy harvesting.

Material	**Temperature range (°C)**	**Harvested energy (mJ/cm^3)**	**Electric field (kV/mm)**	**Type of cycle**	**Author**
PZN-4.5PT<110>	100-130	106	2	H-L Ericsson cycle	Zhu et al. 2009[122]
PMN-10PT ceramics	35-65	80	2	Ericsson cycle	Sebald et al. 2008[76]
PZN-4.5PT<110>	105-140	72	2	Ericsson cycle	Guyomar et al. 2008[77]
P(VDF-TrFE) (60/40)	69.3-87.6	130	20.2-37.9	Ericsson cycle	Nguyen et al. 2010[80]
P(VDF-TrFE) (60/40)	25-110	521	20-50	Ericsson cycle	Navid et al. 2011[81]

Table 3.1 Summary of the development on pyroelectric energy harvesting.

Chapter 4
Energy Harvesting by Nonlinear Capacitance Variation for Relaxor Ferroelectric P(VDF-TrFE-CFE) Terpolymer

The polyvinylidene fluoride (PVDF) and its derivative polymers have attracted a great deal of attention and been widely used as dielectric, piezoelectric, and ferroelectric devices because they are flexible, light weight, large strain, fast response speed and can be conformed to complicated shapes. It is found that the poly(vinylidene fluoride-trifluoroethylene) [P(VDF-TrFE)] copolymers under a proper high-energy electron irradiation treatment exhibit very little room temperature polarization hysteresis and a high electrostrictive strain[123]. In addition, the modified copolymers possess a relatively high room temperature dielectric constant and exhibit many features typical of ferroelectric relaxors[124-125]. All these results demonstrate that the properties of P(VDF-TrFE)-based polymers can be modified and improved markedly by the introduction of 'defect' structures. In this chapter, we present the electrostatic energy harvesting on another polymer based on the concept of the defect structure modification of the P(VDF-TrFE) polymer system, poly(vinylidene fluoride-trifluoroethylene-chlorofluoroethylene) terpolymer [P(VDF-TrFE-CFE)].

4.1 Introduction

In the last chapter, we presented the thermal energy harvesting by pyroelectric effect of single crystal. With the development of miniaturization of integration, the aim of energy harvesting is to power smaller and smaller devices, on the micro-scale, the electrostatic force

becomes significant and so is suitable for electric power generation. Therefore electrostatic energy conversion is of significant interest. Meninger et al. presented a MEMS (Micro-Electro-Mechanical Systems) vibration to an electricity converter based on electrostatic energy harvesting by a variable capacitor[34]. Mechanical vibrations exert an electrostatic force changing the distance between two electrodes (leading to a variable capacitance). With an appropriate energy conversion cycles, as introduced in the first chapter, e.g., charge constrained conversion or voltage constrained conversion, electrical energy can thus be harvested. It is easy to discover that, in essence, these two electrostatic energy conversion cycle is vary similar to the two basic thermodynamic cycles: Stirling cycle and Ericsson cycle. We are still focusing on Ericsson cycle (voltage constrained cycle) in the present case. In order to avoid the external mechanical force, electrostatic energy harvesting can be performed by nonlinear capacitance variation under temperature variation.

In this work, the variable capacitance is realized by dielectric terpolymer P(VDF-TrFE-CFE) due to the dielectric permittivity variation with temperature. Recent experimental results have showed that by defect modification, either through copolymerization with a bulky monomer such as CFE or CTFE (chlorotrifluoroethylene) to form a terpolymer or by direct high-energy irradiation on copolymer films, the normal ferroelectric P(VDF-TrFE) polymer can be converted into a ferroelectric relaxor, which exhibit a large dielectric constant and a very little polarization hysteresis at room temperature[85,126]. Accordingly, the terpolymer P(VDF-TrFE-CFE) 61.3/29.7/9 mol% is chosen to be the active material of this work.

4.2 Material Consideration

4.2.1 PVDF and its Copolymers

Poly(vinylidene fluoride) (PVDF)-based polymers have been some of the most widely researched semicrystalline polymers over the past several decades, due mostly to their ability to exhibit much higher ferroelectric properties and polarization response under an electric field, in comparison with other soft materials. PVDF is a rather typical semicrystalline polymer of approximately 50% crystallinity and possesses most of the same characterisitics of other semicrystalline polymers that make them so desirable for such a wide array of applications. PVDF is commercially synthesized via free radical polymerization at high temperature (50-150°C) and high pressure (10-300 atm), and has a chemical structure of (-

CH_2-CF_2-) repeat units, providing for large chain flexibility due to the very linear structure but also providing some constraints on atomic arrangement due to the high repulsive forces of the fluorine atoms. The most common polymerization process is emulsion or suspension using water as a reaction medium. Since the monomer units of PVDF have a directionality (CH_2 denoted as "head" and CF_2 as "tail"), typically 5% of the monomer units enter the growing chain with a reverse orientation, leading to head-to-head and tail-to-tail defects.

Fig. 4.1 shows the molecular conformations and lattice parameters of PVDF polymer[127]. It has four phases known as phase I(β), phase II (α), phase III (γ), and phase IV (δ)[128-129], α phase is the most common, thermodynamically stable, and easily obtainable phase. The β – phase crystallizes with the molecules being configured in an all-trans (TTTT) zig-zag conformation, giving this phase polarity due to the parallel packing of polymer chains, i.e., the C-F dipoles are all aligned in the same direction. This gives the β-phase crystals a spontaneous lattice polarization which is necessary to observe ferroelectricity in PVDF. The γ-phase is intermediate between the α and β-phases consisting of a (T_3GT_3G') conformation. A fourth polymorph of PVDF is the δ-phase, which is a polar version of the α-phase, with essentially the same unit cell parameters but a varying symmetry.

PVDF is the first organic material found that exhibits significant piezoelectric and ferroelectric properties. For many years, there was debate over the origins of the piezoelectric and pyroelectric properties in PVDF. The arguments seem to have reached the conclusion that the properties primarily arise from the dipole orientation, rather than from trapped space charge. The discovery of the enhancement of piezoelectric activity in PVDF in 1969, by Kawai[130], led to the revelation of other properties, such as pyroelectricity[131] and ferroelectricity properties. Although there is no obvious evidence of the Curie transition in PVDF, the existence of polarization loops, together with polarization reversal and the switching phenomena, is generally accepted as proof of ferroelectricity in PVDF.

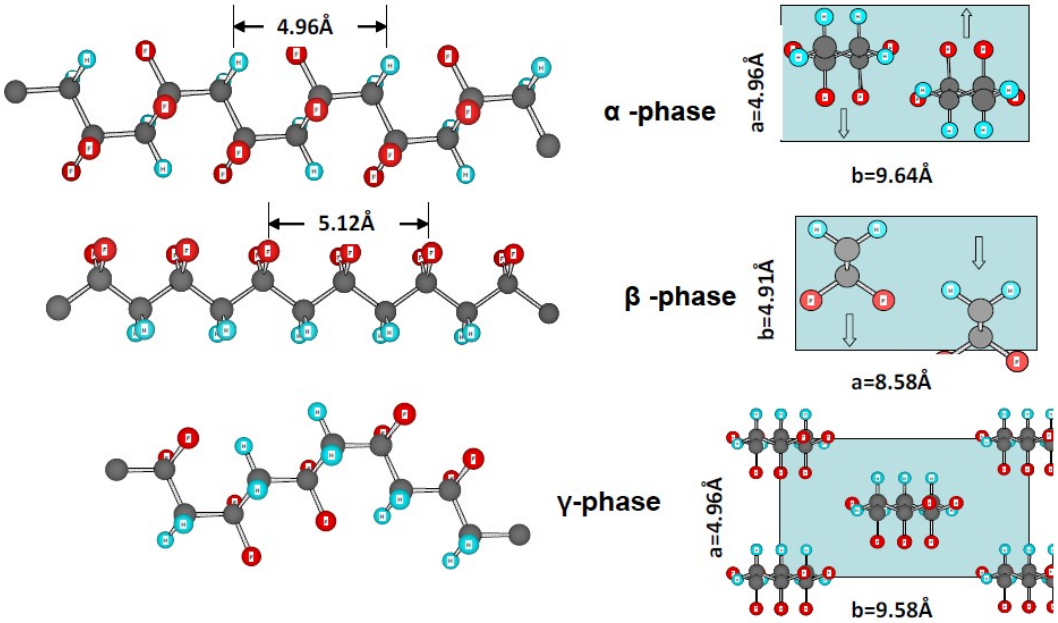

Fig. 4.1 Molecular conformations and unit cells of the three common polymorphs of PVDF.

Although the PVDF exhibits strong piezoelectric and pyroelectric properties, one of the downfalls of utilizing PVDF as a ferroelectric material is the fact that it does not easily crystallize into the ferroelectric β-phase without some specialized processing such as uniaxial drawing. This problem was addressed with investigations on how to alter the stereochemistry of the PVDF chain such that it could naturally crystallize into the polar phase. Some improvement has been achieved by synthesizing copolymers of vinylidene fluoride with trifluoroethylene (TrFE), tetrafluoroethylene (TFE), or vinyl fluoride (VF), and indeed, some of these copolymers exhibit even higher piezoelectric and pyroelectric properties.

P(VDF/TrFE) is the most studied copolymer because of its relatively high piezoelectric response and thermal and chemical stability[132]. In the early of 1980's, Yagi et. al.[133] investigated a ferroelectric to paraelectric (F-P) phase transition at Curie temperature θ_c in P(VDF/TrFE) evidenced by peaks in the dielectric constant and piezoelectric activity and also with changes in structure evidenced by x-ray and infrared analysis. This was the first such phase transition reported in a polymeric material, and it has been found to be affected by several factors, especially the VDF content. A phase diagram for the compositions of P(VDF-TrFE) has been developed as shown in **Fig. 4.2**[134]. It can be seen that the copolymers with composition of VDF<80% and TrFE>20% undergo a phase transition below the melting[127]. The phase transition T_C of all VDF/TrFE copolymers occurs at high temperatures (>60°C). Neese et. al.[85] have found that, among all of available P(VDF-TrFE) compositions, the polymer with 55/45 mol% exhibits the lowest F-P transition temperature (~70°C), which is

useful because we are interested in practical applications at near-room-temperature. They provided the dielectric permittivity of P(VDF-TrFE) 55/45% copolymers with different frequencies as in **Fig. 4.3**. The sharp dielectric constant peak demonstrates that it is a typical normal ferroelectric polymer.

As we stated above, the phase transition temperature θ_c of all VDF/TrFE copolymers occurs at high temperatures (>60°C) and the transition is relatively sharp. In addition, the early experimental results showed a large hysteresis (remnant polarization) associated with the phase transition, which is not desirable for practical applications. Therefore, many attempts have been devoted to achieving the general goal of broadening and reducing the phase transition to room temperature and to minimizing or eliminating the hysteresis[135-137]. Zhang et al. found that the dielectric peak, which is associated with F-P transition in the normal ferroelectric P(VDF-TrFE), is broadened markedly and moved to near room temperature for the irradiated copolymer[136]. In addition, they also reported that P(VDF-TrFE) 50/50 film measured at room temperature before irradiation exhibited a well-defined ferroelectric polarization hysteresis loop. In contrast, the sample irradiated with 4×10^5 Gy at 120°C exhibited a slim hysteresis loop[137].

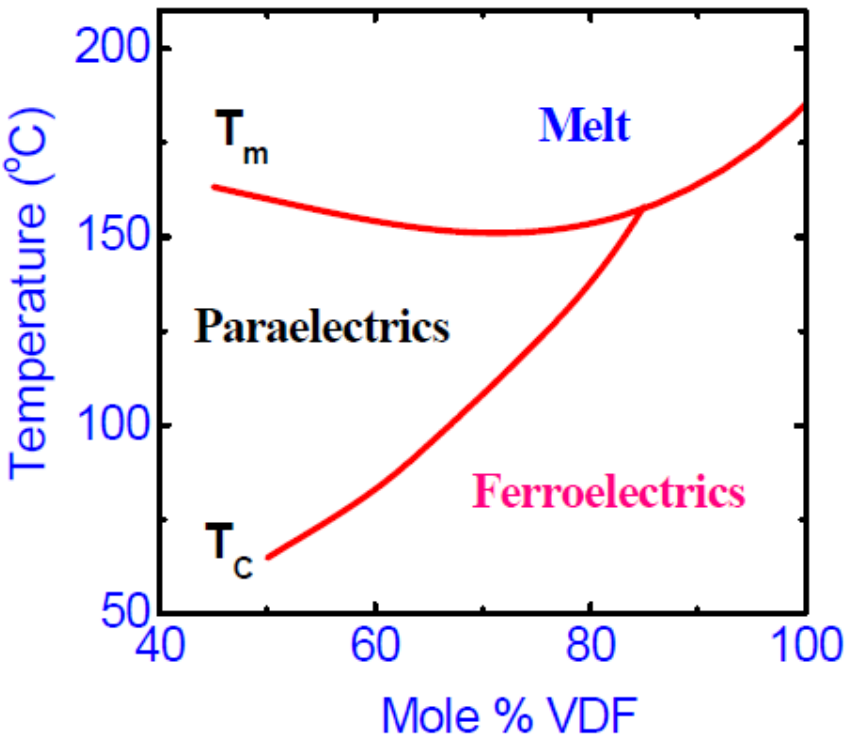

Fig. 4.2 P(VDF-TrFE) phase diagram[134].

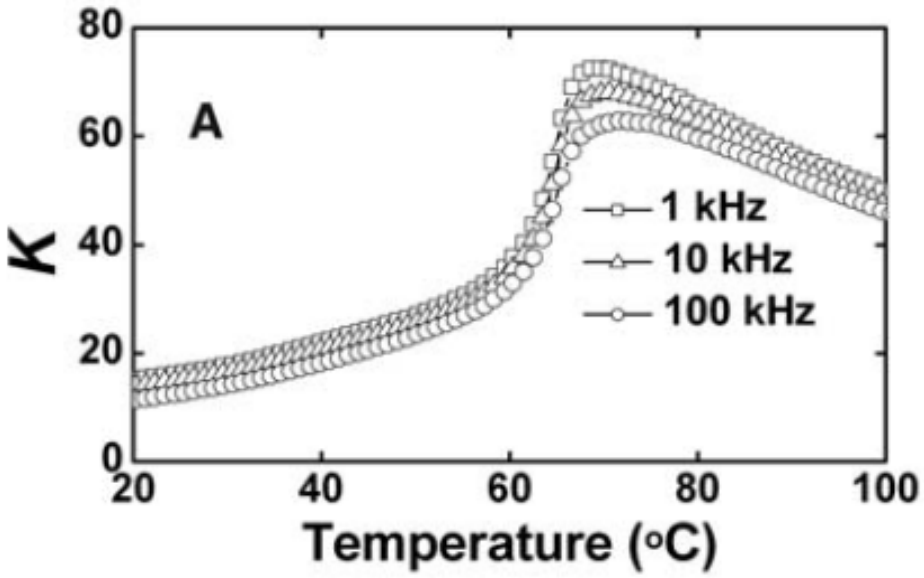

Fig. 4.3 The dielectric constant of P(VDF-TrFE) 55/45 mol% copolymer films as a function of temperature measured at frequencies of 1, 10, and 100 kHz[85].

4.2.2 PVDF-based Terpolymer

Although high-energy irradiations can be used to convert the normal ferroelectric copolymer P(VDF-TrFE) into a relaxor ferroelectric with low phase transition temperature and low ferroelectric hysteresis, the irradiations also introduce many damages to the copolymer, for instance, the formation of cross-linking, radicals, and chain scission. From the basic ferroelectric response consideration, the defect structure modification of the ferroelectric properties can also be realized by introducing randomly in the polymer chain a third monomer, which is bulkier than VDF and TrFE. Compared with the high-energy electron irradiation, the terpolymer approach to modify the copolymer to ferroelectric relaxor is more attractive since it reduces the manufacture cost and significantly simplifies the processing steps. In addition, it greatly reduces the undesirable side effects introduced by the irradiation to the polymers.

Zhang et al. developed a method of converting the polymer to a relaxor ferroelectric by introducing defects into the P(VDF-TrFE) copolymers, i.e., terpolymer containing the chlorofluoroethylene (CFE,-CH_2-CFCl-) or chlorotrifluoroethylene) (CTFE) as the ter-monomer[126,136]. The introduction of the third monomer into the polymer chain serves to break up the ferroelectric domains into local nano-polar regions surrounded by an amorphous matrix, thereby reducing their size. The resulting nano-polar regions are more mobile and increase the polarization response and overall pomittivity. Random defect introduction, as in the irradiated copolymer samples, broadens the ferroelectric transition and reduces the ferroelectric-

paraelectric transition temperature. The random incorporation of the bulky third monomer into the polymer chains forces a conformation change from the all-trans or conformation to the transgauche (TG) and T_3G conformations. Addition of defects in the form of chemical monomers, CFE or CTFE which are copolymerised with the VDF-TrFE, eventually favour the TG conformation and eliminate the normal ferroelectric phase, leading to a relaxor ferroelectrics. By co-polymerization of CFE or CTFE with the P(VDF-TrFE), the polymer could be converted to a relaxor ferroelectric which eliminated the polarization hysteresis (dielectric heating) at room temperature associated with the change of polarization in **Fig. 4.4**[134]. These relaxor-ferroelectric terpolymers P(VDF-TrFE-CFE) and P(VDF-TrFE-CTFE) exhibit a room temperature dielectric constant greater than 50. These values are among the highest ones reported in the literature, and makes the terpolymers suitable in our study for energy harvesting by nonlinear capacitance variation.

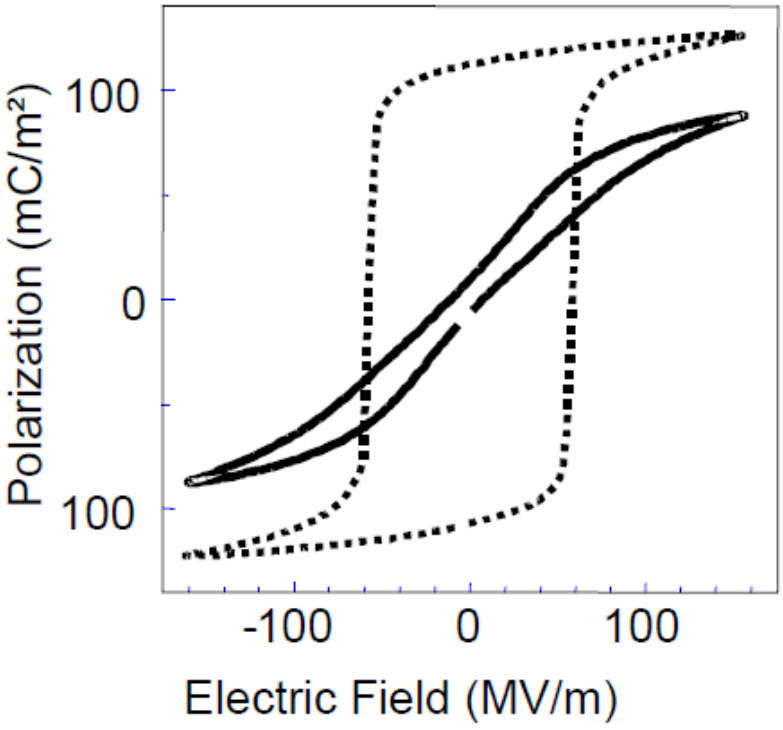

Fig. 4.4 Comparison of the polarization hysteresis of the normal ferroelectric polymer (dashed curve, large hysteresis) and relaxor ferroelectric polymer (black curve) at room temperature.[134]

4.2.2.1 Terpolymer P(VDF-TrFE-CTFE)

Xu et al. synthesized and evaluated terpolymer P(VDF-TrFE-CTFE) using the bulk polymerization method[138]. As the bulky and less polar termonomer CTFE is randomly

introduced into P(VDF-TrFE) normal ferroelectric crystals, there are three main features in the dielectric data of the polymer due to the addition of CTFE observed from **Fig. 4.5**: (1) the original FP transition peak of the copolymer is moved to room temperature; (2) the peak becomes much broader and its position shifts progressively with frequency towards higher temperature; (3) there is no thermal hysteresis in the dielectric data, i.e., the broad dielectric peak stays at the same temperature when measured in the heating and cooling cycles. They also measured the polarization hysteresis loops at room temperature and -40°C in **Fig. 4.6**[138]. The terpolymer exhibits a slim polarization loop at room temperature, and as the temperature is lowered, the coercive field increases and the polarization at maximum electric field decreases. All these features are remarkably reminiscent of ferroelectric relaxor behaviour. In addition, the polarization reduction with temperature proved that, at lower temperature range (lower than FP transition temperature), the dielectric affect shows overwhelming advantage, while the pyroelectric effect becomes negligible. It gives a strong proof for our study in energy harvesting from capacitance variations by lowering the temperature of terpolymer.

Large electrostrictive strain can be also induced by external electric field in P(VDF-TrFE-CTFE), the nonlinear behaviour in strain change on cast film solution which shows both the quadratic dependence of strain at low electric fields and the saturation in strain as the polarization approaches saturation at high fields, has been observed and measured by Petchsuk[139].

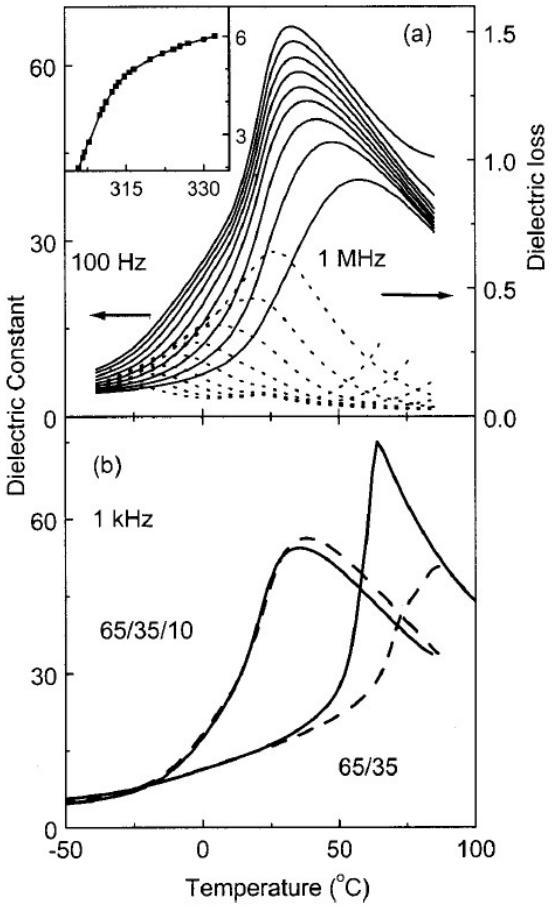

Fig. 4.5 Terpolymer P(VDF-TrFE-CTFE) 65/35/10 mol%.
(a) Dielectric constant (solid curves) and dielectric loss (dashed curve) as a function of temperature at frequencies (from top to bottom for the dielectric constant and for the dielectric loss from bottom to top): 100, 300, 1, 3, 10, 30 kHz, 0.1, 0.3, and 1 MHz. (b) Dielectric constant at 1 KHz of the 65/35/10 terpolymer and 65/35 copolymer for both heating (dashed curves) and cooling (solid curves) cycles measured at room temperature[138].

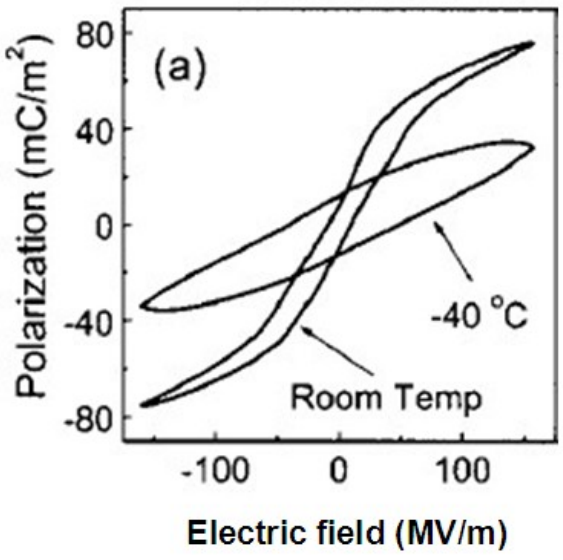

Fig. 4.6 Polarizaiton hysteresis loop measured at 20°C and -40°C and 10 Hz on terpolymer P(VDF-TrFE-CTFE) 65/35/10 mol%.[138]

4.2.2.2 Terpolymer P(VDF-TrFE-CFE)

There were also experimental results on terpolymer P(VDF-TrFE-CFE). Zhang et. al compared the terpolymer P(VDF-TrFE-CFE) with P(VDF-TrFE-CTFE), and concluded that the CFE is more effective on improving their electromechanical response compared with CTFE, shown in the following aspects: (1) In the containing CFE, 4-5 mol% of CFE seems to be adequate to nearly eliminate the polarization hysteresis, while in the terpolymers containing CTFE, nearly 10 mol% is required. (2) P(VDF-TrFE-CFE) 62/38/4 mol% terpolymer exhibits a much higher elastic modulus in comparison with P(VDF-TrFE-CTFE) 65/35/10 mol% terpolymer, resulting in much higher elastic energy density and electromechanical coupling factor in the P(VDF-TrFE-CFE) terpolymer[136].

Klein et al. revealed that the addition of CFE leads to two types of crystalline regions within the polymer, where a non-polar phase coexists with a polar phase. At high CFE mol% (>8.5 mol%) in the compositions range of VDF/TrFE mole ratio between 64/36 to 75/25, the polar phase region is no longer detectable, indicating a complete conversion to the relaxor ferroelectric phase and the terpolymer exhibits the highest strain level with very little hysteresis. They compared the measured strain as a function of the applied field for two compositions of 65/35/8.6 mol% and 75/25/5.3 mol% in **Fig. 4.7**[140]. The presence of the polar-phase in the terpolymer of 75/25/5.3 mol% greatly reduces the electrostrictive strain in the polymer. On the other hand, increasing CFE content causes reduction in crystallinity, which will affect the elastic modulus and the induced polarization level of the polymer [140]. There competing effects determine the desired terpolymer compositions for given application.

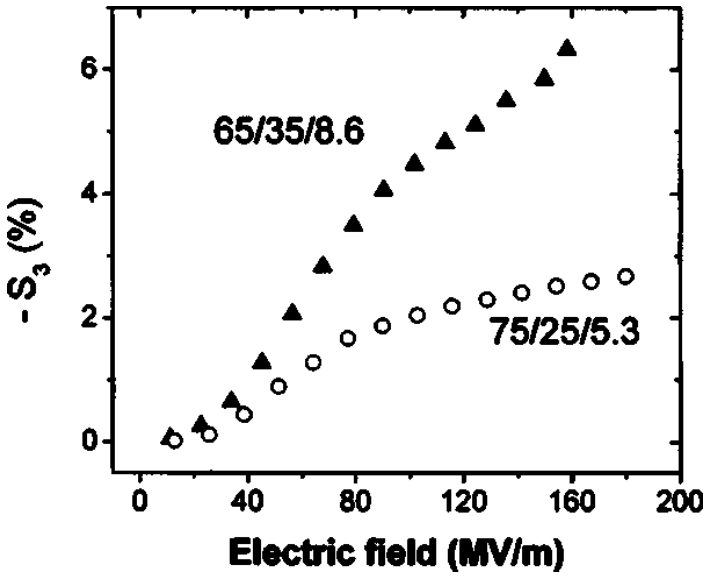

Fig. 4.7 Thickness strain for unoriented samples of composition 65/35/8.6 mol% and 75/25/5.3 mol% VDF/TrFE/CFE.[140]

In 2008, Neese et al. studied the other important property on terpolymer P(VDF-TrFE-CFE)--Electrocaloric effect (ECE)[85]. As we have presented before, electrocaloric is an effect associated with the temperature variation and occurred on the most dielectric materials. A large ECE requires a large entropy change associated with polarization change, and the dielectric material must be capable of generating large polarization changes. In regard to it, ferroelectric polymers are better than ceramics due to the ordering and disordering of dipoles which can result in a large entropy change. The relaxor ferroelectric polymers have the potential for processing attractive ECE properties due to their large polarizability, small polarization hysteresis, and dielectric peak near room temperature. Neese et al. concluded that with an electric field of 307 MV/m at 55°C applied on terpolymer P(VDF-TrFE-CFE) 59.2/33.6/7.2 mol%, temperature variation $\triangle T = 12°C$ and entropy change $\triangle S=55$ J/(kgK) were obtained as presented in **Fig. 4.8**. Especially, the entropy change is about 7 times greater than that in the ferroelectric ceramics and 2 times greater that the best MCE materials[85]. Their study indicates that the large entropy change can be achieved associated with the electric field-induced dipole ordering – disordering (O-D) processes at temperature near O-D transitions. This transition becomes the critical technique during the process of energy harvesting on terpolymer that we will discuss it in the following part.

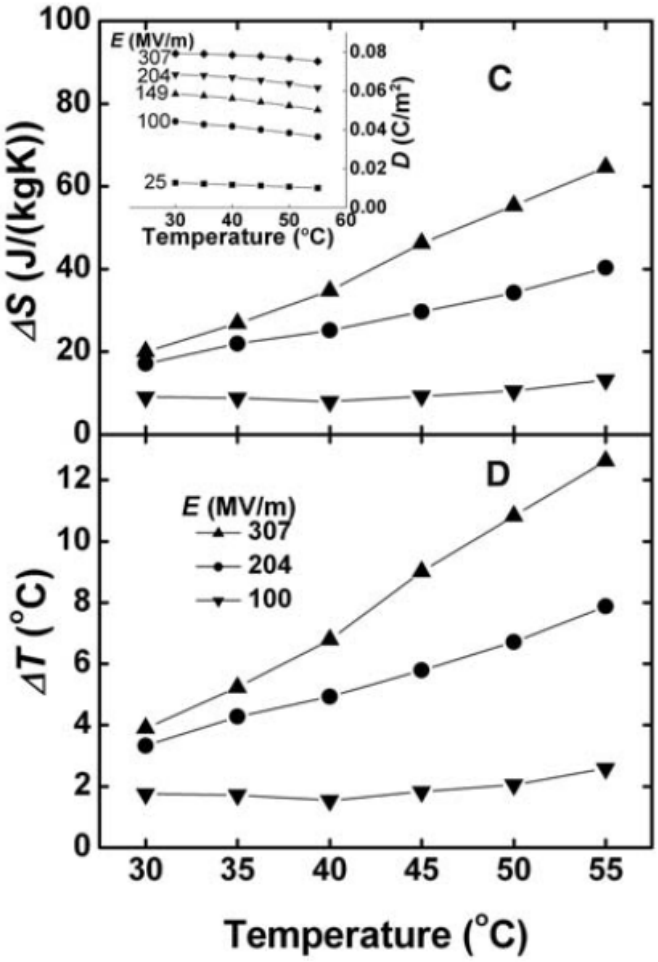

Fig. 4.8 △S and △T vs. temperature for P(VDF-TrFE-CFE) (59.2/33.6/7.2 mol%).[85]

In view of the favorable properties above, low ferroelectric hysteresis, the temperature of the dielectric constant peak shifts to room temperature, large polarization variation induced by the O-D transition, high elastic energy density of PVDF-based terpolymer make it attractive for energy harvesting by temperature variation. Moreover, Ren et al.[141] also reported energy harvesting using a ferroelectric polymer, possessing high electromechanical response and elastic energy density, which make it possible to generate high electrical energy density and attractive for the active energy harvesting scheme. This study shows that combining the active energy harvesting scheme and high electromechanical response of the polymer yields a harvested electric energy density of ~40 mJ/cm^3 with a 10% efficiency at very low frequency.

The outstanding properties of electroactive terpolymer, such as high room temperature dielectric constant, high polarization variation induced by temperature, and high electrostriction etc., make it seem to be the promising candidate for active harvesting of energy, no matter from thermal or mechanical energy sources. The investigation of polymers

opens up novel possibilities for multi-source energy harvesting technique. In view of thermal energy harvesting, the use of copolymer P(VDF-TrFE) to harvest waste heat by pyroelectricity has been explored both experimentally and theoretically[67,80-81]. In this part, we are interested in energy harvesting from nonlinear capacitance variation by temperature on terpolymer P(VDF-TrFE-CFE)[142].

This part focused on the the literature review on PVDF-based polymers, including their crystallinity, molecular conformations and phase diagram etc. We knew that, by introducing defects, such as CFE, into the P(VDF-TrFE) copolymers, polymers could be converted to a relaxor ferroelectric terpolymers, which exhibit low ferroelectric hysteresis. Because of these favourable properties above, the relaxor P(VDF-TrFE-CFE) becomes attractive to for energy harvesting by temperature variation.

4.3 Energy Harvesting by Nonlinear Capacitance Variation for a Relaxor Ferroelectric P(VDF-TrFE-CFE) Terpolymer

4.3.1 Introduction

Harvesting energy from ambient environments is an emerging technology attractive for many applications, ranging from portable electric devices to renewable energy. These generators are highly reliable, silent, and environmentally friendly electrical power sources. With the rapid development of portable electronics and wireless sensors, energy harvesting, i.e., the process of extracting energy from ambient energy and converting it to available electrical energy, has attracted more and more interest in order to find an alternative to traditional energy harvesting devices. Of the available ambient energy sources, which include, for instance, light energy, mechanical energy, and thermal energy, most of innovative solutions deal with energy harvesting from vibration, but very few deal with harvesting with temperature variation. Therefore, the advantages together with the capability of recycling waste heat as an energy source make them as an attractive renewable power supply.

In the last several decades, thermoelectric devices have received significant attention[92]. They make use of the Seebeck effect to directly convert a steady-state temperature difference to electricity at the junction of two dissimilar metals or semiconductors into electrical energy.

However, the precondition of steady-state heat flow greatly restricts the practical applications. On the contrary, pyroelectric energy conversion directly converting time-dependent temperature oscillations to electricity could be promising owning to the university of this temperature mode, by applying a proper thermodynamic cycle, the high conversion efficiency would be obtained. Presently, it is found that thin polymer films have enormous potential for energy harvesting from heat, due to their characterization such as small volume possession, light weight, flexibility, low cost, tough quality. In 2010, Nguyen et al. developed the pyroelectric energy converter using copolymer 60/40 P(VDF-TrFE) and based on Ericsson cycle[80]. A maximum energy density of 130 mJ/cm^3 was achieved at 0.061 Hz frequency with temperature oscillating between 69.3 and 87.6°C ($\triangle$T=18.3°C). In 2011, Navid et al. improved this energy converter by changing the mode of temperature change[81]. They implemented the Ericsson cycle by successively dipping the films in cold and hot silicone oil baths at 25 and 110°C, and compared three different copolymer samples: commercial purified, and porous films. A maximum energy density of 521 mJ/cm^3 and 426 mJ/cm^3 per cycle were produced by commercial and purified films, respectively, under applied electric fields ranging between 20 and 50 kV/mm, and a maximum energy density of 188 mJ/cm^3 per cycle under electric fields between 20 and 40 kV/mm.

With the development of miniaturization of integration, the aim of energy harvesting is to power smaller and smaller devices, and electrostatic energy conversion is of significant interest and so is suitable for micro-scale electrical power generation. Meninger et al. presented a MEMS (Micro-Electro-Mechanical Systems) vibration to an electricity converter based on electrostatic energy harvesting by a variable capacitor. Mechanical vibrations exert an electrostatic force changing the distance between two electrodes (leading to a variable capacitance)[34]. With an appropriate thermodynamic cycle, electrical energy can thus be harvested.

Having taken into account the statement above, a variable capacitance is the critical element for electrostatic energy harvesting. To our best knowledge, the dielectric material can be considered as a capacitor by sandwiched between metallic electrodes, and its dielectric constant is the function of temperature, based on above, we proposed that electrostatic energy harvesting on a relaxor ferroelectric P(VDF-TrFE-CFE) terpolymer, the variable capacitance could be achieved by the dielectric permittivity variation with temperature.

4.3.2 Preparation of Terpolymer P(VDF-TrFE-CFE)

The terpolymer films were prepared through a solution casting method. The terpolymer P(VDF-TrFE-CFE) 61.3/29.7/9 mol%, supplied by PIEZOTECH, France, was firstly dissolved in N-dimethylformamide by stirring at room temperature for one day. Put the uniform solution opened in the vacuum for removing the bubbles. Then deposited the film onto a plat of glass by the solution casting method using a doctor blade applicator (Elcometer 3700). Subsequently put it into the oven of 60°C for one day. After which the film were annealed at 85°C for 6 h in a vacuum oven to remove residual solvent. Gold electrodes were sputtered on the two surfaces of the 20-µm films which was stuck to a steel substrate as shown in **Fig. 4.9**, for accelerating heat exchange during the temperature variation step of energy harvesting cycle. The results presented below were obtained at least on five samples.

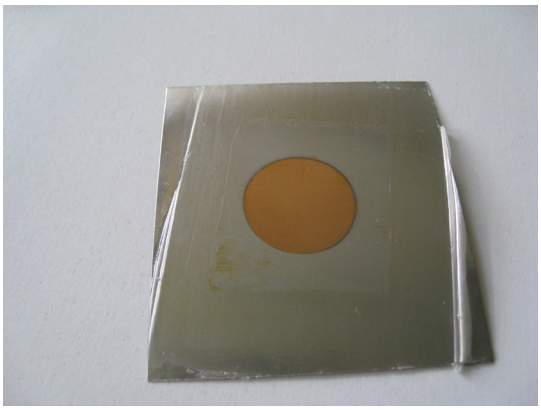

Fig. 4.9 Sample used in this study: P(VDF-TrFE-CFE) terpolymer film stuck to steel substrate.

4.3.3 Principle of Electrostatic Energy Conversion

In the first chapter, we have presented generally the electrostatic energy conversion and its two possible conversion cycles: charge constrained and voltage constrained cycles. We put the scheme of cycles below again in order to quantitatively discuss their capability of energy harvesting on P(VDF-TrFE-CFE) 61.3/29.7/9 mol% terpolymer.

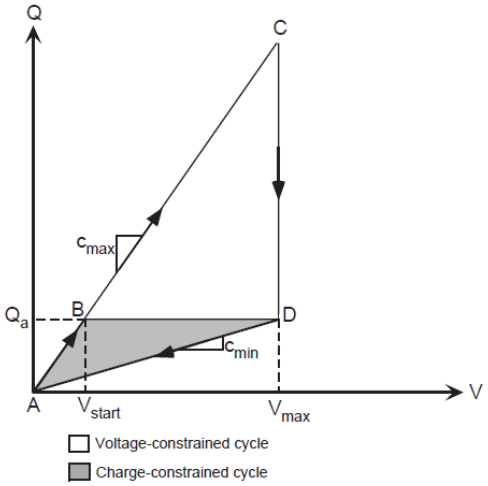

Fig. 4.10 Scheme of electrostatic energy conversion cycles.[34]
(Same as **Fig. 1.7** for reading easily)

4.3.3.1 Charge Constrained Conversion (Stirling Cycle)

For the charge constrained case, it is the cycle analogous to one of general thermodynamic cycles - Stirling cycle[77], which consists of two isothermal and two constant electric displacement processes. Firstly, the capacitor is charged to some initial voltage while its capacitance is at a constant maximum (C_{max}), which corresponds to path A-B in **Fig. 4.10**. The initial energy is injected to the capacitor during this process:

$$W_{inject} = \frac{1}{2} C_{\max} V_{start}^2 \tag{4.1}$$

When constraining charge by keeping the capacitor opened circuited, voltage must increases to the maximum as point D, with decreasing capacitance ($Q_{CONSTANT} = C_{VAR}V$), increasing the potential energy stored in the capacitor; the increasing squared effects of voltage on energy offset the decreasing linear effects of capacitance (i.e., $W_{CAP} = 1/2CV^2$). During the transition from point B to D, the capacitor is isolated (open-circuited) with respect to the rest of the system, so that there is no current path existing. Then short-circuiting the capacitance, it is discharged and the voltage decreases to zero, which corresponds to path D-A. The net harvested energy is the shaded area ABD, and may be expressed as

$$W_{harvest} = -\frac{1}{2}(C_{\max} - C_{\min}) V_{\max} V_{start} \tag{4.2}$$

Owing to the condition of charge constraint as $C_{max}V_{start}=C_{min}V_{max}$, it could also be expressed as

$$W_{harvest} = -\frac{1}{2} C_{\max} V_{start}^2 \left(\frac{C_{\max}}{C_{\min}} - 1\right) \quad (4.3)$$

Here, the segment A-B and D-A corresponds to the two isothermal processes in Stirling cycle, in our study, terpolymer films P(VDF-TrFE-CFE) with two sides of gold electrodes is used as variable dielectric capacitor. So during the charging and discharging processes, the associated polarization originated from the dielectric permittivity changes with the electric field. The segment B-D of charge constrained corresponds to the constant electric displacement process of terpolymer. As a consequence, the gain is defined as the ratio between injected energy and harvested energy (Eq. 3.6).

4.3.3.2 Voltage Constrained Cycle (Ericsson Cycle)

In the voltage constrained case, it is the cycle analogous to the other thermodynamic cycle-Ericsson cycle, which consists of two isothermal and two constant electric field processes[122]. The cycle starts when the capacitor is charged up to V_{max} from reservoir. This is done when the capacitance is at maximum. The injected energy corresponding to the AC segment of the cycle is calculated as

$$W_{inject} = \frac{1}{2} C_{\max} V_{\max}^2 \quad (4.4)$$

During this time, the value of capacitor is taken to be constant, and so the segment of A-C is a straight line. This is a valid assumption since the charge-up time to traverse path A-C (and discharge path D-A) is transient, while the segment C-D, which corresponds to the capacitance variation, is relative longer (in our case, the time is equal to that of temperature variation around 20 seconds). It is evident from the **Fig. 4.10** that during this step in the conversion process, the voltage is held constant. (Hence the name voltage contained conversion.). As the capacitance decreases, path segment C-D is traversed, where the capacitance is at a minimum. In our case, the capacitance is changed by decreasing the temperature of terpolymer, the electrotatic force does work by causing charge to move from the capacitor back into the reservoir. The charge remaining on the plates is then recovered while capacitance of terpolymer reducing to minimum C_{min} following path D-A, the terpolymer is discharged (D-A). Since the segments C-D and D-A, the energy is harvested from heat to electric power, $W_{harvest}$, is the area ACD in **Fig. 4.10**.

$$W_{harvest} = -\frac{1}{2} (C_{\max} - C_{\min}) V_{\max}^2 \quad (4.5)$$

This method sets a maximum limit on the conversion process. The major obstacle for this approach is that some method must be employed to hold the voltage across the capacitor of the device during the conversion process, which would require another source of value V_{max}. This is an additional source to that of the conversion charge reservoir, which is of a lower voltage and is also used to power the control electronics.

Comparing Eq. 4.2 and 4.5, it is clear that the energy available from the charge constrained case is less than that from the voltage constrained case by a factor of V_{start}/V_{max}. From the perspective of energy harvesting, the method of voltage constrained is superior to charge constrained under the same maximum voltage undertaken by material. However, from the perspective of ratio, the method of charge constrained is better than voltage constrained by a factor of V_{max}/V_{start}, another advantage of this approach is that only a single charge source is needed to begin the process, and its value can be much less than V_{max}, that is the reason for higher efficiency of charge constrained conversion. In this study, energy harvesting is our focus.

4.3.4 Characterization of terpolymer P(VDF-TrFE-CFE)

As mentioned earlier, the discovery of high electromechanical performance in P(VDF-TrFE-CFE) based terpolymer opens a new avenue for developing high performance electroactive polymers. Also, by introducing the ter-monomer, for example CFE, to form P(VDF-TrFE) based terpolymer, the normal ferroelectric P(VDF-TrFE) could be converted into a ferroelectric relaxor with high room-temperature dielectric constant peak and a very slightly polarization hysteresis. In a consequence, the terpolymer P(VDF-TrFE-CFE) 61.3/29.7/9 mol% was processed, and the characterization would be investigated in detail in this part.

4.3.4.1 Thermal DSC measurement

The thermal analysis of terpolymer P(VDF-TrFE-CFE) 61.3/29.7/9 mol% was performed using Differential Scanning Calorimetry with DSC 131Evo (SETARAM, France) under an argon atmosphere. The specimens (~10mg) were placed in a closed aluminium pan and were cooled from ambient temperature down to -60°C then heated to 200°C and finally cooled to 25°C at a scanning rate of 10°C/min. The DSC measurement was used to characterize the phase transitions and crystalline structures of the terpolymers. In order to detect the thickness effect on crystallization, we measured the specimens with different

thickness: 6, 12, 20, 50, 80, 100µm. The DSC results depict that the endothermic and exothermic peak is almost at the same temperature and with the same associated energy, namely, the thickness of films does not influence the crystallinity of terpolymer. **Fig. 4.11** records the DSC traces of the samples 20µm-thickenss during the heating and cooling run. The endothermic peak (125°C) and the exothermic peak (115°C), which result from the melting process and crystallization process respectively, are presented apparently in this figure.

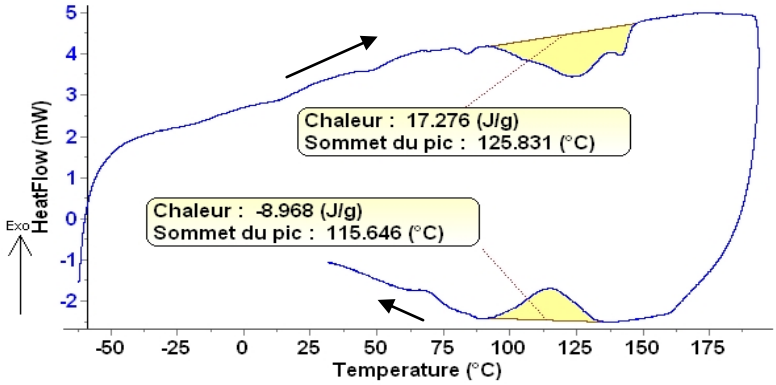

Fig. 4.11 The DSC trace of P(VDF-TrFE-CFE) 61.3/29.7/9 mol% terpolymers at the heating and cooling run.

4.3.4.2 Dielectric and Ferroelectric Characterization

A dielectric material is an electrical insulator that may be polarized by the action of an applied electric field. However, the exact response of a certain material to an applied electric field is quite hard to predict. When a dielectric material is placed in an electric field, electric charges do not flow through the material, like in conductor, but only slightly shift from their average equilibrium positions causing dielectric polarization, positive charges are displaced along the field and negative charges shift in the opposite direction. This creates an internal electric field which partly compensates the external field inside the dielectric. If a dielectric is composed of weakly bonded molecules, those molecules not only become polarized, but also reorient themselves so that their symmetry axis aligns to the field. If the material is conducting, the electric field will give rise to charge transport, due to which the effects of polarization will be obscured. The following part of this chapter considers insulating, non-conductive materials.

A typical model of an insulating material regards the material as composed of small dipoles, which are electrically neutral, but possess internal charge separation. When exposed to an external electric field, the tendency of a single dipole is to align itself with the electric field, such that the positive end points toward lower potential, and the negative end points toward the higher potential[143]. When all the dipoles in a material align in this way to an applied electric field, the material is known as a *dielectric*. Fig. 4.12 (a) depicts the situation when a constant voltage is applied to a set of juxtaposing capacitor plates. Electric field lines may only begin on free positive charges, and end on free negative charges. Thus, surface charge concentration builds up on the capacitor plates. The charge build up continues, until the voltage drop over the capacitor plates matches that of the voltage source. The relation between the amount of free charge, Q, and the voltage drop, V, is $Q = C_r V$, where C_r is the capacitance of the capacitor[144],

$$C_r = \frac{\varepsilon_0 A}{d} \tag{4.6}$$

A is the area of the plates, and d is the distance between them. ε_0 is the vacuum permittivity, $\varepsilon_0 = 8.85*10^{-12}$ F/m. The density of the field lines is known as the electric flux density, or just flux density, and is given by

$$D = \varepsilon_0 E \tag{4.7}$$

where E are the components of the electric field between the capacitor plates.

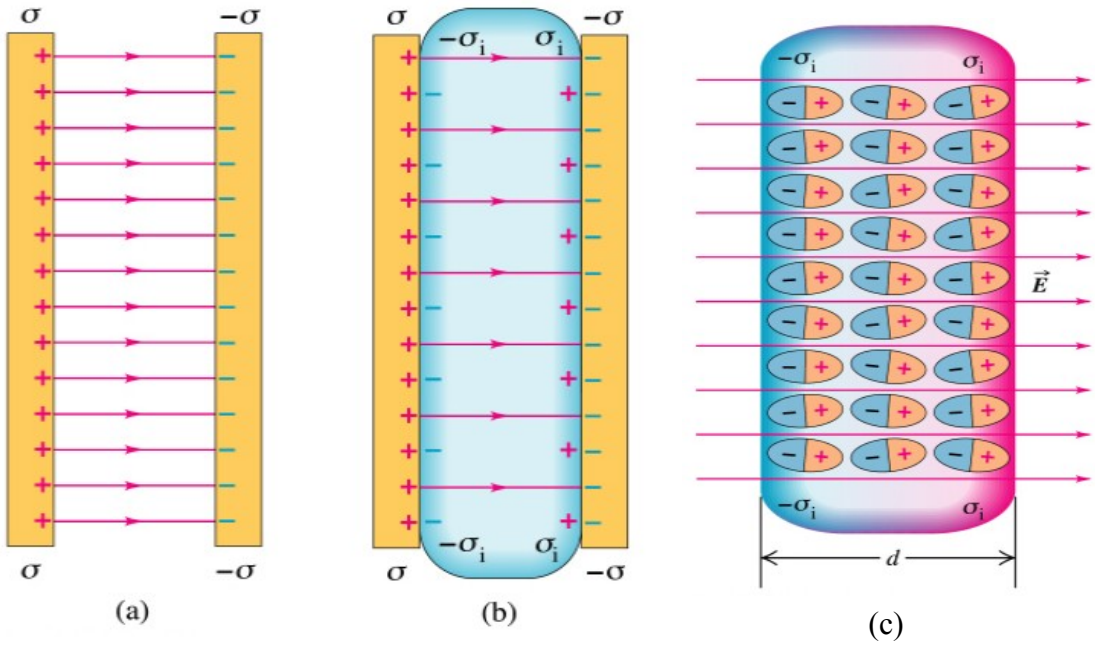

Fig. 4.12(a) Electric field lines with vacuum between the plates (b) The induced charges on the faces of the dielectric decrease the electric field (c) Polarization of a dielectric in an electric field gives rise to thin layers of bound charges on the surfaces, creating positive and

negative surface charge densities. The sizes of the molecules are greatly exaggerated for clarity. (**http://www.physics.sjsu.edu/becker/physics51/capacitors.htm**)

If a piece of dielectric material is inserted between the plates, Fig. 4.12 (b) and (c), the dipoles in the material will reorient such that the positive end of the dipole points toward the negative potential. The flux density is also known as the electric displacement, because it is a measure of the displacement of the dipoles in the material[144].

Part of the electric displacement originates from the vacuum displacement, the other part from actual polarisation of the dielectric. The electric displacement D is related to the polarization density P by

$$D=\varepsilon_0 E+P \qquad (4.8)$$

Due to the insert of dielectric material, the flux density in the material could be also expressed as

$$D=\varepsilon E=\varepsilon_r \varepsilon_0 E \qquad (4.9)$$

where ε is the dielectric of the material. ε_r is referred to as the dielectric constant.

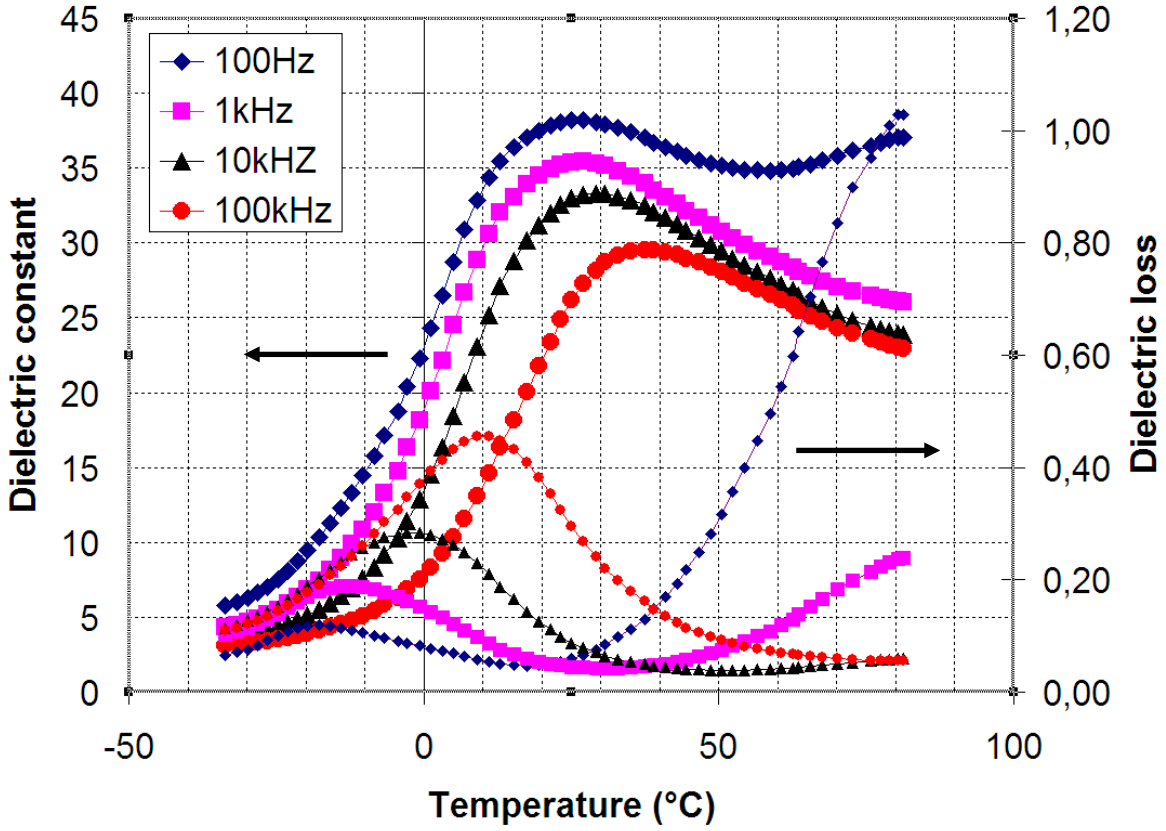

Fig. 4.13 Temperature dependence of weak field dielectric properties of terpolymer P(VDF-TrFE-CFE) measured at different frequencies.

The weak field dielectric properties were measured as a function of temperature by an impedance/GAIN-phase Analyzer (HP4194A). The terpolymer films (20µm-thickness) stuck

with the steel was put into a controlled temperature chamber and connected with an impedance/GAIN-phase Analyzer. **Fig. 4.13** shows the temperature- and frequency-dependent dielectric constant and loss tangent of terpolymer. As expected, due to the introduction of defect structure, the sharp dielectric constant peak in copolymer turns into a broad peak in terpolymer, and the O-D transition peak is moved to around room temperature. Especially, the broad dielectric peak position of dielectric constant shifts slightly with the frequency towards higher temperature[136], such a behaviour is a typical feature to all the known relaxor ferroelectric materials.

As seen in **Fig. 4.13**, it indicates that the dielectric constant shows maximum at nearly room temperature, and decreases more rapidly at the lower temperature range than that at the higher temperature range, the large dielectric constant variation can result in the large electrical displacement variation. On the other hand, Xu et al. have confirmed that the pyroelectric effect could be ignored at this temperature range (i.e., below θ_{max}, see **Fig. 4.6**[138]). Consequently, the high nonlinearity of dielectric permittivity (capacitance) together with the negligible pyroelectric effect could be an important favorable factor for harvesting energy in our study.

In order to investigate the temperature effect of basic ferroelectric characterization on terpolymer, we measured the ferroelectric hysteresis loops at different temperature as shown in **Fig. 4.14**. D-E loops were carried out every 5°C between 20°C and -20°C in descending order, and the unipolar sine electric field was applied with the average slope of dE/dT=40000 kV $mm^{-1}s^{-1}$ which is the same slope with the bipolar cycle at 100 Hz. This frequency was chosen due to its lower hysteresis loss than other frequency.

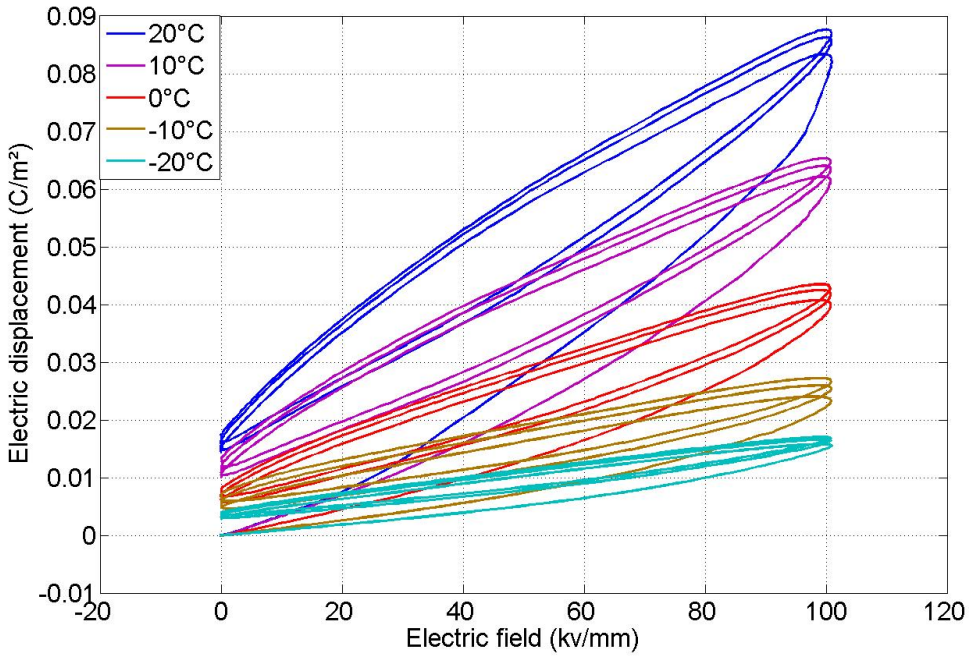

Fig. 4.14 Unipolar D-E loops at different temperature under 100 kV mm^{-1}.

Fig. 4.14 presents that the electric displacement displays an obvious reduction with the decrease of temperature under the maximum electric field 100 kV mm^{-1}, it is consistent with reduction of the dielectric constant in **Fig. 4.13**. As we know, there exists two kinds of polarization mechanism in the relaxor ferroelectrics: thermally activated flips of the nanopolar regions at high temperature and the breathing of frozen nanopolar regions at lower temperature[145]. In the relaxor ferroelectric terpolymers, since the temperature lowered from high temperature to the temperature of the dielectric constant peak, the population of the nanopolar regions increases. The polarization response under high electric field is mainly obtained from the relaxation polarization which is associated with the thermally activated flips of the nanopolar regions. Around the temperature of the dielectric constant maximum, the polarization behavior reaches the maximum due to the largest quantity of the thermally active nanopolar regions. Further lowering the temperature, partial nanopolar regions become frozen, polarization behavior is mainly determined by the breathing of the frozen nanopolar regions. The large electric displacement variation is achieved due to the nanopolar regions transition from thermally activated flip behavior to breathing behavior. Take the two extreme cases for instance in our measurement, at 20°C, the thermally activated flips of the nanopolar regions are predominant, so the large polarization response could be observed, as shown in **Fig. 4.14**, the electric displacement comes up to 0.086 C/m^2. Lowering the temperature down to -20°C, the breathing of frozen nanopolar regions is predominant, although still the same

electric field, the electric displacement is just 0.0165 C/m^2. The variation of electric displacement is satisfactory for harvesting energy.

4.3.5 Electrostatic Energy Harvesting by Nonlinear Capacitance Variation for a Relaxor Ferroelectric P(VDF-TrFE-CFE)

Based on the characterization mentioned above, we indicate that, as relaxor ferroelectrics, terpolymer P(VDF-TrFE-CFE) 61.3/29.7/9 mol% is a promising candidate for electrostatic energy harvesting on Ericsson cycle by nonlinear capacitance variation, due to the high non-linear property of the dielectric constant in the vicinity of the polarization mechanism transformation.

4.3.5.1 Experiment Setup

A waveform generator (Agilent 33220A), a high voltage amplifier (TREK Model 10/10B) and a current preamplifier (STANDFORD Model 570) were used to determine the dielectric constant under a DC electric field and to carry out the Ericsson cycle as **Fig. 3.20**. An elaborate sample holder with closed protecting-cell is used to fix the sample, protect the polymer during the temperature change and applying the external electric field.

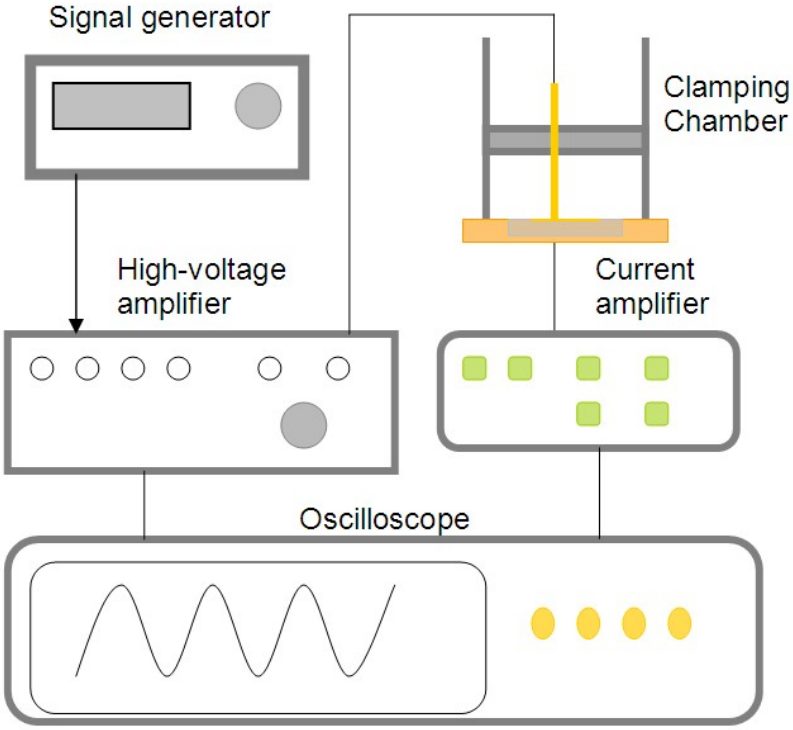

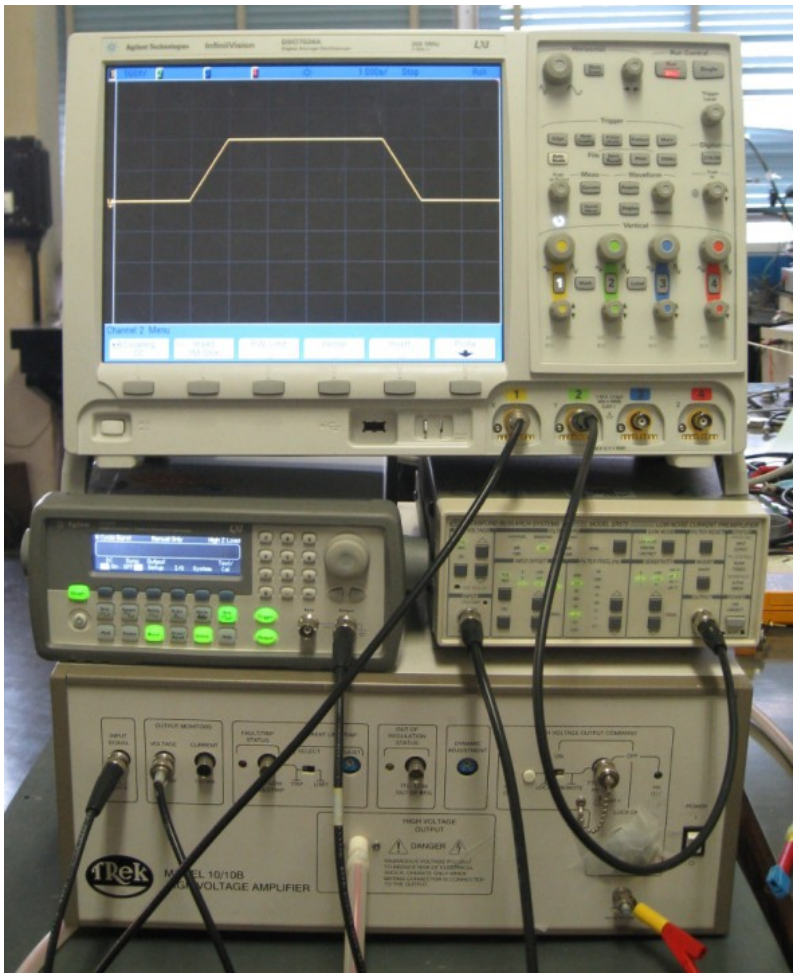

Fig. 4.15 A schematic (upper) and a picture (lower) of the experimental setup for measuring the energy harvesting system in the terpolymers.

4.3.5.2 Theoretical Model

An Ericsson cycle can be used for harvesting energy[77,80,122]. It consists of two isothermal processes (charge at θ_1 and discharge at θ_2) and a process for cooling the sample from θ_1 to θ_2 under a constant electric field. Assuming that there is a linear relationship between the electric field and the dielectric displacement:

$$D = \varepsilon_{33}(\theta)E \tag{4.10}$$

where $\varepsilon_{33}(\theta)$ and θ, denote respectively the permittivity and temperature. The injected energy during the charging process (applied electric field from 0 to E_1) is given by

$$W_{inject} = \int_0^{E_1} EdD \tag{4.11}$$

After the discharging process, the electric displacement returns to zero. Here, the other constant electric field process of the Ericsson cycle no longer exists since there is no remnant polarization for relaxor ferroelectrics. The whole cycle is described in a clockwise path leading to harvested energy which is equal to the area of the cycle:

$$W_{harvest} = \oint EdD \tag{4.12}$$

When changing the electric field and the temperature of a relaxor material, electrocaloric[146] (change in entropy and temperature induced by the application of an electric field) and pyroelectric (change in electric polarization induced by a temperature variation) effects[76] inevitably occur, but, in the present study, both were negligible. The electrocaloric effect was too small to change the temperature of the terpolymer in a significant manner (maximum 1K for the electric field applied in this study)[85]. Similarly, the pyroelectric effect, during cooling from 25°C to 0°C, was too low to lead to a significant increase of the electric displacement as described in the work performed by Xu et al.[138] where the electric displacement was remarkably decreased for a relaxor terpolymer when going from room temperature to a lower temperature.

Assuming that, theoretically, the permittivity is constant during the charging and discharging processes, the injected and harvested energy can be expressed as follows:

$$W_{inject} = \frac{1}{2}\varepsilon_1 {E_1}^2 \tag{4.13}$$

$$W_{harvest} = -\frac{1}{2}(\varepsilon_1 - \varepsilon_2){E_1}^2 \tag{4.14}$$

where ε_1 and ε_2 are the permittivity during the charging and discharging processes, respectively.

4.3.5.3 Results and Discussion

The theoretical analysis indicate that the harvested energy mainly depend on the capacitance variation, which in turn depends on the temperature. **Fig.** 4.16(a) shows the weak field dielectric properties (measured at 100 Hz) as a function of temperature, which has been verified on five samples. The permittivity demonstrated a maximum at the transition temperature (25°C), and then decreased rapidly in the lower temperature range. Benefiting from this transition, a large capacitance variation was obtained. According to these results, the temperatures of 25°C and 0°C were chosen as the charging and discharging temperatures,

respectively, for the Ericsson cycle. The time for charging and discharging the sample corresponds to a frequency of 100 Hz in order to compare simulation and experiment without frequency effect.

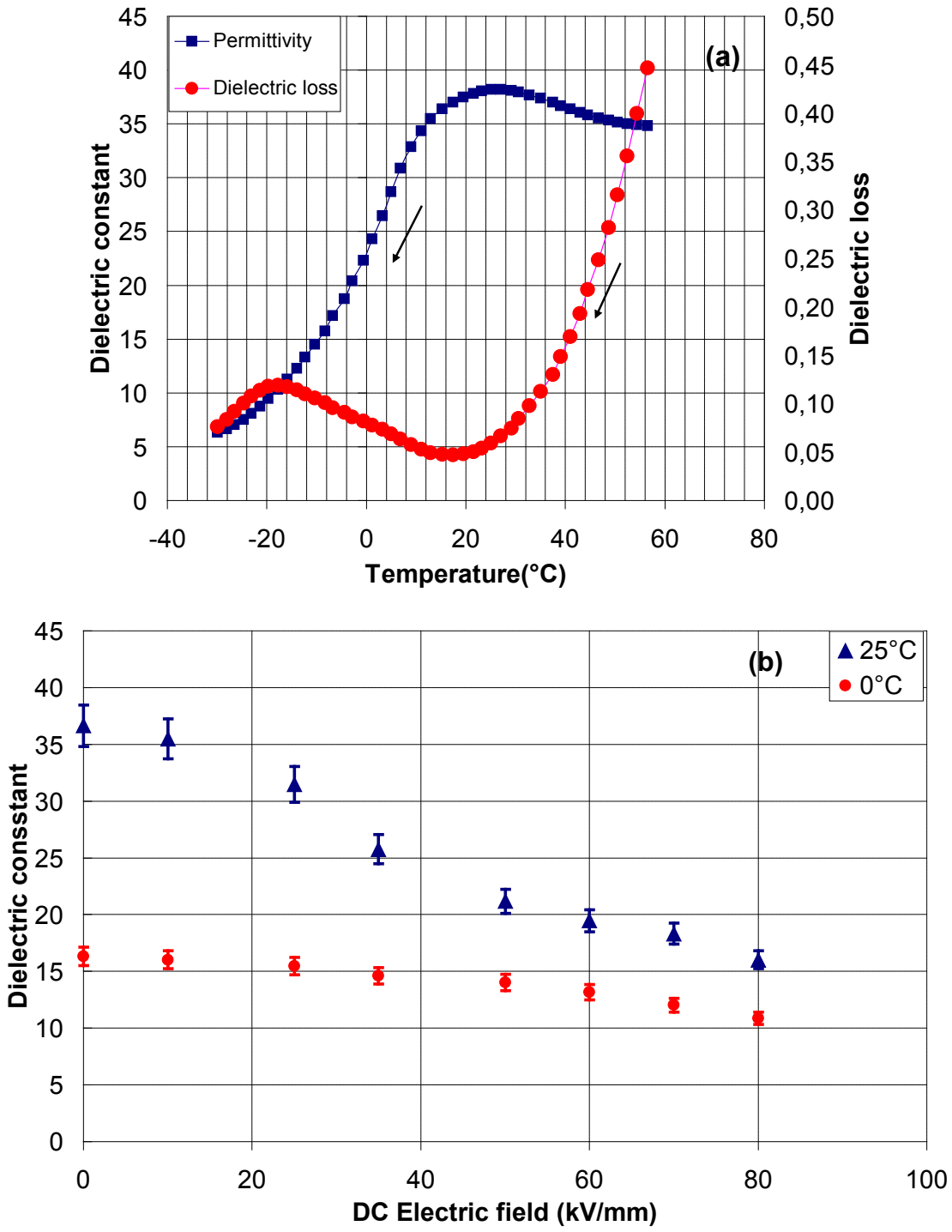

Fig. 4.16 Dielectric property on P(VDF-TrFE-CFE) 61.3/29.7/9 mol%.
(a) dielectric constant (black squares)and dielectric loss (red circles) as a function of temperature under a weak field, (b) dielectric constant under a DC electric field at 25°C (blue triangles) and 0°C (red circles).

The terpolymer was under a DC electric field during the temperature change in the Ericsson cycle. Lu et al. showed that the permittivity of PVDF-based polymers (poly vinylidene-fluoride) exhibits a tunability under a DC electric field[147]. This tunability is a

function of temperature, especially in the vicinity of the dielectric peak where the polymer has the largest tunability. Therefore, the dielectric constant (relative permittivity) was measured under different DC electric fields (E_{DC}) with a small AC field (E_{AC}) at 100 Hz and at 25°C and 0°C, as shown in **Fig. 4.16** (b). The experimental uncertainties correspond to a 95% confidence interval. Two main points are emphasized: (1) there existed a tunability of the permittivity under a DC electric field (the tunability was larger at 25°C than at 0°C) and (2) this tunability presented a non linear behavior with temperature.

As the DC electric field increased from zero to 80 kV/mm, the capacitance variation between 25°C and 0°C decreased significantly (the dielectric constant variation was 21 at E_{DC}=0, and 5 at E_{DC}= 80 kV/mm, corresponding to a reduction by 75%). In physical terms, this can be understood as there existing no macroscopic domain for relaxor ferroelectrics and the polarization mainly depending on the thermally activated flips of the nanopolar regions[148]. An external electric field cannot produce a large domain reorientation, just an alignment of nanopolar regions along the field. At the dielectric peak temperature of 25°C, the quantity of the thermally active nanopolar regions was at a maximum. Nevertheless, at the lower temperature, i.e., 0°C, a majority of the nanopolar regions became frozen[145]; the dielectric behavior thus mainly received contributions from the shape change of the frozen polar regions due to the external DC electric field. Consequently, the tunability was larger at 25°C.

The Ericsson cycle was simulated from the measurements of permittivity presented in **Fig. 4.16** and by using Eq. (4.14). **Fig. 4.17** shows the harvested energy versus the DC electric field considering or not the tunability of the dielectric constant with the electric field. Measurements were undertaken on five samples and the discrepancy is around 10%. The two simulation results almost coincided in the lower electric field range, i.e., at 10 and 25 kV/mm, but at higher electric field, the difference became increasingly pronounced, reaching 46% at 80 kV/mm. These simulations underlined that the tunability needed to be taken into account in order to avoid an overestimation of the harvested energy, especially for high DC electric fields. The harvested energy increased with the maximum DC electric field, and from simulation, a maximum energy of 240 mJ/cm^3 could be harvested at 80 kV/mm. However, electric conduction and the breakdown electric field are two inevitable factors, which restricted the experimental harvested energy, need to be resolved.

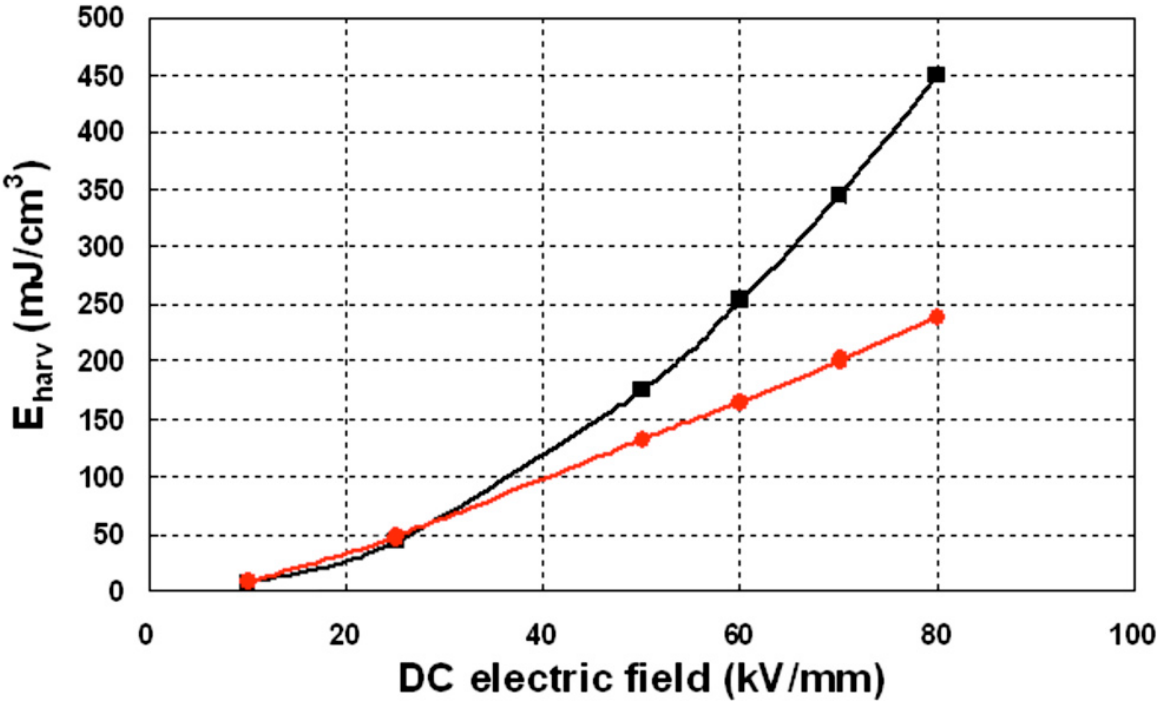

Fig. 4.17 Harvested energy as a function of the DC electric field by a simulated Ericsson cycle for the terpolymer P(VDF-TrFE-CFE) 61.3/29.7/9. Harvested energy simulated by permittivity under a DC field (red circles) and permittivity without a DC field (black squares).

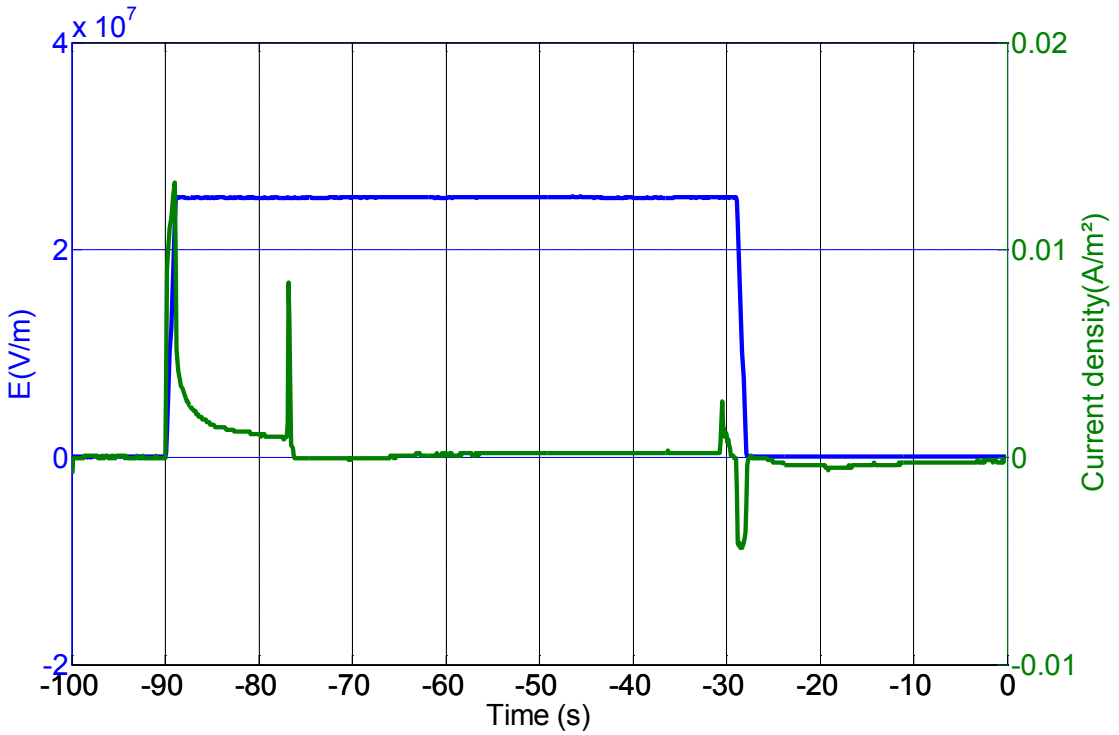

Fig. 4.18 Electric field waveform and the induced current in Ericsson cycle.

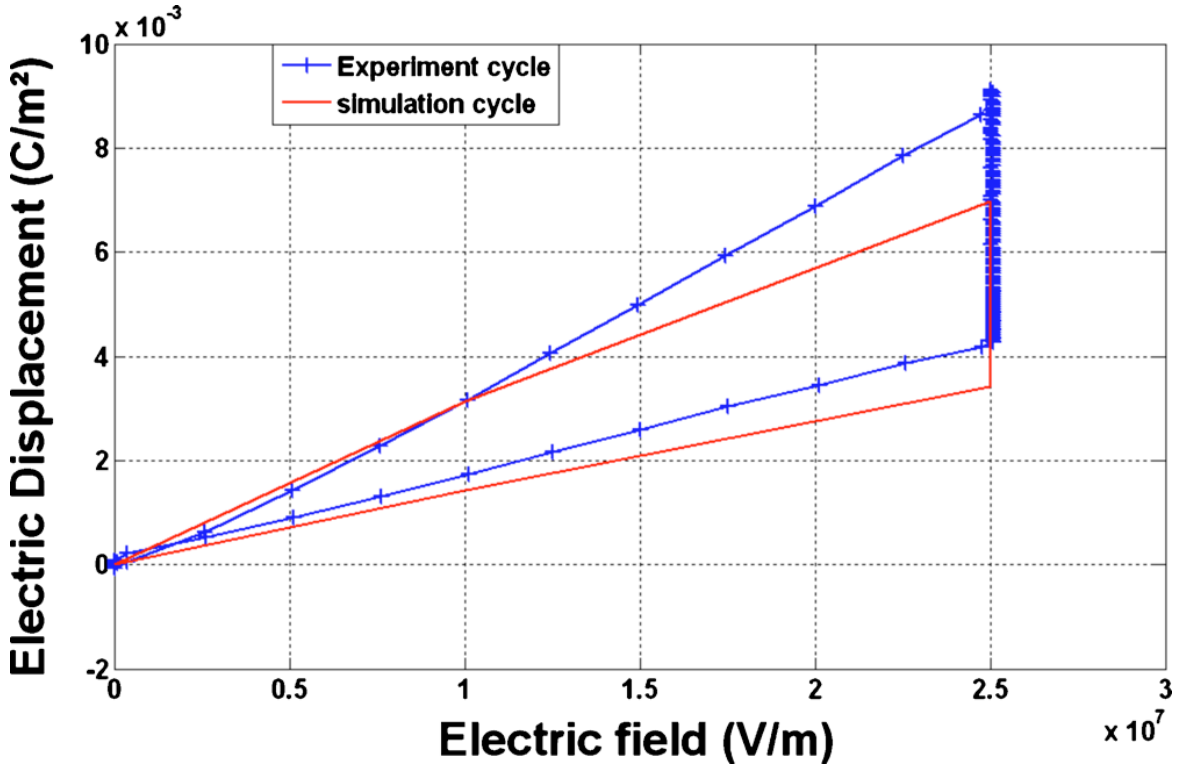

Fig. 4.19 Simulated Ericsson cycle using a dielectric constant (red circles) and its experimental counterpart (blue crosses) for P(VDF-TrFE-CFE) 61.3/29.7/9 mol%.

In order to confirm the simulation experimentally, an experimental Ericsson cycle was also undertaken. **Fig. 4.18** is the applied electric field and the induced current density in the whole cycle. The energy in each segment could be obtained by the electric field integral with respect to current. **Fig. 4.19** presents the simulated and experimental Ericsson cycles at 25 kV/mm. The direct measurement of the Ericsson cycle was carried out with a slope of dE/dt=25kV/mm.s for the charging and discharging processes. The experimental measurement showed the same type of closed Ericsson cycle as the simulation considering the tunability of the dielectric constant. For the experimental cycle, the conduction of the terpolymer is observed while the DC electric field was applied during the temperature change. An Arrhenius law was used to remove the conduction from the experimental data. **Fig. 4.19** presents the experimental Ericsson cycle after eliminating the conduction. The harvested energy was computed by Eq. (4.12), and was found to be 50 mJ/cm^3, which was consistent with the simulation (48 mJ/cm^3). The experimental Ericsson cycle was performed over several cycles on five samples and gave nearly the same harvested energy with a deviation of 10%, as well as simulation, it is the same deviation for harvested energy due to that on dielectric constant, the most representative cycle was chosen corresponding to the average of measured cycles.

In this part, we presented our work on thermal energy harvesting by electrostatic technique. It was realized by utilizing the nonlinear capacitance variation of relaxor terpolymer P(VDF-TrFE-CFE). We prepared the terpolymer through the solution casting method, and then, we investigated their characterizaztion in detail, including the thermal DSC measurement, dielectric properties, and the temperature effect of basic ferroelectric properties. In order to simulate the harvested energy accurately, we also studied the tunability of the dielectric constant of terpolymer.

The direct measurements of Ericsson cycle were implemented, the harvested energy was reached around 50 mJ/cm^3 between 25°C and 0°C under 25 kV/mm, which was consistent with our simulation.

4.4 Simulation of Ericsson and Stirling Cycle

4.4.1 Introduction

Since the first time Ericsson cycle (Olsen cycle) is proposed in 1983[66], the study of waste heat energy harvesting using Ericsson cycle has achieved great development. In this dissertation, we also present our fruitful research on it, however, the study of the other thermodynamic cycle – Stirling cycle is not as prosperous as Ericsson cycle. Guyomar et al. operated the Stirling cycle on PZN-4.5PT single crystal using FE-FE transition for energy harvesting[77]. Consequently, based on the dielectric measurement on terpolymer P(VDF-TrFE-CFE) 61.3/29.7/9 mol%, we attempt to compare the two cycles for electrostatic energy harvesting by simulation.

4.4.2 Theoretical Model for Simulation

The simulation of Ericsson cycle has been introduced in the previous section. Here we mainly concentrate on Stirling cycle. The only difference of the two cycles occurs during the cooling process, Stirling cycle is in open-circuit, whereas Ericsson cycle is under high constant electric field. Two hypotheses are set in the simulation: (1) the permittivity is constant during charging and discharging processes; (2) neglecting the conduction loss in the whole cycle. When increasing the electric field from 0 to E_{START}, the electric displacement increase from 0 to D_{START} following the equation

$$D_{START} = \varepsilon_1(\theta_1)E_{START} \tag{4.15}$$

and the energy is injected into the sample.

$$W_{inject} = \frac{1}{2}\varepsilon_1(\theta_1)E_{START}^2 \tag{4.16}$$

Then cooling the sample under open-circuit, the dielectric constant decreases but the charge is held on the terpolymer. It makes the electric field undertaken by terpolymer raise from E_{START} to E_{MAX} following

$$\varepsilon_1(\theta_1)E_{START} = \varepsilon_2(\theta_2)E_{MAX} \tag{4.17}$$

Finally switching the system to short circuiting condition at the final temperature, electric field reduces quickly to 0, the cycle is end. The harvested energy is the area of the closed cycle which abide by equation below:

$$W_{harvest} = -(\frac{1}{2}\varepsilon_2 E_{MAX}^2 - \frac{1}{2}\varepsilon_1 E_{START}^2) \tag{4.18}$$

4.4.3 Result and Discussion

Whatever the thermodynamic cycles, the key point determining the harvested energy is the permittivity of the specimen. Out of the same reason in the Ericsson cycle simulation, we measured the dielectric constant (relative permittivity) under different DC electric fields (E_{DC}) with a small AC field (E_{AC}) at 100 Hz and different temperature (**Fig. 4.20**), the temperature range is from 20°C to -20°C with an interval of 5°C. The DC electric field was measured from 0 to 60 kV/mm with an interval of 10 kV/mm.

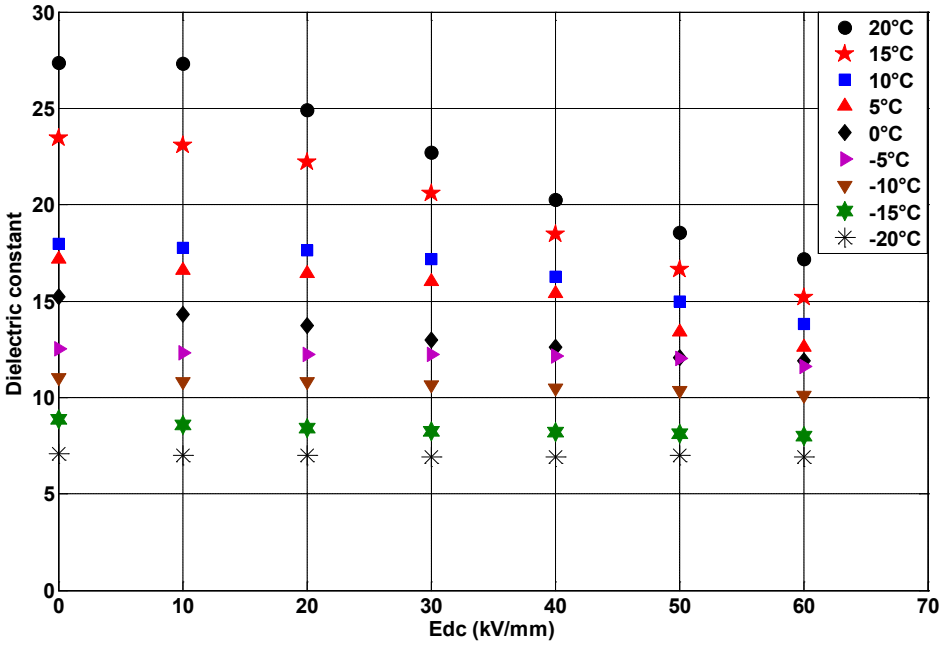

Fig. 4.20 Dielectric constant under DC electric field at different temperature on terpolymer P(VDF-TrFE-CFE) 61.3/29.7/9 mol%.

It can be seen from **Fig. 4.20**, the tunability of the permittivity under DC electric field exists in the whole temperature range, but manifests more significantly at higher temperature than lower temperature. It has been explained in the view of nanopolar regions in the previous part. Thus the Ericsson cycle is simulated directly from the dielectric permittivity by Eq.4.14. **Fig. 4.21** depicts the simulation result in Ericsson cycle versus different temperature range and different maximum electric field. The capacitance variation (permittivity variation) becomes larger with the temperature variation increasing, thus the harvested energy increases. In addition, the maximum electric field is another important factor which influences the harvested energy more greatly (an effect of square in Eq. 4.14) than temperature variation. We also find that, even at the maximum electric field and temperature variation, the harvested energy is still impossible to surpass the injected energy, hence, the ratio is always lower than 1.

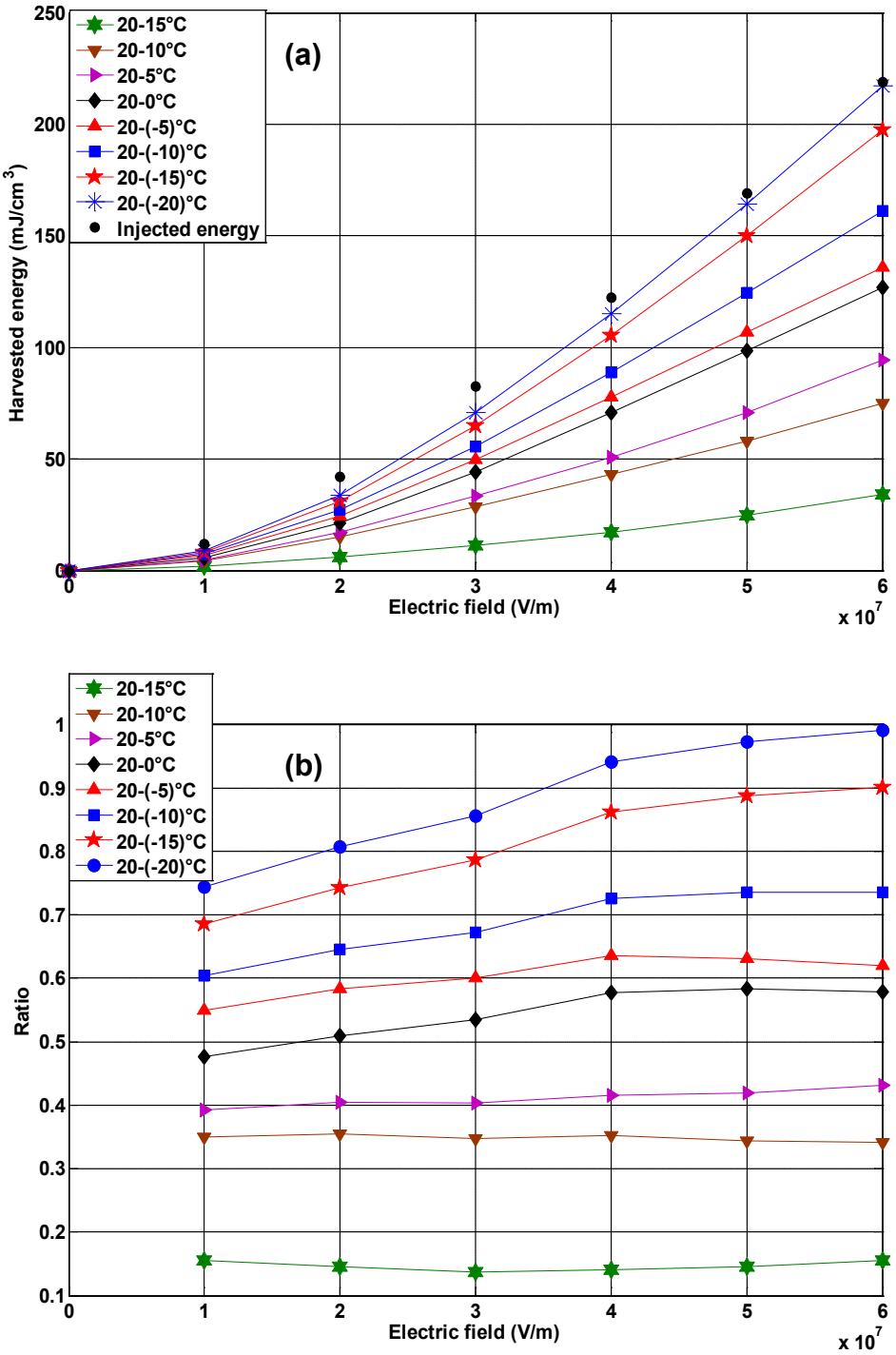

Fig. 4.21 Simulation of Ericsson cycle on terpolymer P(VDF-TrFE-CFE) 61.3/29.7/9 mol%. (a) simulation of harvested energy (b) ratio VS. different temperature range or different electric field.

Stirling cycle is also simulated based on permittivity under DC electric field by Eq.4.18, **Fig. 4.22** shows the simulated Stirling cycle operated under different electric fields. The dashed line in this figure indicates the cooling process from 20°C to 0°C under constrained charge. Keeping the temperature variation constant, it is obviously in **Fig. 4.22** that the

harvested energy (area of the closed cycle) increases evidently with the increase of the initial driving voltage.

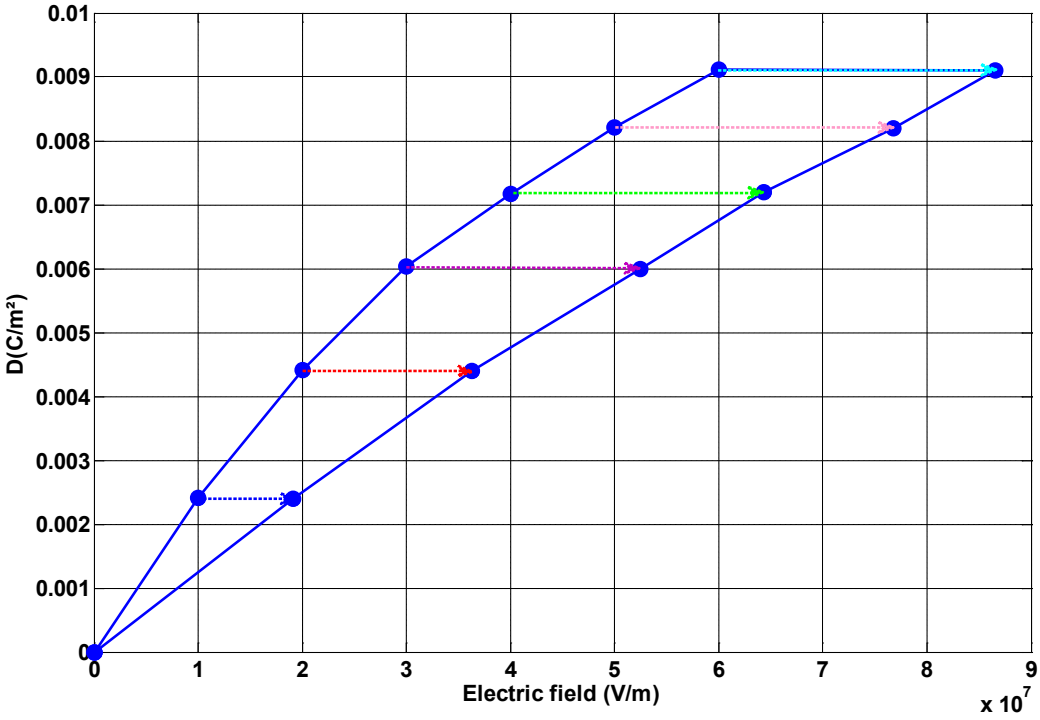

Fig. 4.22 Simulation Stirling cycle (D-E) between 20°C and 0°C under different maximum electric field.

Fig. 4.23 displays that the harvested energy in Stirling cycle is function of temperature variation and initial electric field on terpolymer P(VDF-TrFE-CFE) 61.3/29.7/9 mol%. It shows the same harvested energy tendency as Ericsson cycle, however, for Stirling cycle, the increased range of harvested energy is enormous. The maximum harvested energy (450 mJ/cm^3), under the same temperature range and same initial electric field, is around two times of that in Ericsson cycle (220 mJ/cm^3). Since the injected energy is independent of temperature variation, but just depends on initial voltage and initial temperature, in our case, the injected energy are same in both thermodynamic cycles (the black spots appeared in **Fig. 4.21** (a) and Fig. **4.23** (a)). It is clear that, since the temperature variation larger than 25°C, e.g., between 20°C and -10°C, harvested energy of Stirling cycle becomes larger than injected energy, the ratio is larger than the maximum ratio in Ericsson cycle. Meanwhile, the ratio decreases with the increase of initial electric field. The maximum ratio could be obtained at the maximum temperature variation and the lowest electric field, it equals nearly 3 at 10 kV/mm between 20°C and -20°C. Based on these analysis, we could predict in theory that the Stirling cycle is a more efficient way for energy harvesting from capacitance variation on

terpolymer. Whereas, the disadvantage still exist, like uncontrollability of the maximum voltage on polymers, especially in experimental measurement, the overhigh electric field may lead to the breakdown of polymer. On the other hand, charge losses occur when open circuit and the conduction losses would make a negative impact on energy harvesting. So the further studies should concentrate on how to overcome these restriction, and carry the direct measurement of Stirling cycle.

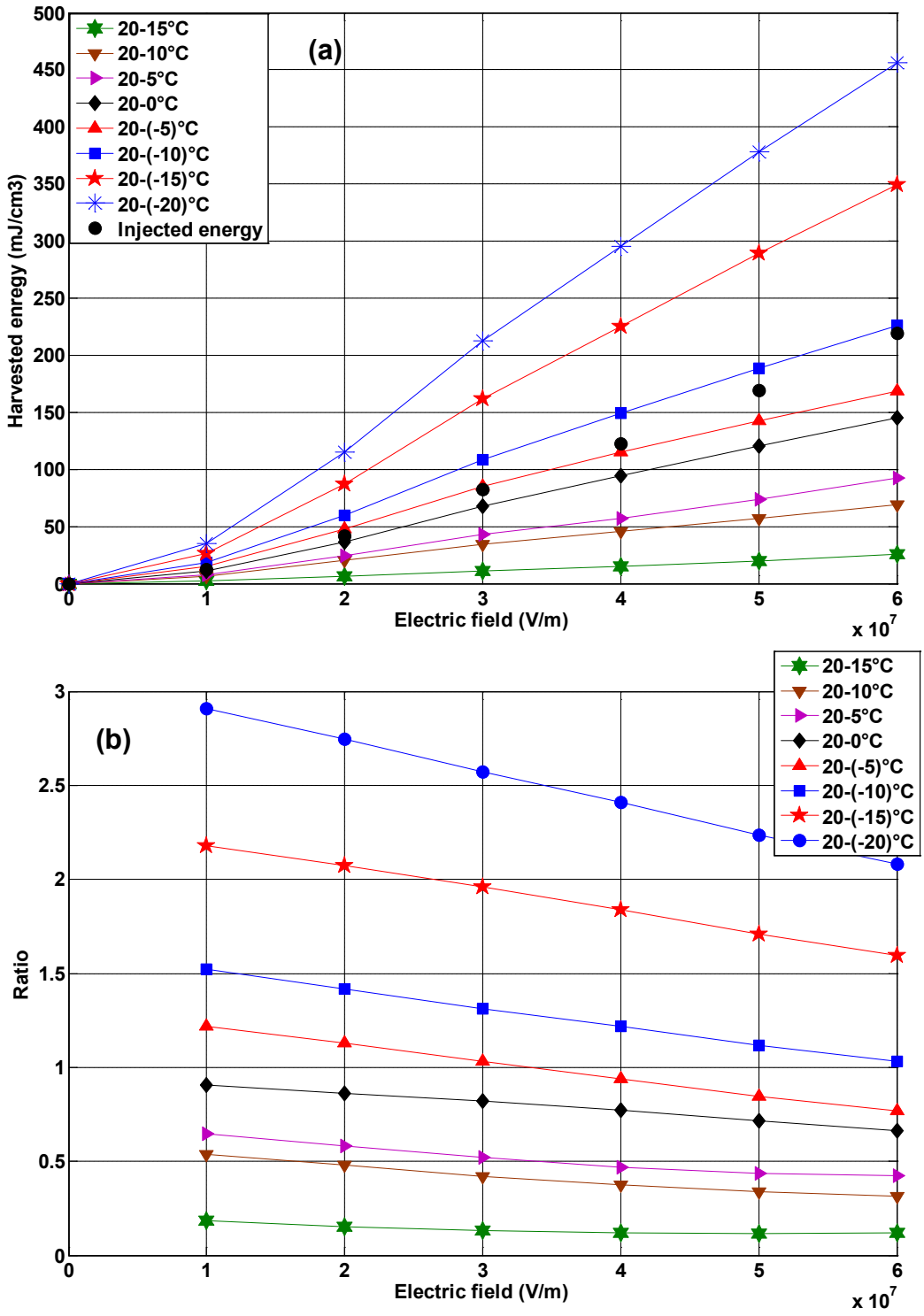

Fig. 4.23 Simulation of Stirling cycle on terpolymer P(VDF-TrFE-CFE) 61.3/29.7/9 mol%. (a) simulation of harvested energy (b) ratio VS. different temperature range or different electric field.

4.5 Conclusion

PVDF-based polymer was introduced in detail in this chapter, especially for terpolymer P(VDF-TrFE-CFE). By copolymerizing the P(VDF-TrFE) with a third monomer to form a terpolymer, the defect structures introduce inhomogeneity in the ferroelectric phase which broadens the transition region and reduce or eliminate the hysteresis. As a result, the normal ferroelectric is transformed into a relaxor ferroelectric polymer. Due to the high room-temperature dielectric peak and slightly polarization hysteresis, terpolymer P(VDF-TrFE-CFE) 61.3/29.7/9 mol% was chosen as the active material for electrostatic energy harvesting. In addition, two basic electrostatic energy harvesting cycles: Charge constrained cycle and voltage constrained cycle, were studied. The main work concentrated on the following aspects:

A. Ericsson Energy Harvesting by Nonlinear Capacitance Variation between 25°C and 0°C

The weak field dielectric properties were measured in order to determine the working temperature during Ericsson cycle. The largest variations in capacitance were obtained between 25°C and 0°C due to a dipolar ordering-disordering transition. In order to evaluate the harvested energy by simulation, the dielectric permittivity under DC electric field was also measured and exhibited tunability of dielectric constant as a function of temperature. Especially in the vicinity of the dielectric peak, the tunability expressed more obviously. This phenomenon was analyzed and explained perfectly from the viewpoint of nanopolar regions.

By characterizing the tunability of the dielectric constant under DC electric field, the simulated harvested energy, between 25°C and 0°C under 80 kV/mm, was equal to 240 mJ/cm^3. The direct measurement of Ericsson cycle was also carried out with a maximum electric field of 25 kV/mm. When subtracting the conduction, the harvested energy was equal to 50 mJ/cm^3 which was consistent with the simulation (48 mJ/cm^3). It proved the reliability of our theoretical evaluation and experimental feasibility in practice.

B. Simulation of Ericsson and Stirling cycle

Simulation on Ericsson and Stirling cycles were also studied in this chapter to estimate energy harvesting under high electric field. The harvested energy versus temperature variation and electric field in Stirling cycle displays the same tendency with Ericsson cycle, but in contrast to Ericsson cycle, Stirling cycle can harvest more energy and have a higher efficiency under the same conditions. After determining the transition temperature, there are two key factors to thermal energy harvesting: temperature variation and applied electric field. The two different cycles exhibit the same dependency on each factors.

Electric conduction and the breakdown electric field are two inevitable negative factors, which restricted the experimental harvested energy, need to be resolved. The next work aims to improve the quality of polymer so as to overcome these restrictions of the experiment. Previous work dealt with the purification of a P(VDF-TrFE) copolymer and the effect of the porosity of the film. It appears that the presence of residual solvent or pores inside the film reduces its resistivity by one order of magnitude[149]. Fujisaki et al. stated that the conduction emerging at a 'defect' part (TrFE and CFE) was much smaller in amorphous regions as compared to in crystal grains[150]. Therefore, it can be reduced by optimizing the proportion of the crystal grains and amorphous regions in the mixture and their respective distribution in the film. In addition, the interface between the film and the electrode also plays an important role for the film's conduction. The improvement of the process of the film is in progress.

Conclusions and Future Work

The work presented in this dissertation focused on finding a novel method to directly convert waste heat into electricity. The specific need that drove the research for new energy harvesting devices is the desire to self-power wireless sensor networks and mobile devices without batteries. Locating a renewable power source with a sensor will enable the sensor unit to be wireless and require minimal maintenance. In the last decades, direct energy conversion devices for medium and low grades waste heat have received significant attention due to the necessity to develop more energy efficient engineering systems. Pyroelectric effect and capacitance variation through temperature fluctuations are the major avenues to convert waste heat into electrical power in this dissertation. This chapter restates the contributions of this work and presents the conclusions of the research on this subject.

Author's Contributions

The research presented in this study is the development of new energy harvester from heat to electrical energy by temperature fluctuations. To maximize the amount of harvested energy involves several factors, including selection and configuration of the active materials, appropriate operating temperature range, efficient thermodynamic cycles for energy conversion. Two major avenues help us to realize this goal: (1) pyroelectric effect and (2) capacitance variation of relaxor.

Pyroelectric energy harvesting directly converts waste heat into electrical power by alternatively heating and cooling a pyroelectric material resulting in electricity generation. It requires dielectric material whose charge storing capabilities are a function of temperature. For pyroelectric single crystals, this property can be exploited by heating these materials after they are charged, due to the rising of temperature, their charge storage capability decreases, forcing them to eject a portion of their surface charge, this ejected charge can then be supplied

to an appropriate electric storage device. PZN-4.5PT single crystal was chosen as the objective sample which displays high pyroelectric effect under electric field. Weak field dielectric property was measured in order to determine the operating temperature range and the FE-FE phase transition temperature. The objective of this study was to evaluate the performance of pyroelectric power generation principle that may be particularly suited to satisfy the small scale power generation demands for application. The pyroelectric energy harvesting system was carried out according to Ericsson cycle. Benefiting from the just perfect utilization of phase transition during the Ericsson cycle, the harvested energy was improved abruptly. On this basis, we studied the frequency effect on energy harvesting of Ericsson cycle, and explained the origin of this effect from the viewpoint of the domain engineering. More interesting point is that the study of frequency effect provided some enlightenment for modification of traditional Ericsson cycle. We designed the asymmetric Ericsson cycle, including L-H and H-L Ericsson modelling, and realized it by experimental measurement, and finally confirmed that the H-L Ericsson cycle exhibited a surprising capability for energy harvesting.

Bearing in mind that the ultimate aim for energy harvesting device is that they can be further and further miniaturised to power smaller and smaller devices, the electrostatic transducer provides a very attractive approach. The most common MEMS actuation mechanism is the electrostatic actuator, which makes use of the force between charges stored on the plates of capacitor to change their capacitance, and eventually to couple the energy from the mechanical domain into the electric domain. On the other hand, thermal energy (temperature variation) is commonly presented in a variety of daily situations. To our best knowledge, an important feature of relaxor ferroelectrics is their dielectric constant as function of temperature. So the second major contribution is to develop an electrostatic energy harvesting model using the capacitance variation with temperature of relaxor ferroelectric polymers. Among all the known polymers, PVDF and its copolymer with trifluoroethylene (PVDF-TrFE) have been accorded a great amount of scientific attention, by introducing defects CFE into the PVDF-TrFE ferroelectric structure, the polymer could behave like typical relaxor ferroelectric features, the more valuable behavior is the dielectric constant maximum occurs at near room temperature, accordingly, terpolymer P(VDF-TrFE-CFE) 61.3/29.7/9 mol% was chosen as active material in this work. Besides the measurement of the weak field dielectric properties as a function of temperature in order to confirm the transition temperature, we also studied the tunability under DC electric field. The dielectric constant was measured under different DC electric fields (E_{DC}) with a small AC field (E_{AC}) at

a given frequency and different temperature. Then, the mechanism of tunability was explained from the relationship of nanopolar regions in the terpolymer and temperature. By these values of dielectric constant under DC electric field, we made the simulation of Ericsson cycle to evaluate the harvested energy under high electric field which can not realized in present stage. The identical result between simulation and experiment proved the reliability of our theoretical evaluation and experimental feasibility in practice. In order to broaden avenue and find the more efficient way for thermal energy harvesting, we still simulated the Stirling cycle by dielectric constant under DC electric field on terpolymer.

Research Conclusions

The work in this dissertation demonstrates the ability to enhance the direct energy conversion from waste heat into electric power on relaxor ferroelectrics. Chapter 1 serves as an introduction to the scheme and general principle of energy harvesting, and provides the different techniques of energy harvesting and their development. Chapter 2 focuses on the principle of thermal energy harvesting, we mainly explored the model of pyroelectric energy harvesting, including Ericsson cycle and Stirling cycle, and presents the background information on ferroelectric materials. Chapter 3 embarks into the frequency effect on pyroelectric energy harvesting in PZN-4.5PT single crystal, in order to enhance the harvested energy, we designed the two asymmetric Ericsson models and put them into practice, one optimal model was confirmed to improve the harvested energy abruptly. Chapter 4 proposes a novel approach for thermal energy harvesting on terpolymers P(VDF-TrFE-CFE): electrostatic energy harvesting modeling using capacitance variation at low temperature. The main valuable results are summarized below.

1) Thermal energy harvesting from $Pb(Zn_{1/3}Nb_{2/3})_{0.955}Ti_{0.045}O_3$ single crystals phase transition

The effect of the frequency on energy harvesting in $Pb(Zn_{1/3}Nb_{2/3})_{0.955}Ti_{0.045}O_3$ single crystals with an Ericsson cycle was successful in practice. At the lowest frequency of 0.01 Hz (which corresponds to the slope for the application of the electric field), the maximum harvested energy was equal to 86 mJ cm^{-3}. With an increase in frequency, the harvested energy demonstrated a nonlinear decrease, and the diminution was particularly rapid at frequencies above the critical frequency of 1 Hz. The inherent mechanism of the frequency effect is discussed in detail. In the present case, the phase transitions due to domain

engineering, e.g., R-O transition during the charge process at low temperature and O-T transition during the discharging process at high temperature, and the high pyroelectric activity in the O phase, greatly improved the harvested energy. The study also revealed that various parameters, such as the electric field associated with the phase transition, the polarization relaxation, and polarization variations, influenced the capability of energy harvesting to a certain extent. This capability depended significantly on the electric field frequency. Especially at high frequency, the reduction in the polarization time resulted in an inadequate phase transition, and subsequently gave rise to the coexistence of orthorhombic and rhombohedral phases. This had an adverse effect on the energy harvesting, and consequently, the harvested energy exhibited a decreasing tendency with an increasing electric field. Based on the result of the frequency effect, two asymmetric Ericsson cycles were attempted: L-H cycle and H-L cycle. These cycles employed different imposed frequencies at the charge and the discharge of the sample. Both asymmetric cycles agreed well with the performed analysis on the influence of the frequency. The H-L cycle greatly promoted energy harvesting, and its harvested energy reached 106 mJ cm^{-3}, thus corresponding to the most effective energy harvesting cycle for this material.

2) Electrostatic energy harvesting by nonlinear capacitance variation for a relaxor ferroelectric P(VDF-TrFE-CFE) terpolymer

The weak field dielectric properties demonstrated that the permittivity exhibited a maximum at the ordering-disordering transition temperature (25°C), and then decreased rapidly in the lower temperature range. It hinted us that there would be a large capacitance variation as a result of this transition. So we measured the tunability of terpolymer in order to obtain the actual dielectric constant during the energy harvesting cycle. This tunability presented a nonlinear behavior with temperature, at the whole DC electric filed range, the capacitance variation between 25°C and 0°C decreased significantly, i.e., the dielectric constant variation was 21 at E_{DC}=0, and 5 at E_{DC}=80 kV/mm. The origin of this phenomenon can be understood as there existing no macroscopic domain for relaxor ferroelectrics and the polarization mainly depending on the thermally activated flips of the nanopolar regions. The simulation of Ericsson cycle was accomplished from the permittivity under DC electric field. By comparing the simulation results considering or not the tunability of the dielectric constant, it is underlined that the tunability needed to be taken into account in order to avoid an overestimation of the harvested energy, especially for high DC electric fields. When going from 25°C to 0°C, it was found that the harvested energy increased up to 240 mJ/cm^3 when the electric field was raised to 80 kV/mm. For confirming the simulation, experiment was

carried out at 25 kV/mm. The harvested energy was computed to be 50 mJ/cm^3, which was consistent with simulation result 48 mJ/cm^3.

To simulate the possible harvested energy at different electric fields and different temperature ranges, we made more elaborate extrapolated results. Analysis of thermal energy harvesting indicated that the key influencing factor of the harvested energy is the permittivity of the sample. We measured the dielectric constant under different DC electric fields (E_{DC}) (from zero to 60 kV/mm) with a small AC field (E_{AC}) at 100 Hz and at different temperature (from 20°C to -20°C). On this basis, Ericsson and Stirling cycle were simulated at different temperature and electric field ranges. The harvested energy versus temperature variation and electric field in Stirling cycle displays the same tendency with Ericsson cycle, but in contrast to Ericsson cycle, Stirling cycle can harvest more energy and have a higher efficiency considering the same injected energy. As for the two important factor for thermal energy harvesting in our case, temperature variation and applied electric field, both cases exhibit different dependency on each factors.

Suggestions for Future Work

This thesis has revealed several effective avenues of research which remain open for further investigation. These will now be discussed.

It is possible to improve the efficiency of thermal energy harvesting from two aspects: energy harvesting cycles and active material. In our study, we designed the energy harvesting cycle with a single sample: single crystal for pyroelectric energy harvesting and terpolymer in low temperature electrostatic energy harvesting. However, it is worth considering that why we can not synthesize the two energy harvesting methods together. When increase the temperature, energy could be harvested by pyroelectric effect, then the temperature decreases, electrostatic technique could be used to harvest energy. By this way, the conversion ratio in one cycle may be increased abruptly. In addition, for pyroelectric energy harvesting, it was initially thought that utilizing the FE-FE phase transition of single crystal during the energy harvesting cycle, while it could also be harvested energy from pyroelectric thin film. Thus in our whole work, no matter pyroelectric or electrostatic energy harvesting system, we can attempt to connect many samples (thin films with metallic electrodes) in a multi-stack structure. By this way, the harvested energy of each cycle would exhibit great increase.

As for material, synthesizing inexpensive material is one possible effort direction, in addition, improving quality is another possibility deserving to attempt. As we have mentioned above, the leakage current of polymer greatly limits the polymer's breakdown electric field, and then restricts the harvested energy. Previous study indicated that a possible mechanism of the electrical resistivity is the accumulation of ionic charge carriers under the electrodes which would cancel the electric field within the film and reduce the leakage current. The low resistivity of the purified and porous films can be attributed to the presence of pores in both films which creates nonuniform electric field in the films. Furthermore, there are the other potential factors such as the presence of residual solvent, proportion of the crystal grains and amorphous regions in the mixture and their respective distribution in the film, the interface between the film and the electrode etc.

Moreover, it is clear that the introduction of chemical defects does have a profound effect on the dielectric and ferroelectric properties of the PVDF polymer backbone. We can tailor the property by changing the composition of the polymer or synthetic process, according to the need for energy harvesting system.

Overall, thermal energy harvesting speeds up the battery-less world's coming, more and more researchers all over the word join in this magical field. Finish of this thesis does not mean the final end of this work, we will continuously make efforts on the future work mentioned above to obtain much more breakthrough on this subject.

List of Publications

Journal Papers

1. **H. Zhu,** S. Pruvost, P.J. Cottinet, D. Guyomar, 2011, "Energy harvesting by nonlinear capacitance variation for a relaxor ferroelectric poly(vinylidene fluoridetrifluoroethylene-chlorofluoroethylene) terpolymer", ***Applied Physics Letters***, **98**, 222901.

2. **Hongying Zhu,** Sébastien Pruvost, Daniel Guyomar, and Akram Khodayari, 2009, "Thermal energy harvesting from $Pb(Zn_{1/3}Nb_{2/3})_{0.955}Ti_{0.045}O_3$ single crystals phase transitions", ***Journal of Applied Physics***, **106**, 124102.

International Conferences

3. G.SEBALD, S. PRUVOST, **H. ZHU**, D. GUYOMAR, **Invited talk,** "**Electrocaloric materials for giant pyroelectric energy harvesting**", International Symposium on Integrated Functionalities 2010, June 13-16, Puerto Rico.
4. S. Pruvost, **H. Zhu**, G. Sebald and D. Guyomar, "**Thermal energy harvesting using phase transitions",** IEEE 19th International Symposium on the Applications of Ferroelectrics. 9-12 August 2010, Edinburgh, United Kingdom.

French Part

Résumé chapitre 1

Avec le développement récent de l'électronique sans fil et intégrée, la demande en électronique portable et en capteurs sans fil a montré une croissance rapide. Ces dispositifs devenant portatifs, il est alors nécessaire de les rendre autonomes électriquement. L'effort important dans la capacité de stockage de batteries a mené à des évolutions significatives sur les capacités des dispositifs mobiles et sur leur fiabilité. Cependant, cette tendance doit être pondérée par le problème lié par exemple à leur temps de vie limité. Une voie possible pour pallier à ces problèmes est la récupération d'énergie, qui est une solution optimale permettant de réaliser des systèmes auto-rechargeables incluant un microgénérateur qui convertit l'énergie ambiante disponible en énergie électrique.

Ce chapitre est consacré à la description détaillée des recherches effectuées dans le domaine de la récupération d'énergie en utilisant différentes sources d'énergie et différentes techniques. La récupération d'énergie, ou extraction de l'énergie, peut être définie comme «la conversion des énergies ambiantes en énergie électrique en utilisant des matériaux ou des structures de conversion d'énergie, énergie électrique qui sera stockée pour alimenter les dispositifs électriques". Certaines sources possibles d'énergie ambiante sont par exemple : l'énergie thermique, l'énergie lumineuse, l'énergie mécanique ou encore l'énergie magnétique. L'énergie solaire et l'énergie issue des océans sont aussi fréquemment exploitées comme la plupart des sources d'énergies renouvelables disponibles dans la nature en raison, respectivement, de l'importante des énergies rayonnante (lumineuse et thermique) et mécanique disponibles. La récupération d'énergie à partir de telles sources renouvelables a stimulé de nombreuses recherches au cours de ces dernières années.

Les techniques de récupération d'énergie sont nombreuses et listées ci-dessous :

- Photovoltaïque : l'énergie solaire est directement convertie en énergie électrique. en utilisant des cellules solaires (dispositifs semi-conducteurs).
- Radiofréquence : besoin d'une antenne de réception reliée à un circuit de production d'énergie capable de convertir une tension alternative en tension continue utilisable.

- Mécanique (vibrations):
  - ❖ Via l'électromagnétisme : une induction électromagnétique résultant du mouvement relatif (rotatif ou linéaire) entre un flux magnétique et un élément conducteur est utilisée.
  - ❖ Via l'électrostatique : des plaques chargées et électriquement isolées d'un condensateur sont en mouvement les unes par rapport aux autres. Le travail s'opposant à la force électrostatique entre les plaques permet de récupérer de l'énergie électrique.
  - ❖ Via des matériaux piézoélectriques : l'élément piézoélectrique est utilisé pour générer de l'énergie électrique lorsqu'il est sollicité mécaniquement.
  - ❖ Via des matériaux magnétostrictifs : utilisant l'effet Villari où les vibrations induisent la déformation de l'élément magnétostrictif produisant ainsi un changement dans son aimantation. Ce changement d'aimantation est converti en énergie électrique.
- Énergie thermique (sujet de cette thèse)
  - ❖ L'énergie thermique (gradient de température) est convertie en énergie électrique utilisant l'effet thermoélectrique.
  - ❖ L'énergie thermique (variation de température) est convertie en énergie électrique par effet pyroélectrique.
  - ❖ L'énergie thermique (variation de température) est convertie en énergie électrique par l'intermédiaire d'une variation non linéaire de capacité.

L'objectif de cette thèse a porté sur la récupération de l'énergie thermique fondée sur des variations de température. L'effet pyroélectrique et la variation non linéaire de la capacité d'un matériau sont les principales techniques pour réaliser cet objectif.

Résumé chapitre 2

Dans ce chapitre, nous allons introduire le principe de la récupération d'énergie thermique. Premièrement, nous nous intéresserons au principe de l'effet pyroélectrique pour récupérer l'énergie et à la simulation de cycles thermodynamiques utilisés au cours de cette thèse. Par la suite, nous nous focaliserons sur la variation non linéaire de la capacité, variation induite par une fluctuation de la température. Les matériaux ferroélectriques utilisés ont été choisis de par la présence de transitions de phases induites par le champ électrique et/ou la température. Les techniques de caractérisation des matériaux ferroélectriques ont également été introduites afin de comprendre les mécanismes à l'origine de la récupération d'énergie et ainsi améliorer son efficacité.

L'effet pyroélectrique est l'un des phénomènes les plus simples pour transformer directement la chaleur en électricité. Les matériaux pyroélectriques génèrent des charges électriques sous l'action d'une variation temporelle de température. Les matériaux à haute activité pyroélectrique peuvent être utilisés pour récupérer de l'énergie en convertissant l'énergie thermique en énergie électrique. La modélisation de la récupération d'énergie en utilisant un effet pyroélectrique linéaire a été établie et la figure de mérite pour la récupération d'énergie montre bien que les propriétés pyroélectriques sont très intéressantes pour ce type d'applications.

D'autre part, la variation de température peut également influencer la variation non linéaire de la capacité (variation de permittivité diélectrique) des polymères lorsque l'effet pyroélectrique devient négligeable dans une certaine gamme de température. Cette propriété pourrait être une autre possibilité pour la récupération d'énergie sur la thermique. La modélisation de cette méthode est également présentée.

Dans le cas de la conversion d'énergie pyroélectrique, un cycle de Carnot n'est pas réaliste compte tenu de la difficulté à contrôler les conditions adiabatiques et isothermes successives. Par conséquent, d'autres cycles thermodynamiques ont été étudiés comme le cycle de Stirling (deux processus à charge électrique constante et deux processus isothermes)

ou le cycle d'Ericsson (deux processus à champ électrique constant et deux processus isothermes). La modélisation théorique pour la récupération d'énergie thermique a été réalisée pour ces deux cycles.

Les matériaux ferroélectriques ayant été choisis comme matériau actif, il est nécessaire de développer une partie sur la caractérisation de ces matériaux et plus spécifiquement celle permettant d'augmenter l'efficacité de la conversion d'énergie (les transitions de phase ou l'ingénierie des domaines par exemple). Les matériaux ferroélectriques peuvent présenter une ou plusieurs phases ferroélectriques (polaires), chaque phase étant organisée en domaines dans lesquels les dipôles peuvent être réorientés par un champ appliqué. Dans un cristal ferroélectrique, de nombreux domaines (régions avec une polarisation uniforme) coexistent. Dans chaque domaine individuel, tous les dipôles électriques sont alignés dans la même direction. La plupart des matériaux ferroélectriques subissent une transition de phase structurale d'une phase paraélectrique si on se situe au dessus de la température de Curie (θc) à une phase ferroélectrique de symétrie cristalline inférieure si on se trouve en dessous de la température de Curie. De légers changements dans la composition près de la limite de phase morphotropique peuvent changer la maille cristalline du monocristal : quadratique, monoclinique, orthorhombique ou rhomboédrique. Nous avons spécialement axé notre étude sur l'ingénierie du domaine pour les monocristaux ferroélectriques relaxeurs de type PZN-xPT, matériau utilisé pour la récupération d'énergie pyroélectrique. Dans cette partie, les différentes organisations en domaines ou structures cristallines observables dans les monocristaux de PZN-4.5PT orientés et polarisés suivant les directions <111>, <001> et <110> sont également décrites. Les transitions de phase (changement de la maille cristallographique) sont toujours associées à des variations importantes de polarisation qui influencent grandement la récupération d'énergie. La compréhension de ces transitions et de l'ingénierie de domaines nous aidera à mieux expliquer les mécanismes physiques à l'origine de la récupération d'énergie thermique dans les matériaux ferroélectriques.

Résumé chapitre 3

Ce chapitre traite de la récupération d'énergie thermique à base de cycles Ericsson en utilisant des monocristaux ferroélectriques de composition $Pb(Zn_{1/3}Nb_{2/3})_{0.955}Ti_{0.045}O_3$ (PZN-4.5PT) et orientés suivant la direction cristallographique <110>. Cette composition a été choisie en raison de la présence d'une transition FE-FE induite par la température ou par un champ électrique dans le cas d'un échantillon polarisé. Ces transitions de phase pourraient conduire à une amélioration considérable de l'énergie récupérée.

Premièrement, les transitions de phase observées pour les monocristaux de PZN-4.5PT orientés suivant <110> en fonction de la température et du champ électrique sont présentées. Pendant le chauffage sous champ électrique nul, ces monocristaux ont montré les transitions de phase suivantes: à température ambiante, la phase stable est rhomboédrique; dans la gamme de température de 120-130°C, une première transition est observée passant d'une maille rhomboédrique (R) à une maille quadratique (T). En augmentant la température, une seconde transition de phase permet de passer d'une maille quadratique à une maille cubique (C). Par ailleurs, sous champ électrique, une phase intermédiaire ferroélectrique de maille cristalline orthorhombique (O) a été induite à des températures comprises entre celles des phases R et T. La transition R-O génère une augmentation de la polarisation et inversement la transition O-T est associée à une diminution de la polarisation. Ces transitions apportent un intérêt certain pour l'amélioration des propriétés pyroélectriques, et par la suite pour augmenter l'énergie récupérée.

Deuxièmement, la synthèse de monocristaux PZN-4.5PT par la méthode de flux haute température a été présentée. Afin de confirmer la structure des monocristaux, la diffraction des rayons X a été réalisée sur des cristaux broyés. Les propriétés diélectriques bas niveau montrent que la transition de phase rhomboédrique-quadratique se produit à environ 130°C sur un monocristal polarisé. A partir de ces analyses, les cycles d'Ericsson ont été entrepris entre 100 et 130°C pour différentes fréquences. A la fréquence la plus basse (0,01Hz), l'énergie maximale récupérable est égale à 86 mJ/cm^3. En augmentant la fréquence, l'énergie

récupérée diminue de façon non linéaire, diminution particulièrement rapide pour des fréquences supérieures à 1 Hz. L'effet de fréquence observé sur les valeurs d'énergies récupérées est discuté en détail. Les transitions de phase dues à l'ingénierie des domaines, par exemple, R-O pendant le processus de charge à basse température et O-T durant le processus de décharge à haute température, ont considérablement augmenté la quantité d'énergie récupérée. Pour des fréquences plus élevées, la réduction du temps de charge du monocristal conduit à une transition de phase diffuse, et par la suite donne lieu à la coexistence de phases orthorhombique et rhomboédrique. De ce fait, l'énergie récupérée baisse si le champ électrique augmente.

Basé sur l'analyse des résultats expérimentaux, il a été constaté que la fréquence du champ électrique appliqué affecte la transition de phase et la polarisation du matériau dans le cadre du cycle d'Ericsson. Ainsi, nous avons développé un cycle d'Ericsson asymétrique, modifié en appliquant un champ électrique avec des fréquences différentes au cours des processus de charge et décharge. Deux cycles asymétriques d'Ericsson ont été testés : un cycle de L-H, correspondant à un processus de charge du matériau réalisé à basse fréquence et un processus de décharge du matériau réalisé à haute fréquence. Le second cycle, de type H-L, était équivalent au premier mais en inversant les fréquences pour les processus de charge et de décharge. Plusieurs fréquences de charge et de décharge de l'échantillon ont été testées. Le cycle de H-L a permis de récupérer une énergie plus grande que lors d'un cycle classique, l'énergie récupérée atteignant 106 mJ /cm^{-3}. De plus, cette énergie récupérée est égale au double de celle fournie lors de la charge de l'échantillon, ce qui correspond au cycle de récupération d'énergie le plus efficace pour ce matériau.

Résumé chapitre 4

Ce chapitre étudie principalement l'exploitation de l'énergie électrostatique sur les terpolymères ferroélectriques. La récupération d'énergie est réalisée en utilisant la variation non linéaire de la permittivité du matériau sous champ électrique. Le terpolymère P(VDF-TrFE-CFE) de composition 61.3/29.7/9 % mol est un matériau prometteur pour ce type d'applications en raison d'une grande variation de sa permittivité diélectrique induite par la transition ordre-désordre observée à une température proche de la température ambiante.

Premièrement, la caractérisation générale des polymères de la famille des PVDF indique que, par la co-polymérisation de monomère CFE avec le copolymère P(VDF-TrFE), le terpolymère obtenu deviendrait un polymère relaxeur éliminant ainsi l'hystérésis des cycles de polarisation P-E, paramètre intéressant pour la récupération d'énergie. Par ailleurs, nos données expérimentales de cycles unipolaires et des propriétés diélectriques bas niveau sur le P(VDF-TrFE-CFE) 61.3/29.7/9 % mol, confirment une diminution notable du déplacement électrique lorsque la température passe de 20°C à -20°C, principalement due à la diminution de la permittivité diélectrique, l'effet pyroélectrique étant négligeable. Par conséquent, la gamme de température entre la température ambiante et une température plus basse a été choisie pour réaliser les cycles d'Ericsson.

Les films de terpolymère ont été obtenus par dépôt d'une solution liquide (casting). Afin d'assurer un échange thermique rapide, les films ont ensuite été collés sur un substrat en acier. Le principe de la conversion de l'énergie électrostatique a été présenté en détail, y compris les deux cycles de conversion d'énergie possibles: cycle de Stirling et cycle d'Ericsson. La simulation de ces deux cycles de conversion a permis d'évaluer leur capacité de récupération d'énergie à partir des valeurs de permittivité diélectrique en fonction de la température et du champ électrique DC appliqué. Lorsqu'on passe de 25 à 0°C, l'énergie récupérée augmente jusqu'à 240 mJ/cm^3 en appliquant un champ électrique de 80 kV / mm. La mesure directe du cycle d'Ericsson a également été réalisée avec un champ électrique maximum de 25 kV / mm.

En tenant compte de la conduction électrique du matériau, l'énergie récupérée est égale à 50 mJ/cm^3, valeur cohérente avec la simulation (48 mJ/cm^3). La faisabilité de ce type de cycle a ainsi été démontrée.

Enfin, afin d'estimer la récupération d'énergie pour des champs électriques élevés, nous avons étudié sous différentes variations de température et de champs électriques les simulations des cycles d'Ericsson et de Stirling.

Bibliography

[1] B. A. Warneke, M. D. Scott, B. S. Leibowotz, L. Zhou, C. L. Bellew, J. A. Chediak, J. M. Kahn, B. E. Boser, and K. S. Pister. An autonomous 16 mm^3 solar-powered node for distributed wireless sensor networks. *Proc. IEEE Sensors*, vol.1, 1510-1515 (2002).

[2] C. Alippi and C. Galperti. An adaptive system for optimal solar energy harvesting in wireless sensor network nodes. *IEEE Transactions on Circuits and Systems I*, vol.55, 1742-1750 (2008).

[3] H. A. Sodano, G. E. Simmers, R. Dereux, and D. Inman. Recharging batteries using energy harvested from thermal gradients. *Journal of Intelligent Material Systems and Structures*, vol.18, 3-10 (2007).

[4] O. M. Nielsen, L. R. Arana, C. D. Baertsch, K. F. Jensen, and M. A. Schmidt. A thermophotovoltaic micro-generator for portable power applications. *Transducers '03*, Boston,USA, 714-717 (2003).

[5] S. Baligo, L. Castorina, L. Fortuna, and N. Savalli. Photo-thermoelectric power generation for autonomous microsystems. *IEEE Internationsl Symposium on Circuits and Systems*, vol.4, 760-763 (2003).

[6] W. Wang, F. Jia, Q. Huang, and J. Zhang. A new type of low power thermoelectric microgenerator fabricated by nanowire array thermoelectric material. *Microelectronic Engineering*, vol.77, 223-229 (2005).

[7] J. B. Lee, Z. Chen, M. G. Allen, A. Rohatgi, and R. Arya. A high voltage solar cell array as an electrostatic MEMS power supply. *Micro Electro Mechanical Systems, Proceedings of IEEE Workshop*, 331-336 (1994).

[8] D. M. Bennett, R. Selfridge, P. Humble, and J. N. HARB. Hybrid power systems for autonomous MEMS. *Proceedings of SPIE, Smart Structures and Materials*, vol.4334, 354-362 (2001).

[9] M. H. Mickle, M. Lovell, L. Mats, L. Neureuter, and D. Gorodetsky. Energy harvesting, profiles, and potential sources. *International Journal of Parallel and Distributed Systems and Networks*, vol.4, 150-160 (2001).

[10] J. F. Randall.On the use of photovoltaic ambient energy sources for powering indoor electronic devices. Ph.D. dissertation, EPFL (Swiss Federal Institute of Technology, Lausanne), 2003.

[11] S. Suzuki, T. Katane, H. Saotome, and O. Saito. A proposal of electric power generating system for implanted medical devices. *IEEE Transactions on Magnetics*, vol.35, 3586-3588 (1999).

[12] D. N. Fry, D. E. Holcomb, J. K. Munro, L. C. Oakes, and M. J. Maston. Compact portable electric power sources. *Oak Ridge National Laboratory report, ORNL/TM-13360* (1997).

[13] P. Glynne-Jones and N. M. White. Self-powered systems: a review of energy sources. *Sensor Review*, vol.21, 91–97 (2001).

[14] H. A. Sodano, D. J. Inman, and G. Park. A review of power harvesting from vibration using piezoelectric materials. *The Shock and Vibration Digest*, vol.36, 197–205 (2004).

[15] M. A. Qiwai, J. P. Thomas, J. C. Kellogg, and J. Baucom. Energy harvesting concepts for small electric unmanned systems. *Proceedings of SPIE, Smart Structures and Materials 2004: Active Materials: Behavior and Mechanics*, vol.5387, 84–95 (2004).

[16] L. Mateu and F. Moll. Review of energy harvesting techniques and applications for microelectronics. *Proceedings of SPIE 5837, VLSI Circuits and Systems II*, Sevilla, Spain, 359 (2005).

[17] J. A. Paradiso and T. Starner. Energy scavenging for mobile and wireless electronics. *IEEE Pervasive Computing*, vol.4, 18–27 (2005).

[18] S.J. Roundy.Energy scavenging for wireless sensor nodes with a focus on vibration to electricity conversion. Ph.D. dissertation, Department of Mechanical Engineering, University of California, Berkeley, 2003.

[19] Shashank Priya. Advances in energy harvesting using low profile piezoelectric transducers. *Journal of Electroceramics*, vol.19, 167-184 (2007).

[20] S. Roundy, P. Wright, and J. Rabaey. A study of low Level vibrations as a power source for wireless sensor nodes. *Computer Communications*, vol.26, 1131–1144 (2003).

[21] L. Wang and F. G. Yuan. Energy harvesting by magnetostrictive material (MsM) for powering wireless sensors in SHM. *Proceedings of SPIE 6529,14th International Symposium*, 652941 (2007).

[22] Tomas Markvart. Solar electricity. *England: John Wiley & Sons* (1994).

[23] N. Bulusu and S. Jha, *Wireless sensor networks, Artech House, Boston,*. (2005).

[24] H. Ostaffe. RF energy harvesting enables wireless sensor networks. *Sensors (http://www.sensorsmag.com/sensors-mag/rf-energy-harvesting-enables-wireless-sensor-networks-6175)* (October 13, 2009).

[25] T. Starner and J. A. Paradiso. Human generated power for mobile electronics. *Low-Power Electronics,CRC Press*, 45_1- 45_35 (2004).

[26] J. K. Ward and S. Behrens. Adaptive learning algorithms for vibration energy harvesting. *Smart Materials and Structures*, vol.17, 035025 (2008).

[27] An Introduction to Joule-Thief™ vibration based energy harvesting. *Powering the Internet of Things™, www.AdaptivEnergy.com*.

[28] C. R. Saha, T. O'Donnell, H. Loder, S. Beeby, and J. Tudor. Optimization of an electromagnetic energy harvesting device. *IEEE Transactions on Magnetics* vol.42 (2006).

[29] P. D. Mitcheson, E. M. Yeatman, G. K. Rao, A. S. Holmes, and T. C. Green. Energy harvesting from human and machine motion for wireless electronic devices *Proceedings of the IEEE* vol.96, 1457 - 1486 (2008).

[30] C.B. Williams and R.B. Yates. Analysis of a micro-electric generator for microsystems. *Sensors and Actuators A, Physical*, vol.52, 8-11.

[31] P. Glynne-Jones, M.J. Tudor, S.P. Beeby, and N.M. White. An electromagnetic, vibration-powered generator for intelligent sensor systems. *Sensors and Actuators A, Physical*, vol.110, 344–349 (2004).

[32] I. Sari, T. Balkan, and H. Külah. An electromagnetic micro energy harvester based on an array of parylene cantilevers. *Journal of Micromechanics and Microengineering*, vol.19, 105023 (2009).

[33] S. Roundy, P. K. Wright, and J. M. Rabaey. Energy scavenging for wireless sensor networks: with special focus on vibrations,Kluwer Academic, Boston. (2004).

[34] S. Meninger, J. O. Mur-Miranda, R. Amirtharajah, A. P. Chandrakasan, and J. H. Lang. Vibration-to-Electric energy conversion. *IEEE Transactions on Very Large Scale Integration (VLSI) Systems*, vol.9, 64-76 (2001).

[35] E. O. Torres and G. A. Rincon-Mora. Electrostatic energy-harvesting and battery-charging CMOS system prototype. *Circuits and Systems I: Regular Papers, IEEE Transactions on* vol.56, 1938 - 1948 (2009).

[36] L. Solymar and D. Walsh. Lectures on the electrical properties of materials. *5th ed. Oxford, U.K.: Oxford Univ. Press* (1993).

[37] M. UMEDA, K. NAKAMURA, and S. UEHA. Analysis of the transformation of mechanical impact energy to electric energy using piezoelectric vibrator. *Japanese Journal of Applied Physics.* vol.35, 3267–3273 (1996).

[38] N. G Elvin, Alex A. Elvin, and M. Spector. A self-powered mechanical strain energy sensor. *Smart Materials and Structures* vol.10, 293–299 (2001).

[39] H. A. Sodano, G. Park, D. J. Leo, and D. J. Inman. Use of piezoelectric energy harvesting devices for charging batteries. *Proceedings of SPIE*, vol.5050, 101–108 (2003).

[40] Geffrey K. Ottman, Heath F. Hofmann, Archin C. Bhatt, and George A. Lesieutre. Adaptive piezoelectric energy harvesting circuit for wireless remote power supply. *IEEE Transactions on Power Electronics*, vol.17, 669-676 (2002).

[41] G.K Ottman, H.F. Hofmann, and G.A Lesieutre. Optimized piezoelectric energy harvesting circuit using step-down converter in discontinuous conduction mode *IEEE Transactions on Power Electronics*, vol.18, 696 - 703 (2003).

[42] A. Badel, D. Guyomar, E. Lefeuvre, and C. Richard. Efficiency enhancement of a piezoelectric energy harvesting device in pulsed operation by synchronous charge inversion. *Journal of Intelligent Material Systems and Structures*, vol.16, 889-901 (2005).

[43] D. Guyomar, A. Badel, E. Lefeuvre, and C. Richard. Toward energy harvesting using active materials and conversion improvement by nonlinear processing. *IEEE Transactions on Ultrasonics, Ferroelectrics and Frequency Control* vol.52, 584 - 595 (2005).

[44] C. Richard, D. Guyomar, D. Audigier, and H. Bassaler. Enhanced semi-passive damping using continuous switching of a piezoelectric device on an inductor *Proceedings of SPIE 3989, Smart Structures and Materials.* 288-299 (2000).

[45] M. E. Staley and A. B. Flatau. Characterization of energy harvesting potential of Terfenol-D and Galfenol. *Proceedings of SPIE, Smart Structures and Materials*, vol.5764, 630-640 (2005).

[46] L. Wang and F. G. Yuan. Structural vibration energy harvesting by magnetostrictive materials (MsM). *The 4th China-Japan-US Symposium on Structural Control and Monitoring, Zhejiang University Press, Hangzhou, China*, 147-152 (2006).

[47] G. Min, D. M. Rowe, and K. Kontostavlakis. Thermoelectric figure-of-merit under large temperature differences. *Journal of Physics D: Applied Physics*, vol.37, 1301–1304 (2004).

[48] D. M. Rowe. Thermoelectric waste heat recovery as a renewable energy source. *International Journal of Innovations in Energy Systems and Power*, vol.1, 13-23 (2006).

[49] M. Chen, S. Lu, and B. Liao. On the figure of merit of thermoelectric generators. *Journal of Energy Resources Technology,* vol.127, 37-41 (2005).

[50] C. Wu. Analysis of waste-heat thermoelectric power generators. *Applied Thermal Engineering*, vol.16, 63-69 (1996).

[51] M.D. Rowe, G. Min, S.G. Williams, A. Aoune, K. Matsuura, V.L. Kuznetsov, and L.W. Fu. Thermoelectric recovery of waste heat – case studies. *Proc. of the 32nd Intersociety Energy Conversion Engineering Conference*, 1075–1079 (1997).

[52] D. M. Rowe, V. L. Kuznetsov, L. A. Kuznetsova, and G. Min. Electrical and thermal transport properties of intermediate-valence $YbAl_3$. *Journal of Physics D: Applied Physics* 2183–2186 (2002).

[53] M. Stordeur and I. Stark. Low power thermoelectric generator-- self-sufficient energy supply for micro systems. *Proc. 16th Int. Conf. Thermoelectrics* 575-577 (1997).

[54] J. Fleming, W. Ng, and S. Ghamaty. Thermoelectric-based power system for unmanned-air-vehicle/microair-vehicle applications. *Journal of Aircraft*, vol.41, 674–676 (2004).

[55] K. Wojciechowski, J. Merkisz, P. Fuć, P. Lijewski, M. Schmidt, and R. Zybała. Study of recovery of waste heat from exhaust of automotive engine. *5th European Conference on Thermoelectrics, Odessa, Ukraine,*, 194-198 (2007).

[56] U. Birkholz, U. E. Grob, M. Riffel, H. Roth, and U. Stohrer. Conversion of waste exhaust heat in automobile using $FeSi_2$ thermoelements. *Proc. of the 7th International Conference on Thermoelectric Energy Conversion, Arlington, VA*, 124–128 (1988).

[57] K. Matsubara. Development of a high efficient thermoelectric stack for a waste exhaust heat recovery of vehicles. *Proc. of the 21st International Conference on Thermoelectronics, August 25-29th, Portland, OR*, 418–423 (2002).

[58] S. R. Hoh. ferroelectric energy converters. *1TT F edral Labs., Nuttley, N. J., Tech. Memo No. 755, March, 1959; presented at Solid State Devices Research Conf., Cornell University, Itchaca, N. Y. ; June 18, 1959*.

[59] B. Miller. Ferroelectrics generate power. *Electronics*, vol.32, 88-90 (1959).

[60] B. Miller. The ferroelectric converter. *Electromechanical Design*, vol.3, 15-17 (1959).

[61] W. H. Clingman and R. G. Moore. Application of ferroelectricity to energy conversion processes. *Journal of Applied Physics*, vol.32, 675-681 (1961).

[62] J. D. Childress. Application of a ferroelectric material in an energy conversion device. *Journal of Applied Physics*, vol.33, 1793-1798 (1962).

[63] S. R. Hoh. Conversion of thermal to electrical energy with ferroelectric materials. *Proceedings IEEE*, vol.51, 838 (1963).

[64] E. Fatuzzo, H. Kiess, and R. Nitsche. Theoretical efficiency of pyroelectric power converters. *Journal of Applied Physics*, vol.37, 510 (1966).

[65] J. A. Gonzalo. Ferroelectric materials as energy converters. *Ferroelectrics* vol.11, 423-429 (1976).

[66] R. B. Olsen and D. Evans. Pyroelectric energy conversion: Hysteresis Loss and temperature sensitivity of a gerroelectric material. *Journal of Applied Physics*, vol.54, 5941-5944 (1983).

[67] R.B. Olsen, D.A. Bruno, J.M. Briscoe, and E.W. Jacobs. Pyroelectric conversion cycle of vinylidene fluoride-trifluoroethylene copolymer. *Journal of Applied Physics*, vol.57, 5036-5042 (1985).

[68] R.B. Olsen, D.A. Bruno, J.M. Briscoe, and J. Dullea. High electric field resistivity and pyroelectric properties of vinylidene fluoride-trifluoroethylene copolymer. *Journal of Applied Physics*, vol.58, 2854 (1985).

[69] R.B. Olsen. Pyroelectric energy converter and method. *U.S. Patent 4,647,836*.

[70] R.B. Olsen. Apparatus and method for pyroelectric power conversion. *U.S. Patent 4,425,540* (1984).

[71] R.B. Olsen, D.A. Bruno, J.M. Briscoe, and J Dullea. Cascaded pyroelectric energy converter. *Ferroelectrics*, vol.59, 205-219 (1984).

[72] H.V. Tiwary. Ferroelectric polymer for thermodielectric energy conversion. *Japanese Journal of Applied Physics*, vol.24, 878-880 (1985).

[73] M. Ikura. Conversion of low-grade heat to electricity using pyroelectric copolymer. *Ferroelectrics*, vol.267, 403-408 (2002).

[74] D. Guyomar, G. Sebald, E. Lefeuvre, and A. Khodayari. Toward heat energy harvesting using pyroelectric material. *Journal of Intelligent Material Systems and Structures*, vol.20 265-271 (2009).

[75] G. Sebald, D. Guyomar, and A. Agbossou. On thermoelectric and pyroelectric energy harvesting. *Smart Msterials and Structures* vol.18, 125006 (2009).

[76] G. Sebald, S. Pruvost, and D. Guyomar. Energy harvesting based on ericsson pyroelectric cycles in a relaxor ferroelectric ceramic. *Smart Materials and Structures* vol.17, 015012 (2008).

[77] Daniel Guyomar, Sebastien Pruvost, and Gael Sebald. Energy Harvesting Based on FE-FE Transition in Ferroelectric Single Crystals. *IEEE transactions on ultrasonics, ferroelectrics, and frequency control*, vol.55, 279-285 (2008).

[78] G. Sebald, E. Lefeuvre, and D. Guyomar. Pyroelectric energy conversion: optimization principles. *IEEE Transactions on Ultrasonics, Ferroelectrics, and Frequency Control*, vol.55, 538-551 (2008).

[79] D. Vanderpool, J. H. Yoon, and L. Pilon. Simulations of a prototypical device using pyroelectric materials for harvesting waste heat. *International Journal of Heat and Mass Transfer*, vol.51, 5052–5062 (2008).

[80] H. Nguyen, A. Navid, and L. Pilon. Pyroelectric energy converter using co-polymer P(VDF-TrFE) and Olsen cycle for waste heat energy harvesting *Applied Thermal Engineering*, vol.30, 2127-2137 (2010).

[81] A. Navid and L. Pilon. Pyroelectric energy harvesting using Olsen cycles in purified and porous poly(vinylidene fluoride-trifluoroethylene) [P(VDF-TrFE)] thin films. *Smart Materials and Structures* vol.20, 025012 (2011).

[82] K.-H. Chew, F. G. Shin, B. Ploss, H. L. W. Chan, and C. L. Choy. Primary and secondary pyroelectric effects of ferroelectric 0-3 composites. *Journal of Applied Physics* vol.94, 1134-1145 (2003).

[83] S.B. Lang. Pyroelectricity: from ancient curiosity to modern imaging tool. *Physics Today*, vol.58, 31-36 (2005).

[84] F. Jona and G. Shirane. Ferroelectric crystals. *Dover, New York.* , 134 (1993).

[85] B. Neese, B. Chu, S. Lu, Y. Wang, E. Furman, and Q. M. Zhang. Large electrocaloric effect in ferroelectric polymers near room temperature. *Science*, vol.321, 821-823 (2008).

[86] E. Lefeuvre, A. Badel, C. Richard, L. Petit, and D. Guyomar. A comparison between several vibration-powered piezoelectric generators for standalone systems. *Sensors and Actuators A, Physical*, vol.126, 405–416 (2006).

[87] G. Sebald, L. Seveyrat, D. Guyomar, L. Lebrun, B. Guiffard, and S. Pruvost. Electrocaloric and pyroelectric properties of $0.75Pb(Mg_{1/3}Nb_{2/3})O_3–0.25PbTiO_3$ single crystals. *Journal of Applied Physics* vol.100, 124112 (2006).

[88] R. B. Olsen, D. A. Bruno, and J. M. Briscoe. Pyroelectric conversion cycle. *Journal of Applied Physics*, vol.58, 4709-4716 (1985).

[89] Y. Xu. Ferroelectric materials and their applications. *North-Holland Elsevier Sci. Publ., Amsterdam* (1991).

[90] T. Liu and C. S. Lynch. Domain engineered relaxor ferroelectric single crystals. *Continuum Mechanics and Thermodynamics*, 119–135 (2006).

[91] L. Kouchachvili and M. Ikura. Pyroelectric conversion—effects of P(VDF–TrFE) preconditioning on power conversion. *Journal of Electrostatics*, vol.65, 182–188 (2007).

[92] S.B. Riffat and Xiaoli Ma. Thermoelectrics: a review of present and potential applications. *Applied Thermal Engineering*, vol.23, 913–935 (2003).

[93] D. Damjanovic, P. Muralt, and N. Setter. Ferroelectric sensors. *IEEE Sensors Journal*, vol.1 191 - 206 (2001).

[94] M.H. Lee, R. Guo, and A.S. Bhalla. Pyroelectric Sensors. *Journal of Electroceramics*, vol.2, 229-242 (1998).

[95] J. He, J. Chen, Y. Zhou, and J. Wang. Regenerative characteristics of electrocaloric Stirling or Ericsson refrigeration cycles. *Energy Conversion and Management*, vol.43, 2319–2327 (2002).

[96] A. Khodayari, S. Pruvost, G. Sebald, D. Guyomar, and S. Mohammadi. Nonlinear pyroelectric energy harvesting from relaxor single crystals. *IEEE Transactions on Ultrasonics, Ferroelectrics, and Frequency Control*, vol.56, 693-699 (2009).

[97] B. A. Tuttlea and D. A. Payne. The effects of microstructure on the electrocaloric properties of $Pb(Zr,Sn,Ti)O_3$ ceramics. *Ferroelectrics*, vol.37, 603 - 606 (1981).

[98] A. S. Mischenko, Q. Zhang, J. F. Scott, R. W. Whatmore, and N. D. Mathur. Giant electrocaloric effect in thin-film $PbZr_{0.95}Ti_{0.05}O_3$. *Science*, vol.311, 1270-1271 (2006).

[99] E. Birks, L. Shebanov, and A. Sternberg. Electrocaloric effect in PLZT ceramics *Ferroelectrics*, vol.69, 125 – 129 (1986).

[100] H. Qian and L.A. Bursill. Phenomenological Theory of the Dielectric Response of Lead Magnesium Niobate and Lead Scandium Tantalate. *International Journal of Modern Physics B*, vol.10, 2007-2025 (1996).

[101] L. E. Cross. Relaxor ferroelectrics. *Ferroelectrics* vol.76, 241-267 (1987).

[102] T. R. Shrout and H. Arvind. Preparation of lead-based ferroelectric relaxors for capacitors. *American Ceramic Society Bulletin*, vol.66, 704-711 (1987).

[103] C.A. Randall, D.J. Barber, R.W. Whatmore, and P. Groves. Short-range order phenomena in lead-based perovskites. *Ferroelectrics*, vol.76, 277 - 282 (1987).

[104] Metin Ozgul. Polarization switching and fatigue anisotropy in relaxor-lead titanate ferroelectric single crystals *Ph.D. thesis, The Pennsylvania State University* (2003).

[105] J. Kuwata, K. Uchino, and S. Nomura. Phase Transitions in the $Pb(Zn_{1/3}Nb_{2/3})O_3$-$PbTiO_3$ system. *Ferroelectrics*, vol.37, 579-582 (1981).

[106] D. E. Cox, B. Noheda, G. Shirane, Y. Uesu, K. Fujishiro, and Y. Yamada. Universal phase diagram for high-piezoelectric perovskite systems. *Applied Physics Letters*, vol.79, 400-402 (2001).

[107] M. E. Lines and A. M. Glass. Principles and Applications of Ferroelectrics and Related Materials. *Clarendon Press,Oxford 1977*.

[108] H. D. Megaw. Ferroelectricity in Crystals. *Methuen and Co., London 1957*.

[109] F. Jona and G. Shirane. Ferroelectric Crystals. *Pergamon Press, Oxford 1962*.

[110] R. E. Nettleton. Ferroelectrics 1, 3, 87, 93, 111, 121, 127, 207, 221 (1970).

[111] R. E. Nettleton. Ferroelectrics 2, 5, 77, 93 (1971).

[112] W. J. Merz. Domain formation and domain wall motion in ferroelectric $BaTiO_3$ single crysrals. *Physical Review*, vol.95, 690 (1954).

[113] A. Renault, H. Dammak, G. Calvarin, and P. Gaucher. Electric-field-induced orthorhombic phase in $Pb[(Zn_{1/3}Nb_{2/3})_{0.955}Ti_{0.045}]O_3$ single crystals. *Journal of Applied Physics* vol.97, 044105 (2005).

[114] W. S. Chang, L. C. Lim, P. Yang, C.-S. Tu, F.-T. Wang, and C.-T. Tseng. Phase transformations in poled PZN-4.5%PT single crystal revealed by combined property

measurements and high-resolution diffraction technique. *Journal of Applied Physics*, vol.104, 054102 (2008).

[115] M. L. Mulvihill, S. E. Park, G. Risch, Z. Li, K. Uchino, and T. R. Shrout. The role of processing variables in the flux growth of lead zinc niobate-lead titanate relaxor ferroelectric single crystals. *Japanese Journal of Applied Physics*, vol.35, 3984-3990 (1996).

[116] L.C. Lima and K.K. Rajan. High-homogeneity High-performance flux-grown $Pb(Zn_{1/3}Nb_{2/3})O_3$–(6–7)%$PbTiO_3$ single crystals. *Journal of Crystal Growth*, vol.271, 435–444 (2004).

[117] A. Benayad, D. Kobor, L. Lebrun, B. Guiffard, and D. Guyomar. Characteristics of $Pb[(Zn_{1/3}Nb_{2/3})0.955Ti_{0.045}]O_3$ single crystals versus growth method. *Journal of Crystal Growth*, vol.270, 137–144 (2004).

[118] D. Kobor, L. Lebrun, G. Sebald, and D. Guyomar. Characterization of pure and substituted $0.955Pb(Zn_{1/3}Nb_{2/3})O_3$–$0.045PbTiO_3$. *Journal of Crystal Growth*, vol.275, 580–588 (2005).

[119] F.J. Kumar, L.C. Lim, C. Chilong, and M.J. Tan. Morphological aspects of flux grown 0.91PZN-0.09PT crystals. *Journal of Crystal Growth*, vol.216, 311-316 (2000).

[120] A. Benayad, A. Hajjaji, B. Guiffard, L. Lebrun, and D. Guyomar. Electromechanical properties versus polarization and vibration directions of $Pb((Zn_{1/3}Nb_{2/3})_{0.955}Ti_{0.045})O_3$ single crystals grown by the modified Bridgman method. *Journal of Physics D : Applied Physics*, vol.40, 840-845 (2007).

[121] H. Cao, B. Fang, H. Xu, and H. Luo. Crystal orientation dependence of dielectric and piezoelectric properties of tetragonal $Pb(Mg_{1/3}Nb_{2/3})O_3$–38%$PbTiO_3$ single crystal. *Materials Research Bulletin*, vol.37, 2135-2143 (2002).

[122] H. Y. Zhu, S. Pruvost, D. Guyomar, and A. Khodayari. Thermal energy harvesting from $Pb(Zn_{1/3}Nb_{2/3})_{0.955}Ti_{0.045}O_3$ single crystals phase transitions. *Journal of Applied Physics*, vol.106, 124102 (2009).

[123] Z.-Y. Cheng, V. Bharti, T.-B. Xu, Haisheng Xu, T. Mai, and Q.M. Zhang. Electrostrictive poly(vinylidene fluoride-trifluoroethylene) copolymers. *Sensors and Actuators A, Physical*, vol.90, 138-147 (2001).

[124] V. Bharti and Q. M. Zhang. Dielectric study of the relaxor ferroelectric poly(vinylidene fluoride-trifluoroethylene) copolymer system. *Physical Review B* vol.63, 184103 (2001).

[125] Q.M. Zhang, Z.-Y. Cheng, and V. Bharti. Relaxor ferroelectric behavior in high-energy electron-irradiated poly(vinylidene fluoride-trifluoroethylene) copolymers. *Applied physics. A, Materials science & processing,* vol.70, 307–312 (2000).

[126] F. Xia, Z. Cheng, H. Xu, H. Li, and Q. Zhang. High electromechanical responses in a poly(vinylidene fluoride-trifluoroethylene-chlorofluoroethylene) terpolymer. *Advanced Materials*, vol.14, 1574-1577 (2002).

[127] B. P. Neese. The multifunctional properties of PVDF-based Polymers. *PhD Thesis, The Pennsylvania State University* (2009).

[128] A. C. Jayasuriya, A. Schirokauer, and J. I. Scheinbeim. Crystal-structure dependence of electroactive properties in differently prepared poly(vinylidene fluoride/hexafluoropropylene) copolymer films. *Journal of Polymer Science Part B: Polymer Physics*, vol.39, 2793-2799 (2001).

[129] K. Tashiro. In Ferroelectric Polymers. *edited by H. S. Nalwa (Dekker, New York, 1995)*, 63.

[130] H. Kawai. The piezoelectricity of poly(vinylidene fluoride). *Japanese Journal of Applied Physics*, vol.8, 975-976 (1969).

[131] J. G. Bergman, J. H. McFee, and G. R. Crane. Pyroelectricity and optical second harmonic generation in polyvinylidene fluoride films. *Applied Physics Letters*, vol.18, 203-205 (1971).

[132] Ferroelectric polymers. *edited by H. S. Nalwa (Dekker, New York, 1995)*.

[133] T. Yagi, M. Tatemoto, and J. Sako. Transition behavior and dielectric properties in trifluoroethylene and vinylidene fluoride copolymers. *Polymer Journal*, vol.12, 209-223 (1980).

[134] F. Bauer. Relaxor fluorinated polymers: novel applications and recent developments. *Dielectrics and Electrical Insulation, IEEE Transactions on* vol.17, 1106 - 1112 (2010).

[135] V. Bharti, H. S. Xu, G. Shanthi, Q. M. Zhang, and Kuming Liang. Polarization and structural properties of high-energy electron irradiated poly(vinylidene fluoride-trifluoroethylene) copolymer films. *Journal of Applied Physics*, vol.87, 452-461 (2000).

[136] Q. M. Zhang, F. Xia, Z.-Y. Cheng, H. Xu, H. Li, M. Poh, and C. Huang. Poly(vinylidene fluoroethylene-trifluoroethylene) based high performance electroactive polymers. *11th International Syniposium on Electrets IEEE*, 181-190 (2002).

[137] Q. M. Zhang, V. Bharti, and X. Zhao. Giant electrostriction and relaxor ferroelectric behavior in electron-irradiated poly(vinylidene fluoride-trifluoroethylene) copolymer. *Science*, vol.280, 2101-2104 (1998).

[138] H. Xu, Z.-Y. Cheng, D. Olson, T. Mai, Q. M. Zhang, and G. Kavarnos. Ferroelectric and electromechanical properties of poly(vinylidene-fluoride–trifluoroethylene–chlorotrifluoroethylene) terpolymer. *Applied Physics Letters*, vol.78, 2360-2362 (2001).

[139] A. Petchsuk. Ferroelectric terpolymers, based on semicrystalline VDF/TRFE/chloro-containing termonomers : Synthesis, electrical properties, and functionalization reactions *PhD Thesis, The Pennsylvania State University* (2003).

[140] R. J. Klein, F. Xia, Q. M. Zhang, and F. Bauer. Influence of composition on relaxor ferroelectric and electromechanical properties of poly(vinylidene fluoride-trifluoroethylene- chlorofluoroethylene). *Journal of Applied Physics*, vol.97, 094105 (2005).

[141] K. Ren, Y. Liu, H. Hofmann, and Q. M. Zhang. An active energy harvesting scheme with an electroactive polymer. *Applied Physics Letters*, vol.91, 132910 (2007).

[142] H. Zhu, S. Pruvost, P.J. Cottinet, and D. Guyomar. Energy harvesting by nonlinear capacitance variation for a relaxor ferroelectric poly(vinylidene fluoridetrifluoroethylene-chlorofluoroethylene) terpolymer. *Applied Physics Letters*, vol.98, 222901 (2011).

[143] H. Fröhlich. Theory of dielectrics. *Oxford University Press,London, 2nd edition,* (1958).

[144] G. Kofod. Dielectric elastomer actuators. *Ph.D. Thesis,The Technical University of Denmark* (2001).

[145] Z.-Y. Cheng, R. S. Katiyar, X. Yao, and A. S. Bhalla. Temperature dependence of the dielectric constant of relaxor ferroelectrics. *Physical Review B*, vol.57, 8166-8177 (1998).

[146] G. Akcay, S. P. Alpay, J. V. Mantese, and Jr. G. A. Rossetti. Magnitude of the intrinsic electrocaloric effect in ferroelectric perovskite thin films at high electric fields. *Applied Physics Letters*, vol.90, 252909 (2007).

[147] S. G. Lu, B. Neese, B. J. Chu, Y. Wang, and Q. M. Zhang. Large electric tunability in poly(vinylidene fluoride-trifluoroethylene) based polymers. *Applied Physics Letters*, vol.93, 042905 (2008).

[148] V. Bobnar, B. Vodopivec, A. Levstik, M. Kosec, B. Hilczer, and Q.M. Zhang. Dielectric properties of relaxor-like vinylidene fluoride-trifluoroethylene-based electroactive polymers. *Macromolecules*, vol.36, 4436-4442 (2003).

[149] A Navid, C S Lynch, and L Pilon. Purified and porous poly(vinylidene fluoride-trifluoroethylene) thin films for pyroelectric infrared sensing and energy harvesting. *Smart Materials and Structures*, vol.19, 055006 (2010).

[150] Sumiko Fujisaki, Hiroshi Ishiwara, and Yoshihisa Fujisaki. Low-voltage operation of ferroelectric poly(vinylidene fluoride-trifluoroethylene) copolymer capacitors and metal-ferroelectric-insulator-semiconductor diodes. *Applied Physics Letters*, vol.90, 162902 (2007).

List of Figures

List of Tables

FOLIO ADMINISTRATIF

THESE SOUTENUE DEVANT L'INSTITUT NATIONAL DES SCIENCES APPLIQUEES DE LYON

NOM : **ZHU** DATE de SOUTENANCE : **29 September 2011**
(avec précision du nom de jeune fille, le cas échéant)

Prénoms : **Hongying**

TITRE : **Recupération d'Énergie Thermique à partir de Variations de Température**

NATURE : **Doctorat** Numéro d'ordre : 2011-ISAL-0086

Ecole doctorale : **Électronique, Électrotechnique et Automatique de Lyon**

Spécialité : **Énergie et Systèmes**

RESUME : Le développement des équipements portables, des réseaux de capteurs sans fil et systèmes auto-alimentés d'une manière générale génère une forte demande pour les dispositifs de récupération de micro-énergie. Une des voies les plus intéressantes pour auto-alimenter des dispositifs consiste à développer des systèmes recyclant l'énergie ambiante afin de renouveler sans cesse l'énergie consommée par le dispositif. En dehors de la récupération d'énergie électromécanique, il est également intéressant de convertir l'énergie thermique, qui est «disponible» partout, en énergie électrique.
Au cours de cette thèse, la conversion d'énergie thermique en énergie électrique fondée sur des variations temporelles de température a été développée et améliorée. Parmi les matériaux ferroélectriques, des monocristaux de PZN-4.5PT et le terpolymère P(VDF-TrFE-CFE) 61.3/29.7/9 mol % ont été choisis comme matériaux actifs en raison de leurs propriétés remarquables sous champ électrique. En utilisant des cycles thermodynamiques intelligents, par exemple, Ericsson ou à cycle de Stirling, l'efficacité de la conversion de l'énergie pourrait être considérablement améliorée.
Dans la première partie, la récupération d'énergie pyroélectrique en utilisant des monocristaux de PZN-4.5PT a été principalement étudiée sous deux aspects: l'effet de fréquence et des transitions de phase sur les cycles d'Ericsson. Il a été montré que l'énergie récupérée diminue de façon non linéaire avec une augmentation de la fréquence. De plus, l'utilisation optimale des transitions de phase pendant le cycle d'Ericsson permet d'améliorer grandement l'énergie récupérée en choisissant une gamme de température de travail appropriée. A partir de ces résultats, deux cycles d'Ericsson asymétriques (LH et HL) ont été réalisés avec succès. Avec les monocristaux de PZN-4.5PT, le cycle HL est le cycle le plus efficace pour la conversion d'énergie thermique en énergie électrique.
La deuxième partie traite de la récupération d'énergie électrostatique via la variation non linéaire de la capacité du terpolymère P(VDF-TrFE-CFE) 61.3/29.7/9 mol %. Un cycle d'Ericsson a été réalisé entre 25 et 0°C et comparé à sa simulation à partir de la valeur de la constante diélectrique sous champ électrique DC. La concordance entre la simulation et l'expérience a prouvé la fiabilité de notre évaluation théorique. A partir de la simulation, l'énergie récupérée augmente jusqu'à 240 mJ/cm3 en appliquant un champ électrique de 80 kV/mm. Des cycles de Stirling et d'Ericsson ont également été simulés sous différentes variations de température et champ électriques. L'énergie récupérée augmente avec l'accroissment de la variation de température et de la valeur du champ électrique appliqué et ceci quelque soit le cycle réalisé. Contrairement au cycle d'Ericsson, un cycle de Stirling peut récupérer plus d'énergie pour une même énergie injectée.

MOTS-CLES : **Récupération d'Énergie, Pyroélectricité, Monocristaux, Terpolymères Fluorés, Amélioration de la Conversion Energétique, Cycles Thermodynamique**

Laboratoire (s) de recherche : **Laboratoire de Génie Électrique et Ferroélectricité (LGEF) – INSA Lyon**

Directeur de thèse: **Pr. Daniel GUYOMAR**
Co-directeur de thèse : **Dr. Sébastien PRUVOST**

Président de jury : **Pr. Amen AGBOSSOU**

Composition du jury : **Pr. Amen AGBOSSOU**
Pr. Francois BAUER
Dr. Yves BERNARD